AN INVESTIGATION INTO UNDERWATER DATA TRANSMISSION USING AMPLITUDE-SHIFT-KEYING TECHNIQUES

by

ROBERT SAMUEL ANDREWS

A Thesis submitted for the Degree of Doctor of Philosophy in the Faculty of Engineering, University of London

Department of Electrical Engineering
Imperial College of Science and Technology
University of London

MARCH 1977

ABSTRACT

This thesis reports on the results of a general investigation into several aspects of underwater data transmission using acoustic propagation.

A prototype amplitude-shift-keying (ASK) data transmission system was designed and tested in a large fresh-water reservoir. The system design details and the results of experimental tests are described. The experimental results indicate that when using only 50 milli-Watts of peak transmitter power and with a carrier frequency of 150 kHz, it is possible to transmit digital data at rates up to 625 bits/second at ranges up to 650 metres and to do so with an average probability of bit-error of 1 in 10^3.

Results are also presented on several aspects of the amplitude fluctuations of the received signal. It is shown that the experimentally measured data can be separated according to the prevailing wind direction and that the observed results can be interpreted in terms of cross-wind and parallel-wind directions of propagation. Using this technique, two main causes of signal amplitude fluctuations are investigated and compared with relevent theories.

Two models of the signal amplitude probability density function are proposed and the models are used to compute approximate upper and lower bounds of the average probability of bit-error. It is shown that the measured average probabilities of bit-error actually lie within the computed bounds for signal-to-noise ratios greater than approximately 17 dB.

In the final part of the thesis, some preliminary results relating to the channel pulse response are presented and discussed.

TABLE OF CONTENTS

TITLE	1
ABSTRACT	2
TABLE OF CONTENTS	3
LIST OF FIGURES	6
LIST OF TABLES	11
ACKNOWLEDGEMENTS	12
DEDICATION	13
CHAPTER ONE - INTRODUCTION	14
1.1 Historical Introduction	14
1.2 Survey of Underwater Data Transmission Systems.	18
1.3 Aims and Outline of the Thesis	24
CHAPTER TWO - DESCRIPTION OF THE PROTOTYPE ASK DATA TRANSMISSION SYSTEM AND DISCUSSION OF EXPERIMENTAL PROCEDURES	30
Introduction	30
2.1 Factors Affecting Underwater Acoustic Propagation	30
2.1.1 Spreading Loss	30
2.1.2 Absorption Loss	31
2.1.3 Source Level and Transducer Gain	33
2.1.4 Ambient Noise	34
2.1.5 Other Factors Affecting Transmission	35
2.1.6 Derivation of Maximum Transmission Frequency	37
2.2 Test Site	38
2.3 ASK Data Transmission System	40
2.3.1 Transducers	40
2.3.2 Transmitter Details	50
2.3.3 Receiver Details	52

2.4 Test Procedures 55

2.4.1 Tests Relating to the Study of Signal Amplitude Fluctuations 56

2.4.2 Tests Relating to the Study of Bit-Error Probabilities 57

2.5 Data Analysis Techniques 58

2.5.1 Analysis of Tests Relating to the Study of Amplitude Fluctuations 58

2.5.2 Analysis of Tests Relating to the Study of Bit-Error Probabilities 60

CHAPTER THREE - A STUDY OF SIGNAL AMPLITUDE FLUCTUATIONS 62

Introduction 62

3.1 Amplitude Fluctuations and Their Relevance to Underwater Data Transmission 62

3.2 Measured Amplitude Frequency Spectra 63

3.3 Measured Autocorrelation Functions 73

3.4 Coefficient of Variation of the Amplitude Fluctuations 78

3.5 Analysis of the Signal Probability Density Functions 85

3.6 Derivation of Probability Density Function Models 92

CHAPTER FOUR - STUDY OF BIT-ERROR PROBABILITIES 106

Introduction 106

4.1 Test Procedure and Presentation of Results 106

4.2 Interpretation and Analysis of the Summer Results 110

4.3 Interpretation and Analysis of the Autumn Results 122

4.4 A Comparison of Predicted and Measured Error Probabilities 126

4.5 Optimum Fixed Detection Threshold Level 138

CHAPTER FIVE - BASEBAND PULSE RESPONSE 144

Introduction 144

5.1 Practical Derivation of the Baseband Pulse Response 144

5.2 Presentation of Experimental Results 147

5.3 Summary of Results 168

CHAPTER SIX - SUMMARY AND CONCLUSIONS 170

Introduction 170

6.1 General Summary 170

6.2 Summary of Results 170

6.3 Suggestions for Further Research 177

REFERENCES 179

APPENDIX A - MEAN VALUE OF RICIAN DISTRIBUTION 184

APPENDIX B - COMPUTATION OF SPECTRA USING THE FAST FOURIER TRANSFORM (FFT) 186

APPENDIX C - EXPONENTIAL-COSINE AUTOCORRELATION FUNCTION 190

APPENDIX D - COMPUTATION OF NOISE SPECTRUM 193

LIST OF FIGURES

Figure		Page
1.1	Typical Noise Intensities as a Function of Frequency	16
2.1	Fresh-Water and Sea-Water Attenuation Coefficients as a Function of Frequency	32
2.2	RMS Amplitude Fluctuations Due to Thermal Inhomogeneities	36
2.3	Test Site Dimensions	39
2.4	Theoretical Beam Pattern of the 150 kHz Transducer	42
2.5	Cross-Section of 150 kHz Transducer	44
2.6	Measured Directivity Pattern of the 150 kHz Transducer	46
2.7	Electrical Equivalent Circuit Near Resonance	47
2.8	Measured Admittance Circle Diagrams	49
2.9	Block Diagram of Transmitter Section	51
2.10	Block Diagram of Receiver Section	53
3.1	Measured Amplitude Frequency Spectrum at 150 metres with a Parallel-Wind Condition	65
3.2	Measured Amplitude Frequency Spectrum at 200 metres with a Parallel-Wind Condition	66
3.3	Measured Amplitude Frequency Spectrum at 650 metres with a Parallel-Wind Condition	67
3.4	Measured Amplitude Frequency Spectrum at 150 metres with a Perpendicular-Wind Condition	68
3.5	Measured Amplitude Frequency Spectrum at 200 metres with a Perpendicular-Wind Condition	69
3.6	Measured Amplitude Frequency Spectrum at 650 metres with a Perpendicular-Wind Condition	70
3.7	Computed Autocorrelation Function at 150 metres with a Parallel-Wind Condition	74

3.8 Computed Autocorrelation Function at 200 metres with a Parallel-Wind Condition 75

3.9 Computed Autocorrelation Function at 650 metres with a Parallel-Wind Condition 76

3.10 Computed Autocorrelation Function at 650 metres with a Perpendicular-Wind Condition 77

3.11 Average Coefficient of Variation for the Perpendicular-Wind Condition 80

3.12 Average Coefficient of Variation for the Parallel-Wind Condition 82

3.13 Average Coefficient of Variation of the Surface-Reflected Path Signal 83

3.14 Typical PDF Measured at 150 metres with a Perpendicular-Wind 87

3.15 Typical PDF Measured at 150 metres with a Parallel-Wind 88

3.16 Typical PDF Measured at 150 metres - Intermediate Wind Direction 89

3.17 Typical PDF Measured at 150 metres under an Up-Wind Condition 90

3.18a Direct-Path PDF at 150 metres with a Perpendicular-Wind 95

3.18b Surface-Reflected Path PDF at 150 metres with a Perpendicular-Wind 96

3.19a Direct-Path PDF at 150 metres with a Parallel-Wind 97

3.19b Surface-Reflected Path PDF at 150 metres with a Parallel-Wind 98

3.20 Comparison of Predicted and Measured PDFs for the Parallel-Wind Condition 104

3.21 Comparison of Predicted and Measured PDFs for the Perpendicular-Wind Condition 105

4.1	Typical 3-Day Variation in the Temperature-Depth Profile Measured During Summer	108
4.2	Typical 3-Day Variation in the Temperature-Depth Profile Measured During Autumn	109
4.3	Average Probability of Bit-Error vs Range During Summer	111
4.4	Average Probability of Bit-Error vs Range During Summer	112
4.5	Average Probability of Bit-Error vs Range During Summer	113
4.6	Average Probability of Bit-Error as a Function of Data-Rate During Summer	114
4.7	Average Probability of Bit-Error vs Range During Autumn	115
4.8	Average Probability of Bit-Error vs Range During Autumn	116
4.9	Average Probability of Bit-Error vs Range During Autumn	117
4.10	Average Probability of Bit-Error as a Function of Data-Rate During Autumn	118
4.11	Average Probability of Bit-Error During Autumn with an Absolute Fixed Threshold	119
4.12	Daily Variation in System Performance During Summer	120
4.13	Daily Variation in System Performance During Autumn	121
4.14	Illustration of the Variation of the Signal PDFs with Range	125
4.15	Measured and Predicted Peak Signal-to-Noise Ratios	135
4.16	Computed and Measured Error Probabilities	136
4.17	Computed Optimum Fixed Threshold Levels	141
5.1	Perpendicular-Wind Pulse Response at 150 metres (every consecutive pulse)	149
5.2	Perpendicular-Wind Pulse Response at 200 metres (every consecutive pulse)	150

5.3 Perpendicular-Wind Pulse Response at 650 metres (every consecutive pulse) 151

5.4 Parallel-Wind Pulse Response at 150 metres (every consecutive pulse) 152

5.5 Parallel-Wind Pulse Response at 200 metres (every consecutive pulse) 153

5.6 Parallel-Wind Pulse Response at 650 metres (every consecutive pulse) 154

5.7 Perpendicular-Wind Pulse Response at 150 metres (every 50th pulse) 155

5.8 Perpendicular-Wind Pulse Response at 200 metres (every 50th pulse) 156

5.9 Perpendicular-Wind Pulse Response at 650 metres (every 50th pulse) 157

5.10 Parallel-Wind Pulse Response at 150 metres (every 50th pulse) 158

5.11 Parallel-Wind Pulse Response at 200 metres (every 50th pulse) 159

5.12 Parallel-Wind Pulse Response at 650 metres (every 50th pulse) 160

5.13 Perpendicular-Wind Pulse Response at 150 metres (every 150th pulse) 161

5.14 Perpendicular-Wind Pulse Response at 200 metres (every 150th pulse) 162

5.15 Perpendicular-Wind Pulse Response at 650 metres (every 150th pulse) 163

5.16 Parallel-Wind Pulse Response at 150 metres (every 150th pulse) 164

5.17 Parallel-Wind Pulse Response at 200 metres (every 150th pulse) 165

5.18 Parallel-Wind Pulse Response at 650 metres (every 150th pulse) 166

LIST OF TABLES

Table		Page
1.1	Performance Requirements for Future Underwater Communication System	19
2.1	Estimation of Maximum Transmission Frequencies at 1.0 km	38
2.2	Comparison of Element Values	48
3.1	Perpendicular-Wind Statistics	93
3.2	Parallel-Wind Statistics	93

ACKNOWLEDGEMENTS

The author is grateful to his supervisor, Dr. L. F. Turner, for his assistance throughout the course of this research. Special thanks is due to all colleagues who came out to Staines reservoir in 1974, and especially to Alex Lax, William Edmondson and Bill Hodgkiss for their help in many of the circuit design problems.

The author wishes to extend his gratitude for the financial support of both the Athlone Fellowship Committee, London, and the National Research Council of Canada. The authorities of the Admiralty Research Laboratory, Teddington, are also gratefully acknowledged for allowing the use of their facilities at the King George VI reservoir, Staines.

To Ann and Bijou

CHAPTER ONE

INTRODUCTION

1.1 Historical Introduction

Man's interest in using the underwater medium as a means of communication can be traced back to Leonardo da Vinci. Leonardo used a simple form of passive (listening) sonar in an attempt to detect the movement of ships. He inserted a hollow tube partially into the water and, by listening at the other end, was able to detect a distant ship. Passive sonar is now much more sophisticated, but the basic principle, as discovered by Leonardo da Vinci, has changed very little.

Since the First World War, during which time a simple active sonar device known as ASDIC was developed, considerable advances have been made in both passive and active (echo-ranging) sonars. The use of such sonars has spread quickly from pure military applications to both civilian and industrial applications. More recently, off-shore oil exploration and geological mapping of the ocean floor have led to the development of very complex active sonar devices. For example, a high-resolution side-scanning sonar system has been developed by the Institute of Oceanographic Sciences (McCartney, 1975) for the purpose of topographical mapping of the ocean floor, and a sophisticated fish detection and fish density analysis system, based on the electronic sector-scanning sonar (Welsby and Dunn, 1963) has been implemented by the Ministry of Agriculture, Fisheries, and Food (Mitson, 1975).

One of the problems of sonar systems is the erroneous detection of targets. In an active sonar system, a target may be incorrectly identified with respect to range, bearing or target strength. This incorrect identification of sonar targets is obviously undesirable and a detailed and extensive investigation of the effects which can

cause errors in the detection of targets is very important.

There are three main effects which can cause the incorrect detection of sonar targets. The first main source of error is background noise. Background noise effects are most severe when echo-ranging and passive sonars are used to detect targets at very long ranges and when the signal-to-noise ratio at the receiver is low. The background noise in the medium can be divided into three main types - noise due to the thermal activity of the water molecules (thermal noise); noise due to the movement of waves on the water surface (wind noise); and additional noise such as man-made noise (ship noise) and noise caused by sea creatures, etc. An illustration of the variation of noise power, as a function of frequency, is shown in FIGURE 1.1 (Kinsler and Frey, 1962). From the figure, it can be seen that at low frequencies (i.e. less than 50 kHz), the background noise is dominated by wave noise, shipping noise and noise from sea creatures, whereas at high frequencies (i.e. greater than 100 kHz), the background noise is almost entirely thermal in nature.

Since wave noise, sea creature noise and shipping noise are unpredictable and span a wide range of noise levels and frequencies, it would seem sensible to operate sonars at high frequencies where the background noise is thermal and statistically predictable. However, this is not the case since high-frequency sonar waves suffer high attenuation (see Chapter 2) and this limits the effective range. Typically, ranges would be limited to a few hundred metres.

A second major source of error in sonar systems is reverberation. As a propagating sonar wave diverges, it may be reflected from either the surface and the bottom boundaries of the water medium, or it may be reflected several times from the two boundaries. These reflected

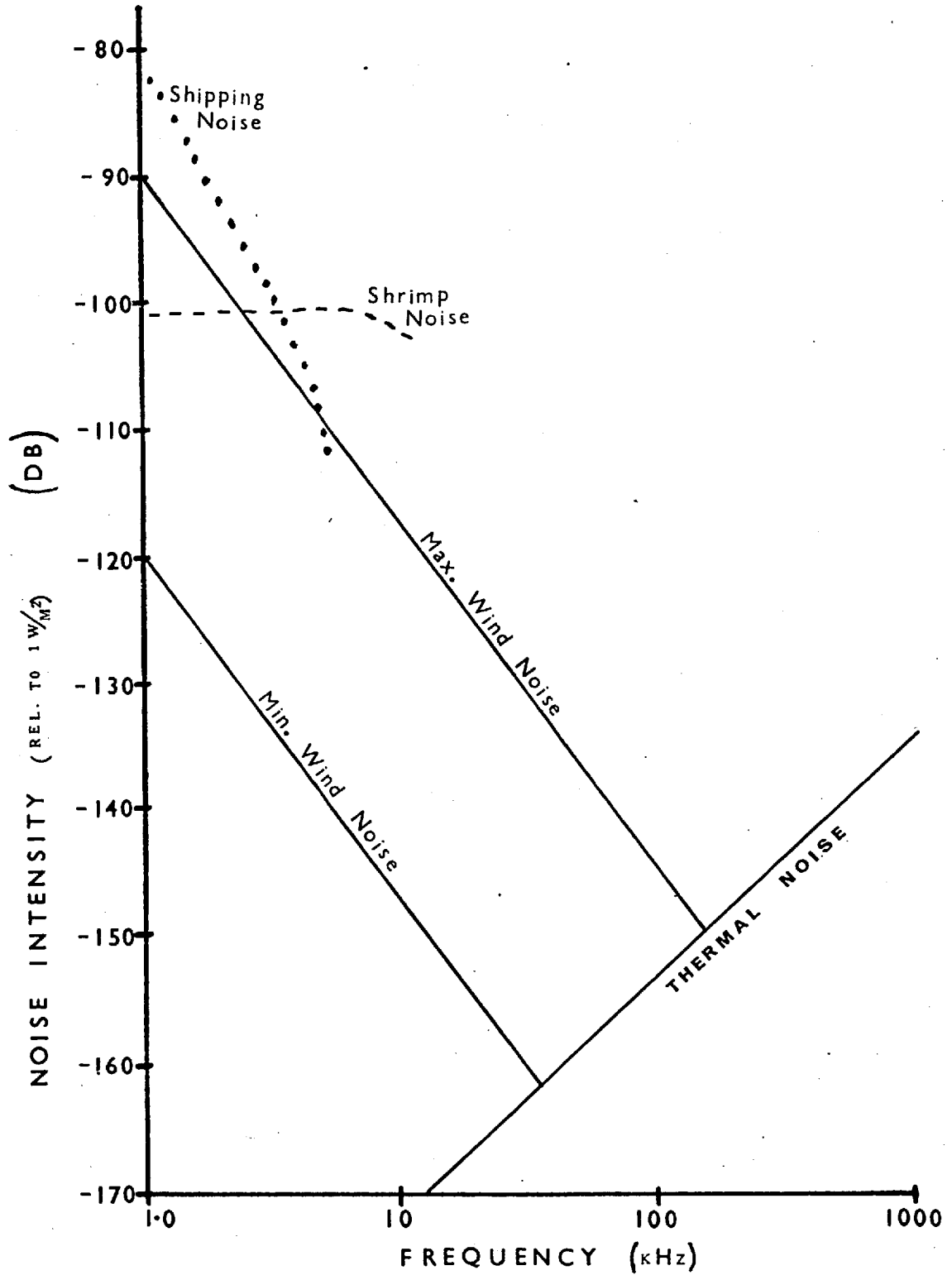


FIGURE 1.1 Typical Noise Intensities as a Function of Frequency

versions, which are known as multipath signals, arrive at the receiver and can result in serious detection errors since the direct-path target signal may be 'masked' by the reflected versions. For a fixed water depth, reverberations increase with increasing range, and can result in poor performance in the case of long-range sonars.

The third source of error in sonar systems arises from thermal inhomogeneities in the medium. These inhomogeneities cause small changes in the refractive index of the water and this results in both amplitude and phase pertubations of the propagating wave-front. It has been shown theoretically (Bergmann, 1946; Lieberman, 1951; Mintzer, 1953; and Chernov, 1967), that the fluctuations are both range and frequency dependent. Experimental investigations into the effects of the thermal inhomogeneities on the amplitude and phase of a propagating acoustic wave have been carried out (Stone and Mintzer, 1962; Campanella and Favret, 1969; and Sagar, 1973) and have provided confirmation of the theoretical models proposed by Bergmann and others.

As well as causing errors in the detection of sonar targets, the three main sources of signal pertubation also have a detrimental effect on underwater communication systems, such as telemetry and digital data links. When digital information is transmitted, the signal pertubations can cause an increase in the bit-error probability and limit the rate at which digital data can be communicated if a prescribed maximum error probability is not to be exceeded. Thus, in order to improve both sonar and underwater communication systems, steps need to be taken to reduce the effects of signal pertubations. In order to reduce the effects of the signal fluctuations, and thereby improve system performance, it is necessary to have a deeper understanding of multipath interference and the other causes of signal fluctuations.

Although some work has been carried out on various aspects of CW signal amplitude fluctuations (i.e. MacKenzie, 1962), there is, at present, a lack of information relating specifically to data transmission. By obtaining more detailed information about pulse amplitude fluctuations, then it may be possible to implement techniques such as adaptive equalisation into underwater data transmission systems. If this was done, then errors in communication might be reduced. Also the rate at which digital information could be communicated might be increased with an improvement in reliability.

1.2 Survey of Underwater Data Transmission Systems

Until recently, there appears to have been little need to develop high data-rate underwater acoustic telemetry systems, but the recent extensive interest into the possibility of exploitation of the oceans for their natural resources has led to the development of many types of underwater data transmission systems. Berktay et al.(1968) gave an indication of the possible future requirements for acoustic telemetry systems in terms of the field of application, range, and data-rate. Since then the interest in these aspects of underwater communication has increased considerably. TABLE 1.1, which is taken from Berktay et al.(1968) provides some indication of the present requirements for underwater acoustic telemetry and data communication systems.

A particularly interesting, and difficult, application of underwater telemetry is to be found in the operation of systems on the continental shelf , where water depths are typically a few hundred metres. This type of situation can be considered as a shallow-water propagation path, and considerable effort has been devoted to this aspect of underwater data transmission. Off-shore oil exploration, and fish-trawling are two important areas for the possible application of

TABLE 1.1 Performance Requirements of Future Underwater Communication Systems

	TRAWL	OCEANOGRAPHY	SPEECH
Range (metres)	1000-2000	8000	500
Angle of Depression (degrees)	5-25	10-90	-90 to 0 to +90
Operational Sea State	6	6	3
Depth (metres)	up to 800	6000	100
Number of Channels	4 * 16-20 +	4	1-2
Information Rate/Channel (bits/sec)	2-20	2-100	2 kHz minimum bandwidth (analogue)
Overall Information Rate (bits/sec)	8-100	8-400	

* For commercial Fishing

\+ For Fisheries Research

underwater speech and data transmission systems. The constraint of shallow-water propagation introduces the effects of boundary reflections which result in multipath propagation and leads to a degradation in system performance.

Early telemetry systems did not, in general, incorporate specific designs to overcome signal degradation. A typical system is that described by Hearn (1966). This telemetry system was used in a fish-trawling application and was designed to transmit, from the trawl net to the trawler, information concerning the 'mouth-spread' of the net, the water temperature, the strain on the net, and the height of the top of the net from the bottom of the ocean. This information was time-multiplexed and transmitted to the trawler using a 40 kHz transducer. The system was used in the situation in which the water depth was approximately 500 metres and the total transmission path length was of the order of 1500 metres. The data-rate of the system was very slow, typically 60 data pulses per second, and the method for reducing multipath interference was to assume that the direct-path signal always preceded the multipath signals at the receiver. Triggering circuits in the decoding section of the receiver were based on the above assumption. Because of the low data-rate, sophisticated techniques for reducing multipath interference were not necessary, and automatic gain control (AGC) was not used.

A few years later, and with the same application in mind, Goddard (1970) and Nesbitt and Berktay (1971) developed two different telemetry systems for use in the fish trawling situation. Because the desired data-rate was much higher (2000 bits/sec) than in Hearn's system, techniques for reducing the effects of multipath interference were implemented. Goddard's system was based on a time-gating principle, in which data

was transmitted for a duration less than the difference in time between the arrival of the direct-path signal and the multipath signals. The transmission was then stopped until the multipath arrivals had ceased and then transmission was resumed. When using a carrier frequency of 104 kHz, a data-rate of approximately 2000 bits per second was achieved at a range of 300 metres. An automatic gain control system was built into the receiver to overcome signal fluctuations.

The system developed by Nesbitt and Berktay (1971) was based on an electronic tracking idea. Using the principle that the direct-path signal always precedes any of its multipath signals at the receiver*, the beam pattern of the receiving transducer was deflected in the direction of the direct-path signal. This provided an attenuation of the multipath signals by the use of the receiving directivity response. In the system, which operated at a carrier frequency of 89 kHz over a range of about 250 metres, an alignment sequence was transmitted every 100 msec in order to effect the tracking operation. No indication of the achieved, or desired data-rate was given in the paper.

A special, and very complicated, signalling format was used to reduce multipath interference effects in the system developed by Miller and Bohmann (1972). Thirty-two frequencies, in multiples of 68.4 Hz, centred at 7.0 kHz, were available to scramble the data bits. The choice of frequency was based on a coding procedure and the data-rate to be transmitted. Four parallel transmission channels, ranging from 17.5 kHz to 42 kHz were available and the already scrambled data bits were encoded into pairs and then transmitted using FSK techniques over the parallel channels. This complicated frequency diversity technique was used to transmit data at ranges up to 700 metres at a maximum data-rate of 1640 bits per second.

* The principle is not generally true but it is valid in many situations.

Another telemetry system, employing a time-gating principle similar to that used by Goddard (1970), has been described by Okerlund (1973). The system was tested at a range of 2000 metres, and data was transmitted for a time interval less than the difference in transmission time between the direct-path signal and the surface-reflected path signal. The transmission was then stopped and resumed after the multipath signals had ceased to exist at the receiver. The data-rate achieved was about 3100 bits per second using a bandwidth of nearly 20 kHz centred at a carrier frequency of 50 kHz.

The systems which have been described appear to have functioned well in the particular environments for which they were designed and tested, but they are likely to be less effective in a more general environment. For example, the time-gating principle, although very effective under certain conditions, does have some limitations. As the difference in transmission time between the direct-path signal and the surface-reflected path signal changes (resulting from a change in range or transducer depth), it becomes difficult to transmit data at a constant rate. This arises from the fact that the time allowed for the transmission of the data changes with changes in range or transducer depth, and in order to maintain a constant data-rate, a change in both the transmitter and receiver timing circuitry may be necessary. This might not be possible in practice, and if the difference in the propagation time between the direct-path and the surface-path becomes small enough, then the system bandwidth could limit the performance of the system. This particular problem can arise in the case of long-range transmission.

Although the idea of frequency diversity may, at first sight, seem to be an effective method for reducing multipath interference,

it also has a limitation. The movement of the water surface causes a Doppler frequency shift of a surface-reflected signal, and frequency shifts of the order of 0.2% of the carrier frequency could be expected under many conditions. At, say 100 kHz, this would mean a frequency shift of about 200 Hz. Thus, for the effective reduction of multipath interference using frequency diversity techniques with only one transmission frequency, quite large frequency shifts would be required in an FSK system. Also, as the data-rate is increased, the time diversity would decrease accordingly, thereby losing the advantages of the frequency diversity. The idea of using several parallel transmission frequencies is attractive, but involves a much more complicated, and costly, data transmission system.

There are also several other techniques which could be used to reduce multipath interference effects and thereby achieve high data-rates. One method, space diversity, offers an effective method of reducing the effects of multipath, but this method can involve the implementation of quite large and complex receivers. In the case of long-range shallow-water propagation, it may become difficult to distinguish the the direct-path from the multipaths in both time and space.

The use of matched filters to recover signals embedded in noise is a well-known technique in radar systems. Tests, using this technique, have been carried out in the underwater environment by Parvelescu and Clay (1965). However, since multipath interference is usually a time-varying phenomenon, matched filters are not often effective when operating in a multipath environment.

In order to optimise the implementation of an underwater data transmission system, many aspects relating to underwater data transmission need to be investigated. At present, little is known

about the manner in which data pulses fluctuate and how these fluctuations affect the data-rate. The time-varying nature of multipath interference has not been completely investigated nor have the achievable data-rates and the related error probabilities for a particular underwater environment and data transmission system. The purpose of this thesis is to investigate some of these problems and thereby provide a clearer understanding of some of the underlying factors which affect underwater data transmission.

1.3 Aims and Outline of the Thesis

The maximum information capacity of an underwater communication channel has been studied by Rowlands and Quinn (1967) using a simple approach, and a more detailed and complicated approach has been adopted by Marsh and Rowlands (1968). Although these theoretical investigations present an indication of the maximum data-rate which can be attained for a particular system bandwidth and signal-to-noise ratio, present-day data transmission systems do not appear to approach these theoretical limits.

Signal amplitude fluctuation is the main reason for the large difference between the maximum theoretical and the actual practical data-rates that have been achieved. These fluctuations originate from three main sources - multipath interference, thermal inhomogeneities, and background noise. The effect of signal amplitude fluctuations on a data transmission system is to increase the probability of detection error, which implies a subsequent limitation of the data-rate if communication is to be carried out with a maximum prescribed probability of bit-error.

Quantitative results relating to the effect of signal amplitude fluctuations on system performance have not been widely reported.

In particular, little has been reported on the effect of signal amplitude pertubations on the bit-error probability of an underwater data transmission system. There have, however, been several papers which have reported on some general aspects of underwater acoustic signal amplitude fluctuations.

A considerable body of literature exists on experimental investigations of signal amplitude fluctuations arising from thermal inhomogeneities (Stone and Mintzer, 1965; Campanella and Favret, 1969; and Sagar, 1973), and on signal amplitude and phase characteristics determined over long propagation paths using low-frequency CW transmissions (MacKenzie, 1962; Steinberg and Birdsall, 1966; Nichols and Young, 1968; and Stanford, 1974). Two other experimental works (Whitmarsh et al, 1957; and Whitmarsh, 1963) have reported on various aspects of signal amplitude fluctuations of both direct-path and surface-reflected path signals. In all the above-mentioned publications, little indication has been given as to the effect that the signal amplitude fluctuations have on the performance of data transmission, or sonar, systems.

The performance of a data transmission system can be evaluated in several ways. An important parameter used to evaluate the performance of a system is the bit-error probability. In order to predict theoretically the bit-error probability of a particular system, it is essential to have some knowledge of the probability density function (PDF) of the received signal amplitude. Some experimental investigations have been carried out to determine the signal PDF under a variety of propagation conditions. The results have indicated that the received signal PDF is quite variable (MacKenzie, 1962) and can range from Rayleigh and Gaussian distributions (MacKenzie, 1962) to a Rician

distribution (Goddard, 1970). The fact that the nature of the PDF is extremely variable and still relatively unknown, suggests that more work is needed on this important aspect. Although some work has been done to evaluate bit-error probabilities for a particular system (Abotteen et al, 1974), it is necessary to know some of the characteristics of the signal PDF in more detail. It is necessary that this be done if the effects of climatic and propagation conditions are to be adequately taken into account. In this way, it may be possible to develop a more detailed and specific model for use in the prediction of system performance.

With many of the above-mentioned ideas in mind, a general programme was undertaken to investigate several aspects relating underwater data transmission. Specifically, the variation in performance of a particular data transmission system was to be investigated. This would involve an analysis of the effect of a variation of both climatic and propagation conditions on the bit-error probability of the system. Other factors, such as data-rate, data-pulse width, and the receiver decision threshold, which might affect system performance, were also to be investigated. An additional factor to be studied was the variation in the signal amplitude characteristics under a variety of climatic and propagation conditions. This included the determination of the signal PDF and its related statistics. It was hoped that the information obtained would be useful as an aid to a more general understanding of the signal PDF, and as an aid in the development of more accurate prediction models.

A prototype underwater data transmission system was designed and tested. The system, which was based on the conventional amplitude-shift-keyed (ASK) method of data transmission, was intended to provide

some information about several aspects of underwater data transmission. The reasons for the choice of ASK modulation over other forms of modulation for the initial investigation can be summarised as follows:

1. with ASK, the demodulation process is simple and, at the start of the work, very little information was available relating to the problems of carrier extraction with systems operating in the water medium;
2. with ASK, the pulse response of the overall system is more easily understood and more easily interpretable because ASK modulation and demodulation are linear operations;
3. as the provision of digital speech facilities is a likely possible application of underwater data transmission, it seems reasonable to expect that such systems will have to operate close to the Nyquist transmission rate. Therefore, steps may need to be taken to eliminate the effect of intersymbol interference arising from pulse dispersion and multipath. One possible method of doing this would be to use adaptive equalisation techniques and these are much easier to apply to ASK systems than to PSK or FSK systems.

Because of the availability of only restricted range facilities (less than 1.0 km), the system was designed to operate as a low-power system, so that information relating to the limiting performance could be obtained. Automatic gain control circuits were not used in the prototype system since one of the main aims of the investigation was to obtain information about the amplitude fluctuations of the received signal.

In Chapter 2, a detailed description of the prototype ASK system is given. Attention is first drawn to the choice of an appropriate carrier frequency to use in the system, with specific reference to the

restricted range facilities and other important factors which would affect transmission. A description of all the components of the ASK system is given and in particular, the design, construction, and testing of the ultrasonic transducers are described. In the last part of Chapter 2, a description is given of the method of evaluating system performance. The testing procedure is explained, as are the techniques used in the analysis of the experimental data.

Chapter 3 is devoted to a consideration of the amplitude fluctuations of the received signal. A presentation and discussion of results relating to specific aspects of the amplitude fluctuations are given. Results of measured PDFs, signal spectra and signal autocorrelation functions are presented and interpreted with reference to some contemporary theories. Using the experimental results presented in the chapter, two models of the signal PDF are proposed, based on climatic conditions.

The presentation and discussion of results of tests relating to the bit-error probability of the ASK system are given in Chapter 4. The results are classified into two main categories in order to interpret the performance of the system more easily. Using the PDF models derived in Chapter 3, bit-error probabilities are predicted and the results of the prediction are compared with experimentally measured error probabilities. A derivation of the optimum fixed detection threshold level is made from a consideration of the PDF models proposed in Chapter 3. Values of the detection threshold level are computed for a range of signal-to-noise ratios.

The baseband pulse response of the system is considered in Chapter 5. Some provisional experimental results are presented and these are interpreted in terms of the propagation and climatic conditions under

which they were measured. The work presented in this chapter is only provisional and much remains to be done. A knowledge of the pulse response, and the way in which it varies with time, is important in any consideration relating to high-rate data transmission, and in any possible application of techniques such as adaptive equalisation.

In Chapter 6, a summary of the work presented in the thesis is given, and some general conclusions are drawn based on the results of the investigation. Also, some suggestions for further research are made.

CHAPTER TWO

DESCRIPTION OF THE PROTOTYPE ASK DATA TRANSMISSION SYSTEM AND DISCUSSION OF EXPERIMENTAL PROCEDURES

Introduction

In the first part of this chapter, some of the factors which affect underwater acoustic propagation are considered. These factors are then used to determine a suitable carrier frequency for an ASK system for use at transmission ranges up to 1.0 km. A complete description of the ASK data transmission system is given. In the last part of the chapter, an outline of the procedures used in the testing of the system is provided and a description of the techniques used in the analysis of the test data is presented.

2.1 Factors Affecting Underwater Acoustic Propagation

In this section of the chapter, some of the factors which affect acoustic propagation are considered briefly. By making several, rather general, assumptions about these factors, an upper limit for a suitable carrier frequency is determined as a function of the desired receiver signal-to-noise ratio.

2.1.1 Spreading Loss

One of the fundamental losses encountered in underwater acoustic propagation is the loss due to the divergence of the acoustic wavefront as it propagates through the medium. In an unbounded medium, this geometrical spreading is spherical, but in the case in which boundary reflections are present, the spreading tends toward a cylindrical divergence (see Tucker and Gazey, 1966). The spreading loss (SPL), expressed in decibels, is

$$SPL = 10n\log_{10}(r) \quad \text{(relative to 1 metre)} \quad \ldots\ldots (2.1)$$

where r = range in metres, and

n = 1 ; for cylindrical spreading

= 2 ; for spherical spreading

2.1.2 Absorption Loss

On account of its non-ideal nature, the water medium absorbs acoustic energy. The absorption losses of a propagating acoustic signal are associated with effects such as viscosity, thermal conduction and, in the case of sea-water, relaxation phenomena. For fresh-water, at 15°C, the absorption coefficient due to these effects is, (Kinsler and Frey,1962),

$$a_1 = (2.4 \times 10^{-7}) f^2 \quad \text{dB/metre} \qquad \ldots\ldots (2.2)$$

where f is the transmission frequency in kHz.

For sea-water, at 15°C, the absorption coefficient is, (Kinsler and Frey,1962),

$$a_2 = a_1 + \frac{0.036 f^2}{f^2 + 3600} \quad \text{dB/metre} \qquad \ldots\ldots (2.3)$$

The second term in equation (2.3) takes account of the increase in acoustic absorption of sea-water at 60 kHz due to the dissociation of dissolved magnesium sulphate. The manner with which the attenuation coefficients, a_1 and a_2, vary as a function of frequency, is shown in FIGURE 2.1. The absorption loss, AL, in terms of the absorption coefficients and the transmission range, is therefore,

$$AL = a_i r \quad \text{dB} \qquad \ldots\ldots (2.4)$$

where i = 1 or 2, depending on whether propagation is in fresh-water or sea-water, and r is the transmission range in metres.

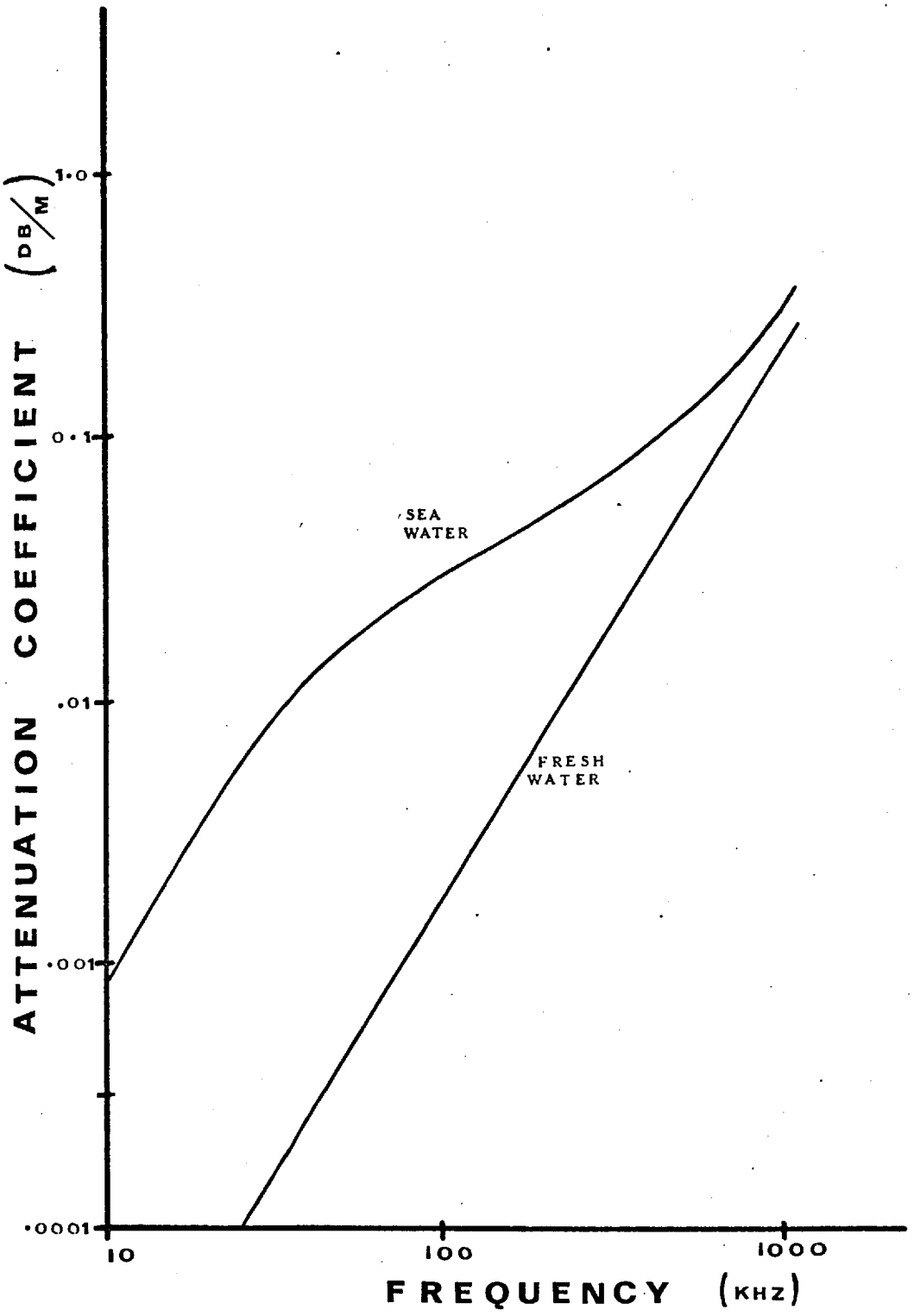


FIGURE 2.1 Fresh-Water and Sea-Water Attenuation Coefficients as a Function of Frequency

2.1.3 Source Level and Transducer Gain

The source level, SL, is expressed in terms of the radiated acoustic power and the gain due to the directivity of the transmitting transducer.

The acoustic intensity of an omnidirectional source is

$$SI = 10\log_{10}\left(\frac{W_r}{4\pi}\right)$$

$$= -11 + 10\log_{10}W_r \quad \text{dB (relative to 1 Watt/m}^2\text{)}$$

(referred to 1 metre) ..... (2.5)

where W_r is the radiated source power in Watts.

To obtain an expression for the source level, SL, for a given source intensity, SI , an additional gain factor has to be included on account of the directivity of the transducer. This gain factor (SD), which is a function of the directivity index of the transducer, is given by,

$$SD = 10\log_{10}\left(\frac{4\pi A_s}{\lambda^2}\right) \quad \text{dB} \qquad \ldots\ldots (2.6)$$

where A_s = area of the transmitting transducer and,

λ = acoustic wavelength of the transmission frequency in the medium.

On including this directivity factor, the source level, SL, of the transmitter is seen to be,

$$SL = SI + SD \quad \text{dB (relative to 1 W/m}^2\text{)} \qquad \ldots\ldots (2.7)$$

Similarly, the receiver has a gain factor (RD) associated with its directivity. This factor is,

$$RD = 10\log_{10}\left(\frac{4\pi A_r}{\lambda^2}\right) \quad \text{dB} \qquad \ldots\ldots (2.8)$$

where A_r is the area of the receiving transducer.

2.1.4 Ambient Noise

In general, the noise generated by the medium is due mainly to the thermal activity of the water molecules and wave motion. The thermal and wave noise powers are approximately proportional to the square of the transmission frequency (Urick, 1967).

The total ambient noise power (AN) can be related to the system bandwidth in the following manner:

$$AN = \int_{f_c - \varepsilon/2}^{f_c + \varepsilon/2} a_n f^2 \, df \qquad \ldots\ldots (2.9)$$

where ε = bandwidth of the system

a_n = constant

and f_c = carrier frequency of the system

If the bandwidth, ε, is much less than the carrier frequency, f_c, then it follows that,

$$AN \doteq a_n f_c^2 \varepsilon \qquad \ldots\ldots (2.10)$$

The noise level, NL, expressed in decibels, can be determined from the noise power, AN, by taking the logarithm of equation (2.10). If this is done, then,

$$NL = k + 10\log_{10}\varepsilon \qquad \ldots\ldots (2.11)$$

where k is a function of the centre, or carrier frequency f_c, and the constant, a_n. This factor has been computed and is shown as a function of frequency in Chapter One (FIGURE 1.1).

2.1.5 Other Factors Affecting Transmission

In addition to the loss of signal power due to spreading and absorption, there are other potential sources which may affect the received signal level. One of these sources is the presence of thermal inhomogeneities within the medium. These inhomogeneities cause a change in the refractive index of the medium and this results in pertubations of the wavefront of the propagating signal. The wavefront pertubations appear as amplitude and phase fluctuations of the received signal.

It has been shown (Chernov, 1967) that the fluctuations of the signal resulting from the thermal inhomogeneities are both range and frequency dependent and it is instructive to investigate, for a particular range, the effects that the fluctuations have over a band of frequencies.

The general fluctuation theory presented by Chernov can be divided into two cases which are based on near-field and far-field approximations. For the ranges and frequencies of interest for the data transmission tests, the special case of the far-field theory (Fraunhofer diffraction) can be applied. This has been done, for a range of 1.0 kilometre, and typical values obtained for amplitude fluctuations are shown, as a function of frequency, in FIGURE 2.2. The two curves shown in the figure correspond to two particular values of the product of the mean-square fluctuation of the refractive index and the spacial correlation distance, which have been experimentally obtained by Sagar (1960).

Another possible source of signal degradation is the effect of the amplifiers in the receiver. Because the signal levels at the input to the receiver amplifiers are expected to be in the μvolt range, it is possible that the noise generated by the amplifiers may cause a reduction in the received signal-to-noise ratio of up to 6 dB.

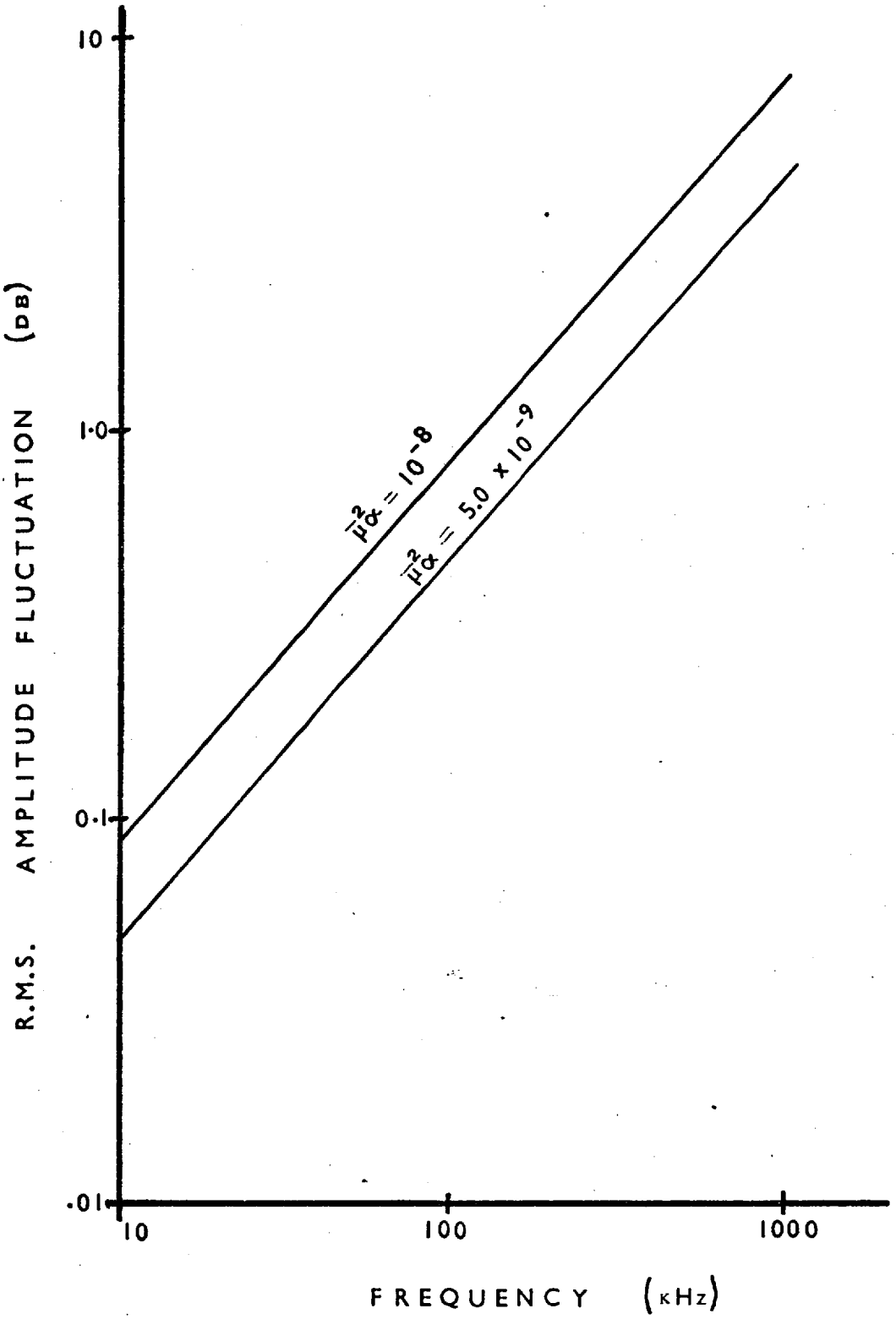


FIGURE 2.2 R.M.S. Amplitude Fluctuation Due to Thermal Inhomogeneities

2.1.6 Derivation of the Maximum Transmission Frequency

By considering and taking account of the factors discussed above, it is possible to estimate, for a desired signal-to-noise ratio at the receiver, the maximum frequency which could be used for communicating over a maximum range of, say, 1.0 kilometre. If a 'worst-case' approach is adopted, then it is possible to provide a conservative estimate of the transmission frequency. With the test site considerations in mind, a worst-case analysis was in fact carried out for the situation in which the desired range of communication was set at 1.0 kilometre. In the analysis, the following assumptions and estimates of the system parameters were made:

a) Spreading in the medium was assumed to be spherical.

b) A low transmitter power of 50 milli-Watts to be used.

c) The system bandwidth to be 10.0 kHz.

d) The directivity of the transducers will result in signal level gains of 3 dB.

e) The ambient noise level is -120 dB relative to 1 Watt/m^2.

f) Fresh-water absorption applies.

g) The transmitting and receiving transducers are identical.

h) Signal level fluctuations due to thermal inhomogeneities will be of the order of 9 dB.

i) The receiver amplifiers result in a signal-to-noise ratio degradation of 6 dB. (very pessimistic estimate)

Under the above assumptions, the maximum usable frequency, as a function of the desired signal-to-noise ratio at the receiver, can be computed by determining the maximum frequency for which the equation,

$$SL + RD - SPL - AL - NL - 9 - 6 = SNR \qquad \ldots\ldots (2.12)$$

is satisfied. In Equation (2.12), SNR is the desired signal-to-noise

ratio at the detector.

If this is done, then the results are as shown in TABLE 2.1. The frequencies in the table are the estimated maximum transmission frequencies which could be used at a range of 1.0 kilometre for the indicated signal-to-noise ratios. It is important to note that the values obtained provide a conservative indication of the possible transmission frequencies because of the 'worst-case' approach used in the analysis.

TABLE 2.1

Estimation of Maximum Transmission Frequncies at 1.0 km.

SNR	MAXIMUM FREQUENCY
20 dB	60 kHz
10 dB	220 kHz
0 dB	280 kHz

2.2 The Test Site

The tests were carried out at the King George VI reservoir at Staines and the facilities were made available by the Admiralty Research Laboratory (ARL), Teddington. The reservoir is approximately 1500 metres long and 600 metres wide and its depth varied from 16 metres during the period from mid-June to mid-September, to 13 metres from mid-September to November. The ARL raft at the reservoir provided electrical power facilities and test ranges of 150, 200 and 650 metres. A diagram of the basic dimensions of the test site is shown in FIGURE 2.3.

In order to centralise the majority of the test equipment and thereby simplify experimentation, a feedback cable link was established, for each test range, between the ARL raft and the receiver. In this way, both the transmitted and received signals could be observed together.

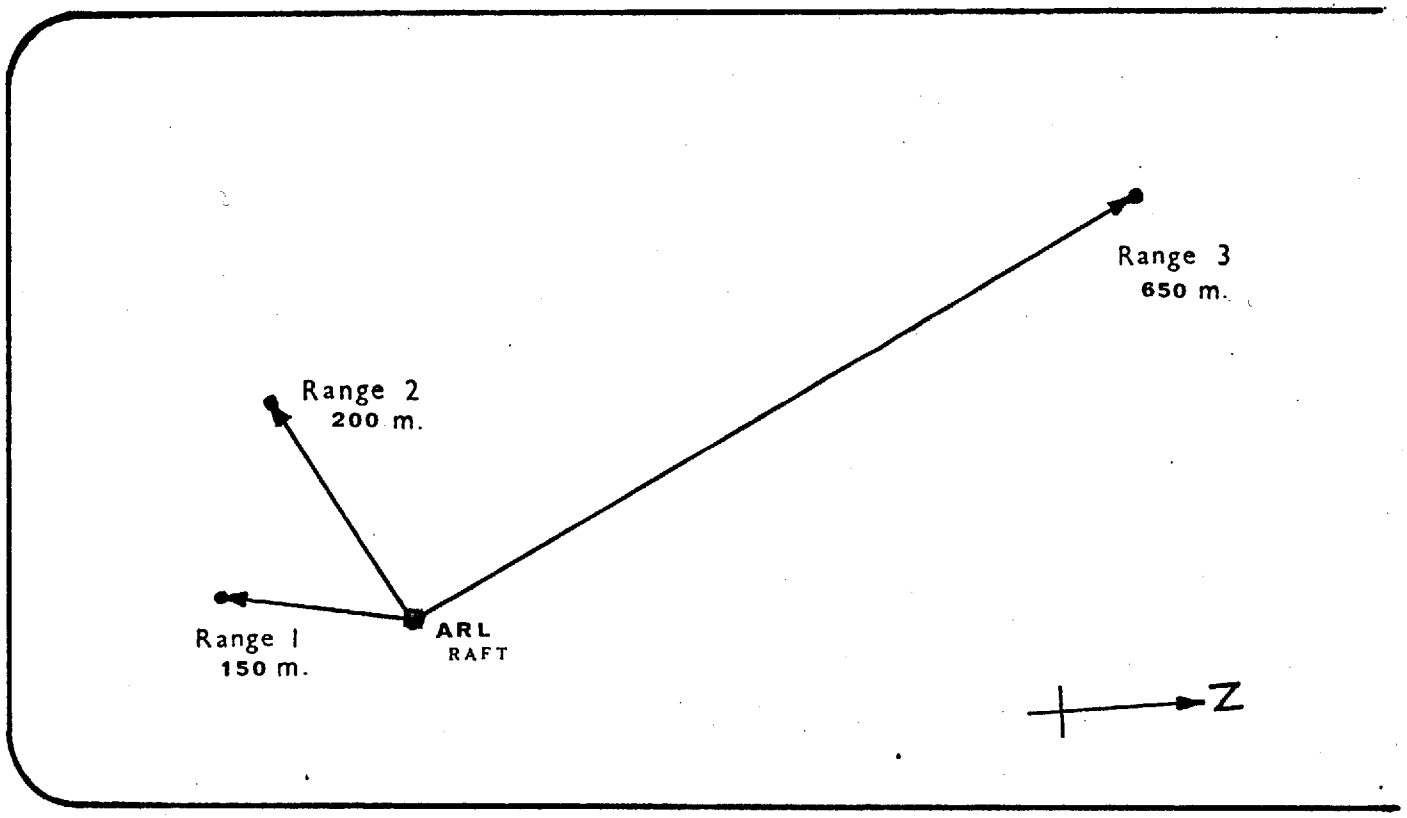


FIGURE 2.3 Test Site Dimensions

2.3 ASK Data Transmission System

2.3.1 Transducers

There were two main reasons for the final choice of the transmission frequency to be used in the ASK system. Firstly, as was shown in Section 2.1.6, the choice depends on the desired signal-to-noise ratio at the receiver. From TABLE 2.1 it can be seen that frequencies varying from 60 kHz to 280 kHz would be suitable at a range of 1.0 kilometre. As the maximum range at the test site was limited to 650 metres, it might be thought that frequencies somewhat in excess of those given in TABLE 2.1 would be most suitable. For example, as the maximum range is 650 metres, this indicates that a transmission frequency of the order of 250 kHz would be suitable and that this would still allow for unpredicted losses and would still provide a sufficiently large signal-to-noise ratio at the receiver. However, a brief investigation into the availability of transducers with resonant frequencies of approximately 250 kHz revealed that transducers of this type were not readily available and could not be constructed from available parts. For this reason, it was decided to construct transducers using easily available electro-acoustic crystal elements.

The particular crystal which was selected was a PZT-5A thickness vibrating ceramic disc, resonant in the thickness mode at 150 kHz. This crystal was readily available and inexpensive. Although the resonant frequency of this particular crystal was somewhat below the intended frequency of 250 kHz, the crystal provided some desirable properties for the transducer beam pattern.

It is possible to reduce the effects of multipath interference by using directional transducers. For example, a transducer which has a narrow vertical response and a wide horizontal response can reduce the effects of multipath interference arising from both surface and

bottom reflections. One of the aims of the experimental investigation was to study the effects of multipath interference on the received signal. Thus, by using a circular disc which has a symmetrical directivity response about an axis perpendicular to the face of the disc, multipath effects could be studied more easily. Another advantage of the PZT-5A type of crystal is that, unlike many other types of lead-zirconate-titanate compounds, the 5A-type material has a low mechanical Q-factor. This means that quite large bandwidths can be obtained.

The diameter of the crystal is 31 mm, or approximately three times the acoustic wavelength of 150 kHz sound in water. The corresponding area of the crystal face results in a transducer gain of $10 \log_{10}\left[\frac{4\pi^2(3.1)^2\lambda^2}{4\lambda^2}\right]$ dB = 19.7 dB but the beamwidth is not very narrow. The directional response of the circular disc is given by (Tucker and Gazey, 1966), as,

$$D(x) = \frac{2J_1(x)}{x} \qquad \ldots\ldots (2.13)$$

where $J_1(x)$ = first Bessel function of x,

$x = \left(\frac{\pi d}{\lambda}\right) \sin\theta$,

λ = acoustic wavelength,

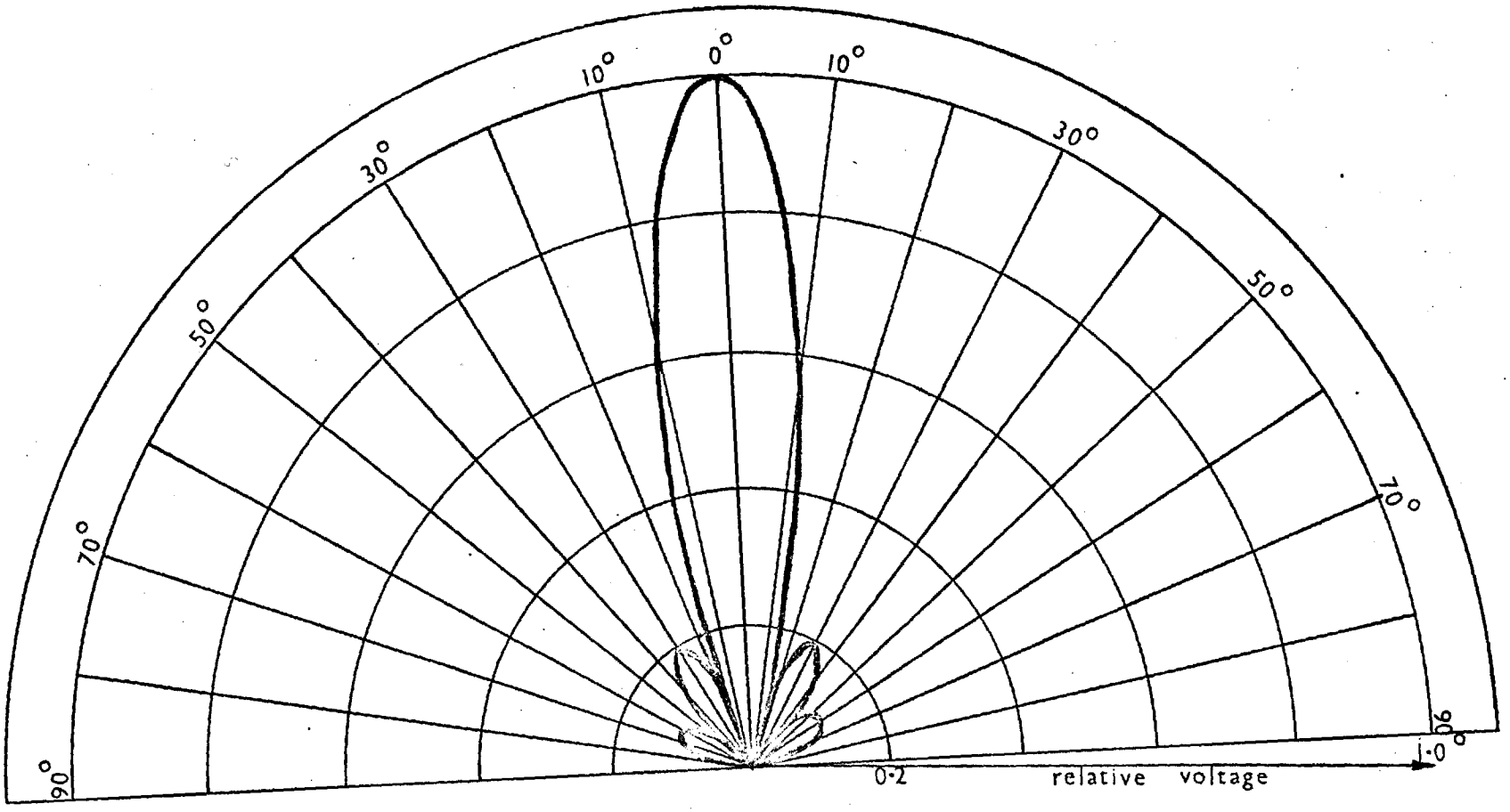
d = diameter of the disc ,

and θ = angle of observation.

Using the appropriate values in Equation (2.13), the beam pattern of the disc was calculated and is shown in FIGURE 2.4. The 3-dB beamwidth of the main-lobe is seen to be $\pm 8^\circ$ from the maximum response, and the first side-lobes occur at $\pm 30^\circ$ from the point of the maximum response. The computed intensity of these side-lobes is -14 dB relative to the maximum intensity.

In order to maximise the power radiated from the transducer, an aluminium casing was designed to load heavily one face of the crystal

FIGURE 2.4 Theoretical Beam Pattern of the 150 kHz Transducer



whilst allowing the other face to radiate freely the acoustic energy into the water. The aluminium casing was of a dimension such that it formed a quarter-wave transformer which provided a large mechanical load on the back face of the crystal. The mechanical load on the crystal face which radiates into the water is simply that of the water, while the load on the opposite crystal face is considerably larger. The loads, expressed in terms of acoustic impedances, on either side of the crystal are,

$$Z_{face\ 1} = Z_{water}$$
$$Z_{face\ 2} = \frac{Z^2_{aluminium}}{Z_{water}} \qquad \ldots\ldots (2.14)$$

The ratio of the acoustic impedances on either side of the crystal is approximately,

$$\frac{Z_{face\ 1}}{Z_{face\ 2}} = \frac{1}{125} \qquad \ldots\ldots (2.15)$$

From equation (2.15), it would be expected that less than 1% of the radiated acoustic energy would be 'back-radiated' into the water through the aluminium casing. A full-scale drawing of the encapsulated PZT-5A crystal is shown in FIGURE 2.5.

The experimental measurement of both the directional response and the electrical equivalent circuit of each of the transducers was performed under somewhat restrictive conditions. A large concrete and glass water tank of dimensions 5.25m x 2.7m x 2.6m was used, and in order to reduce reflections from the bottom and sides of the tank, it was necessary to line some parts of the inside of the tank with acoustic absorbing material. A measured directivity pattern of one of

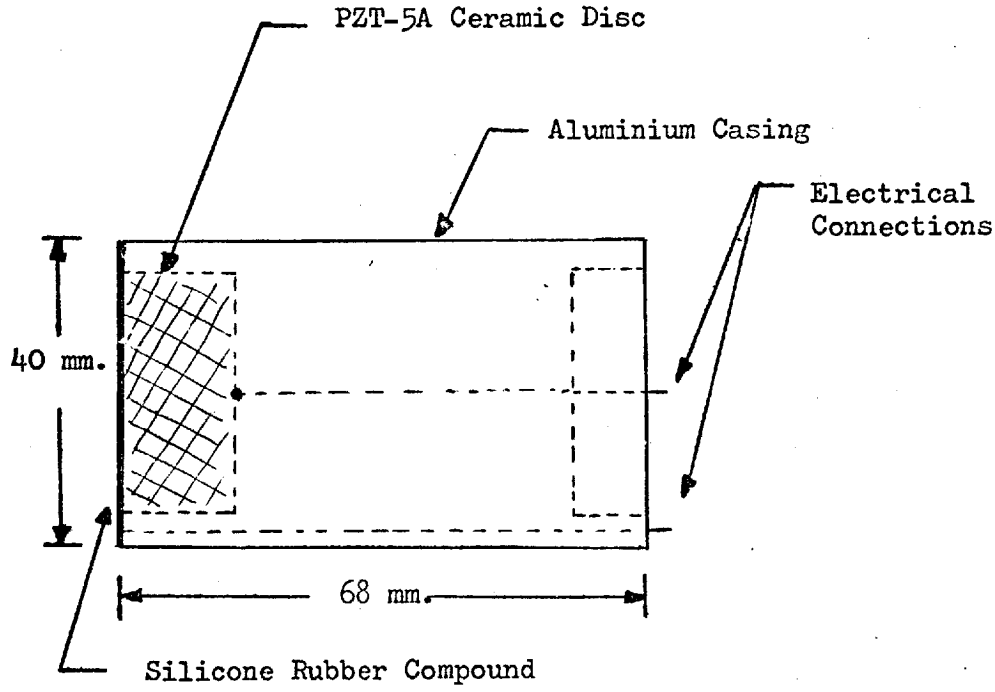


FIGURE 2.5 Cross-Section of 150 kHz Transducer

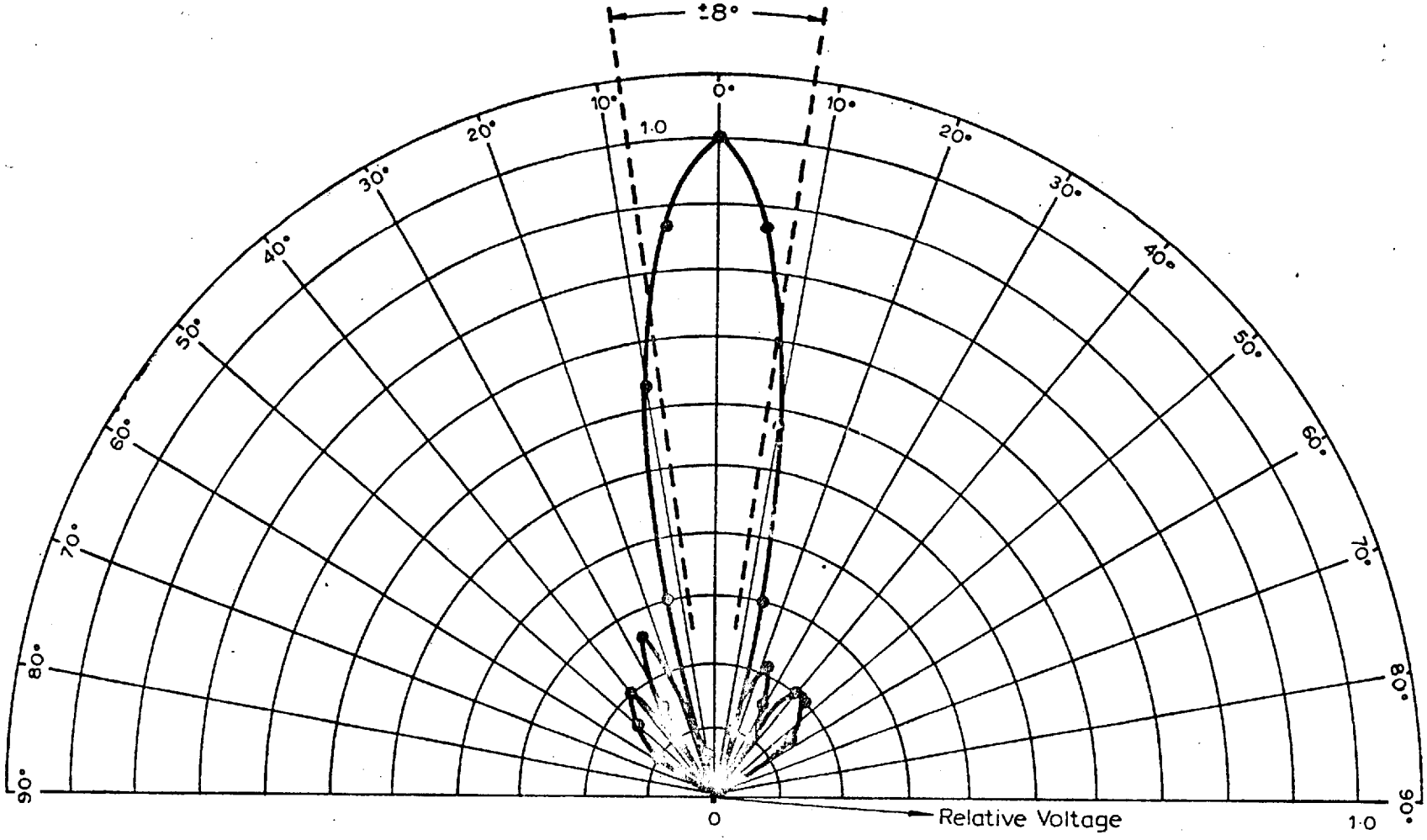
the transducers is shown in FIGURE 2.6. On comparing the measured response shown in FIGURE 2.6 with the theoretical response given in FIGURE 2.4, it is seen that there is considerable agreement between the two. In particular, there is excellent agreement with respect to the value of the 3-dB beamwidth of the main-lobe of the response. The measured value of 16° is identical to the predicted value. Also, the intensity of the first side-lobes with respect to the main-lobe was measured to have values of between -12 dB and -14 dB, which compare well with the theoretical value of -14 dB. There is, however, a discrepency between the theoretical and practical values for the angle between the maximum responses of the main-lobe and the first side-lobe. The measured value of the angle was found to be $\pm 23^{\circ}$, whereas the theoretical value is $\pm 30^{\circ}$. The difference is probably due to two main causes.

A first possible cause of the discrepency between the measured and theoretical angle is that the acoustic absorption of the tank was not sufficient to prevent multipath interference effects from occurring in the tank. A second possibility is that the bond between the aluminium casing and the crystal was not uniform over the crystal face, which could affect the radiating properties of the transducer.

It is possible to obtain an electrical equivalent circuit for the transducer by considering both the piezoelectric properties and the physical dimensions of the crystal. Near to the main resonance of the crystal, the transducer can be modelled by the R-L-C type circuit shown in FIGURE 2.7. This particular form of the electrical equivalent circuit of the transducer was derived mathematically by Mason (1948).

The measurement of the admittance of the transducer over a band of frequencies near the mechanical resonance frequency makes it possible

FIGURE 2.6 Measured Directivity Pattern of the 150 kHz Transducer



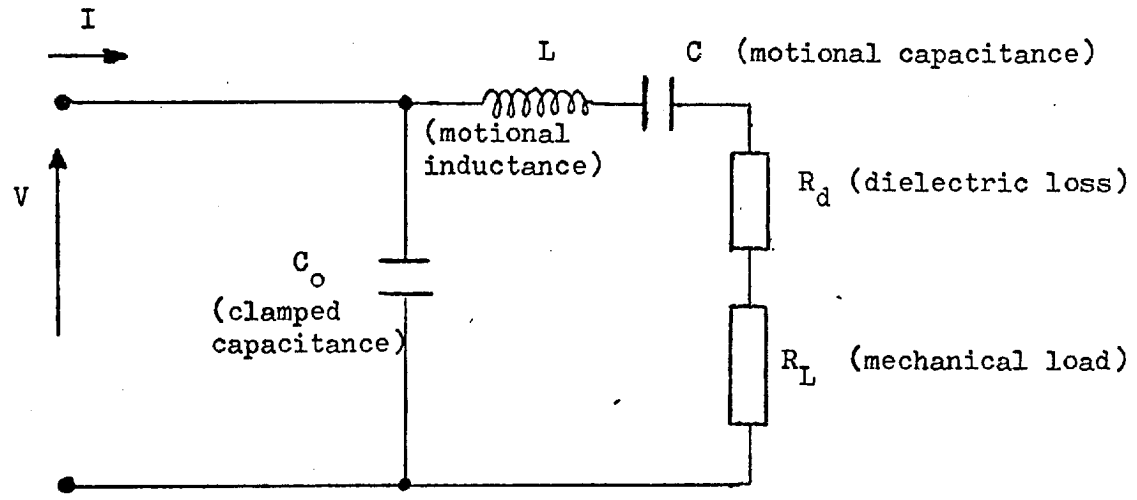


FIGURE 2.7 Electrical Equivalent Circuit Near Resonance

to determine values for the elements of the equivalent circuit. Using frequency as a variable, a circle can be traced out on susceptance and conductance coordinates. By computing two such circle diagrams, as shown in FIGURE 2.8, for the cases of an air load and a water load on the transducer, it is possible to compute values for the elements of the equivalent circuit. A comparison of theoretical and actual computed values from a consideration of the circle diagrams in FIGURE 2.8 is shown in TABLE 2.2, from which it can be seen that the computed and theoretical values are in good agreement.

TABLE 2.2

Comparison of Element Values

Element	Theoretical	Measured
C_o	500 pF	600 pF
R_d	------	570 Ω
L	25 mH	32 mH
C	30 pF	28 pF

The electro-acoustic efficiency of the transducer can also be computed from a consideration of the admittance circle diagrams (see Tucker and Gazey, 1966). A value of 48% has been calculated from the values of the circle diagrams shown in FIGURE 2.8. Another important parameter which can be calculated from a consideration of the circle diagrams is the bandwidth of the transducers. The information contained in the measured circle diagrams indicated that the transducers had a mechanical Q-factor of 22, which corresponds to a bandwidth of 6.5 kHz. Under measurement at the test site, however, the 3-dB bandwidth was determined to be 9.0 kHz, which indicated a Q of 16.5. No obvious

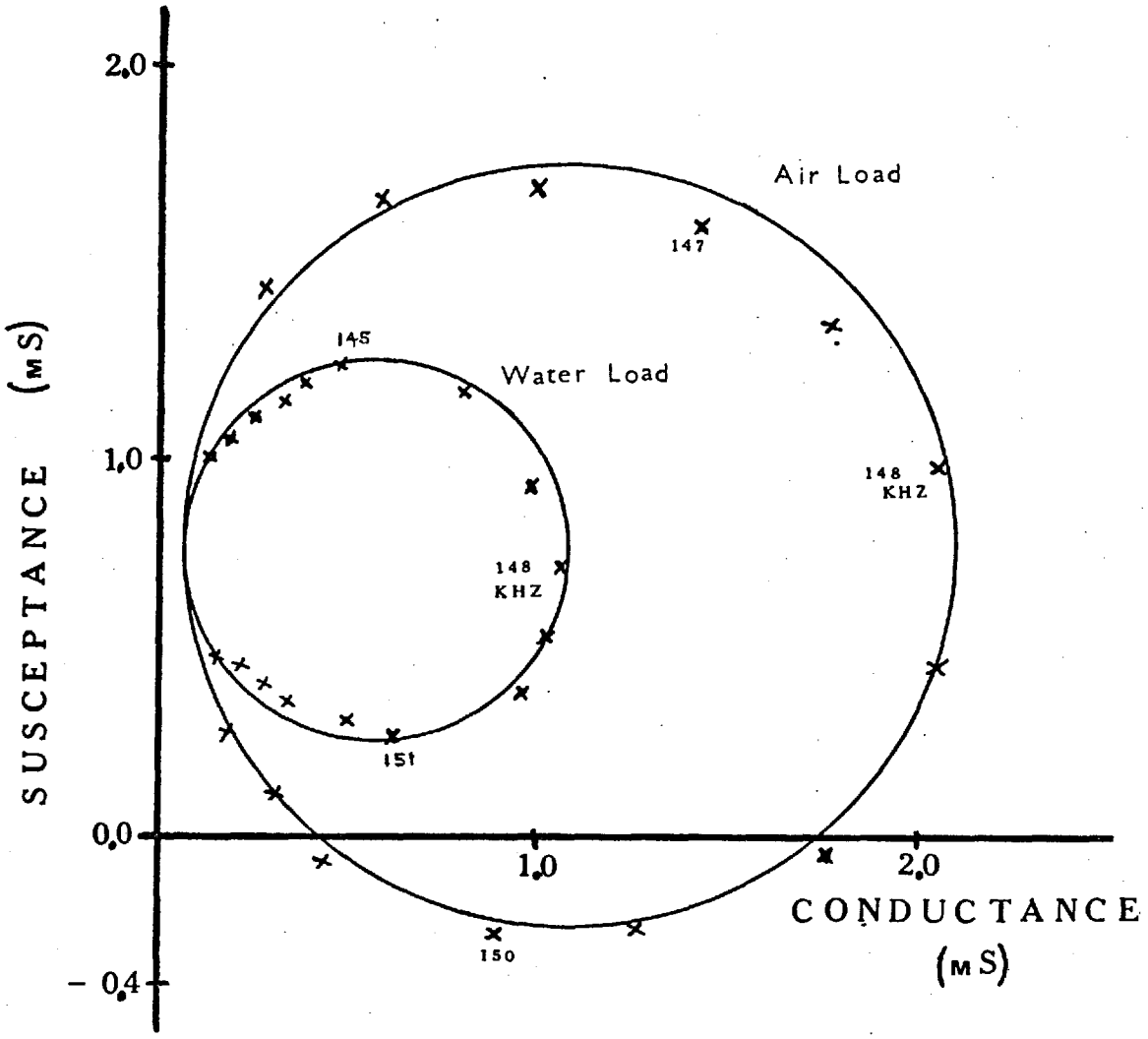


FIGURE 2.8 Measured Admittance Circle Diagrams

reason has been found which explains this discrepency.

Similar measurements to those described above were carried out on the two transducers and they were found to have similar electrical and directional properties. For example, the resonant frequencies of the two transducers were found to differ not more than 300 Hz.

2.3.2 Transmitter Details

A block diagram of the transmitter section of the prototype ASK data transmission system is shown in FIGURE 2.9. The data source consists of a pulse generator, a shaping filter unit, and a pseudo-random scrambler. The pulse generator and shaping filter unit (Andrews, Constantinides and Turner, 1974), produces raised-cosine pulses with 100% roll-off. The raised-cosine frequency spectrum of the pulses is given by,

$$H(\omega) = \tfrac{1}{2}\left[1 + \cos\left(\frac{\pi\omega}{2\omega_c}\right)\right] \quad ; \quad \text{for } |\omega| \leq 2\omega_c$$
$$= 0 \quad ; \quad \text{elsewhere} \qquad \ldots\ldots (2.16)$$

where $2\omega_c$ is the bandwidth of the pulse.

The pulse generator and shaping filter unit was designed to be capable of generating a variety of data-pulse widths and data-pulse sequences. The pulse widths which can be generated are 0.8, 1.0, 1.6, and 2.0 msec in duration. The unit is also capable of producing a large variety of repetitive 'on-off' pulse sequences and, by doing this, a large number of data-rates, ranging from less than 250 bits/second to 1250 bits/second can be generated. The pseudo-random (PR) scrambler can be either switched into operation or left out, as desired. The generation of the PR sequences is based on the time-gating of a

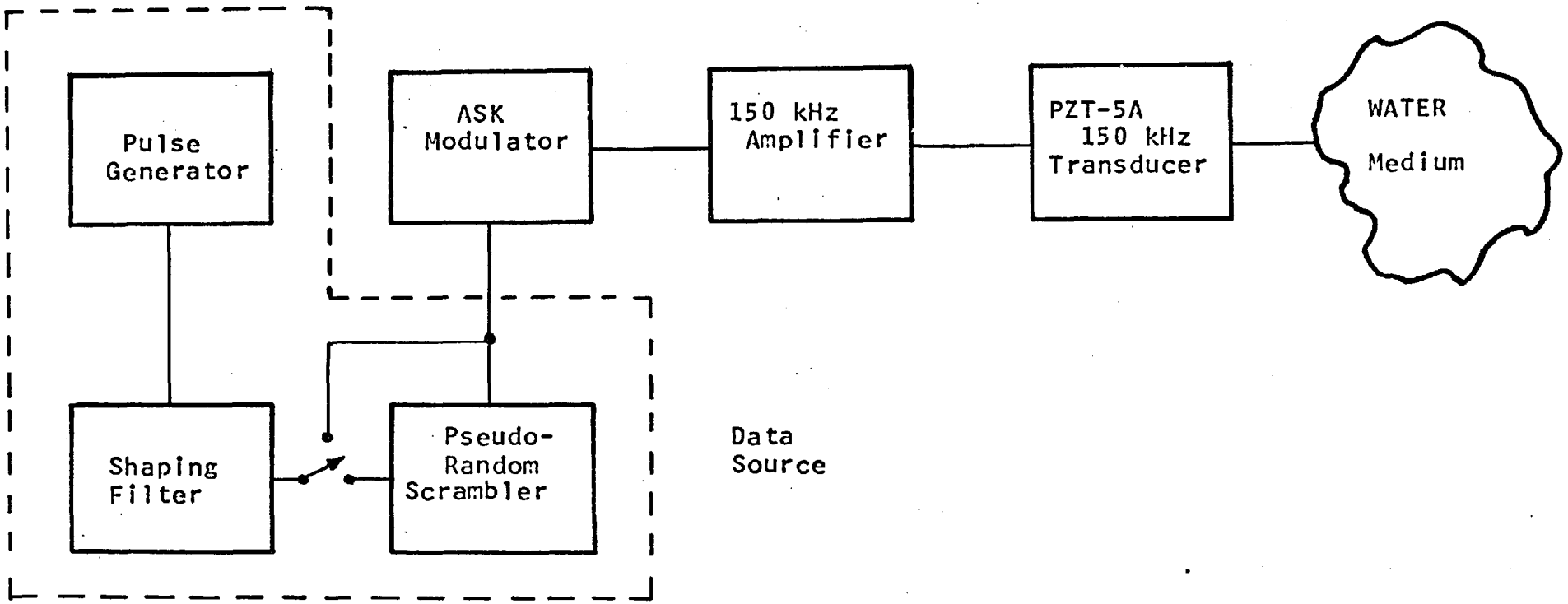


FIGURE 2.9 Block Diagram of Transmitter Section

continuous raised-cosine signal from the pulse generator unit, and the resulting output is a PR sequence, of length (2^7-1) bits, of raised-cosine pulses.

The ASK modulator is a commercially available unit which has a variable depth-of-modulation facility. In the test system, a modulation depth of 95% is used (rather than 100% for true ASK operation), so that the simple and reliable demodulation scheme can be used in the receiver (see Section 2.3.3). The modulator is then connected to a variable-power amplifier which is used to drive the transmitting transducer. This amplifier is capable of producing a peak-to-peak voltage of 50 volts across the input terminals of the transmitting transducer. A simple matching network, consisting of a single inductor, was used to resonate with the static capacitance (C_o) of the transducer. The transmitting transducer has been described previously in Section 2.3.1.

2.3.3 Receiver Details

The receiver section of the ASK data transmission system is shown in block diagram form in FIGURE 2.10. The acoustic signals are received by the receiving transducer which is identical to the transmitting transducer. The electrical signals from the output of the transducer are then amplified by a line amplifier which is connected to an underwater cable linking the receiver and transmitter. The received signals were transmitted back to the ARL raft over this cable. The line amplifier, which is tuned to a centre frequency of 150 kHz with a pass-band of ± 4.5 kHz about the centre frequency, is capable of providing a maximum gain of 30 dB at the transmission frequency. By amplifying the signals prior to transmission over the underwater cable, it was possible to minimise effects such as cable noise and thereby prevent these effects from causing a significant reduction in the signal-to-noise ratio of

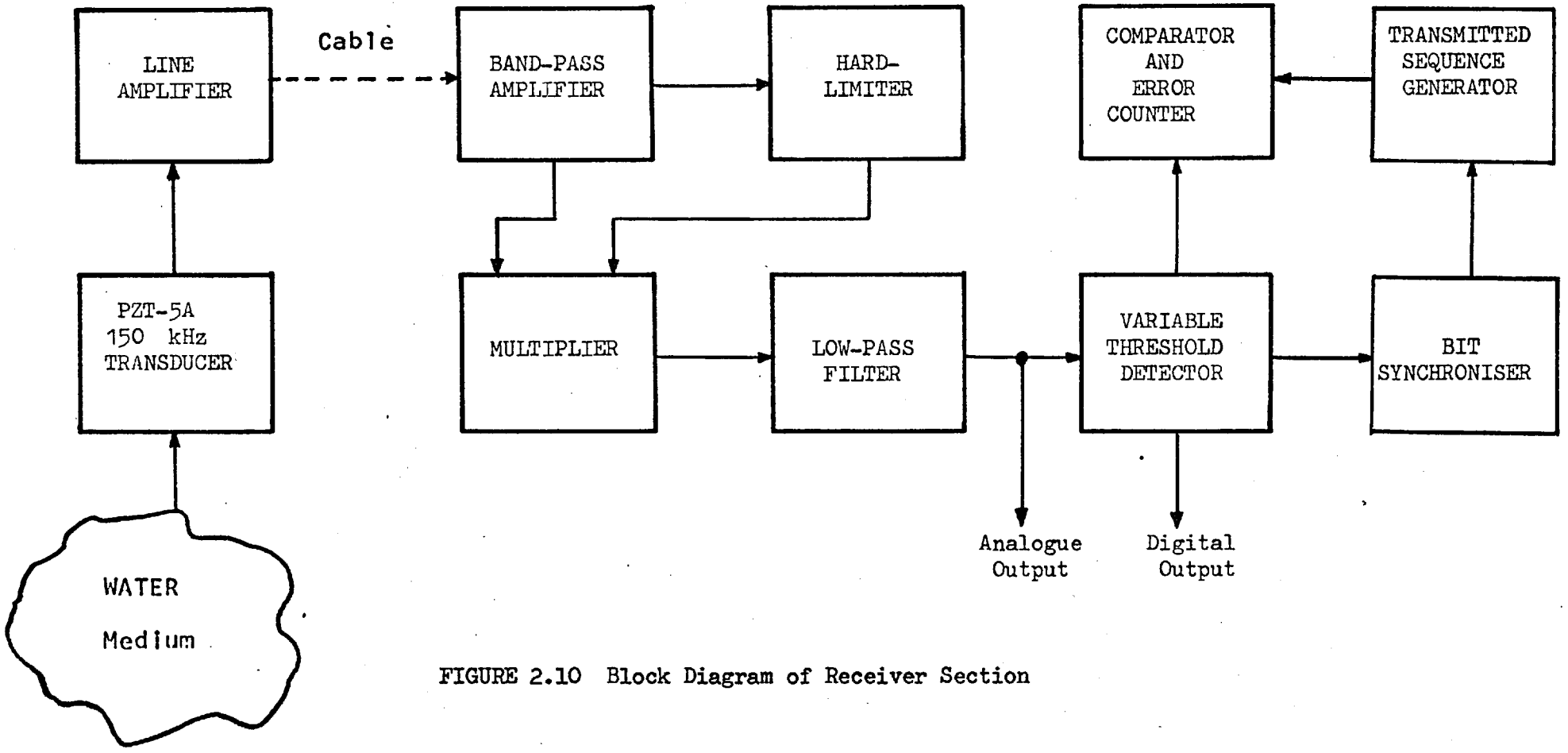


FIGURE 2.10 Block Diagram of Receiver Section

the signal during transmission from the receiving transducer to the ARL raft.

During the tests, the signal received at the ARL raft was amplified using a band-pass amplifier. This amplifier, which can provide a signal gain variable up to 80 dB, has a bandwidth of $\pm$ 4.5 kHz centred at the carrier frequency. The demodulation process, which may be considered as a pseudo-synchronous form of detection (Turner and Andrews, 1974), provides a simple and reliable form of ASK demodulation. The detection process consists of multiplying the band-pass version of the received ASK signal by a hard-limited version of the same signal. The hard-limited version is obtained by using a voltage comparator circuit which produces an output in proportion to the zero-crossings of the received signal. As mentioned previously, a 95% depth-of-modulation was used in the tests and this made it possible to use the pseudo-synchronous detection scheme. On account of the unwanted high-frequency components which are produced by this form of detection, it is necessary to low-pass filter the signal from the output of the detector. In the system, an active low-pass Butterworth filter with a 4.5 kHz cut-off frequency is used. It is important to note that the above detection scheme is the same as a full-wave rectifier detector with a low-pass filter and hence the system used in the ASK receiver operates as an envelope detector.

In order to perform tests capable of providing information about the effect of the decision threshold level on the bit-error probability of the ASK system, a variable threshold decision-making device was built into the receiver. The device is essentially a voltage comparator, which compares the incoming signal with a threshold voltage which can be altered easily.

Because of the relative movement of the transmitting and receiving transducers arising from the motion of the rafts on the reservoir, it was necessary to incorporate an adaptive timing circuit in the receiver.

It was necessary to do this in order to ensure that corresponding digits in transmitted and received sequences could be compared and a count of the number of errors arising from transmission thereby obtained. A bit-synchronising scheme, of the type described by Bennett and Davey (1965), was built into the receiver. The sychroniser extracts timing information from the incoming received bit-stream and uses this information to adjust the timing of a clock generator in the receiver. This clock generator is then used in the generation of a bit-sequence which is identical to the transmitted bit-sequence. By doing this, timing differences between the transmitted and received signals are overcome and a count of the number of errors detected in transmission can be made.

A count of the number of errors detected in transmission was carried out in the receiver. A sampling signal was generated from the receiver clock using a monostable multi-vibrator. The sampling signal, which is a 1.0 μsec duration pulse, is then used sample both the received and transmitted data streams in synchronism. By using a simple 'exclusive-OR' circuit and some additional logic, it was possible to compare the two data sequences and to produce a pulse signal whenever the two signals differed. Thus, the number of errors detected in transmission could be determined by simply counting the number of difference pulses. Both the number of errors and the number of transmitted data pulses were counted in order that information about the bit-error probability could be obtained.

2.4 Test Procedures

The experimental testing of the ASK data transmission system was divided into two groups. The first group of tests were carried out to provide information about the amplitude fluctuations of the received signal, and the second group of tests were carried out to provide

information about the bit-error probability of the system. During the course of the tests, detailed physical and climatic data were recorded at the reservoir. The recorded data included the measurements of bathythermographs (temperature-depth profiles), wind direction, air temperature, and approximate wave heights and speeds. In all the tests, both the transmitting and receiving transducers were located at a depth of six metres below the surface of the water.

2.4.1 Tests Relating to the Study of Signal Amplitude Fluctuations

The tests relating to the study of signal amplitude fluctuations were carried out over a period of approximately twelve weeks, from mid-June until mid-September, and were performed over transmission ranges of 150, 200, and 650 metres. In order to obtain information relating solely to the signal amplitude fluctuations, it is desirable, though not essential, to eliminate intersymbol interference effects that result from multipath propagation. It was found, after an initial investigation, that intersymbol interference effects were negligible if data pulses were transmitted at a rate of less than approximately 600 bits/second, and it was decided, therefore, that if data pulses were transmitted every 6.4 msec (or a rate of 156 bits/second), then intersymbol interference effects would be small. In the tests, two pulse widths of 0.8 and 1.6 msec were used. The pulses which were received at the ARL raft were demodulated and recorded on a wide-band FM tape recorder. Each test consisted of transmitting either a 1.6 or a 0.8 msec duration pulse with the pulses modulating a 150 kHz carrier signal. The duration of each test was approximately three minutes and the entire test was recorded on tape. Several tests were carried out at each range under a variety of climatic and propagation conditions. The peak signal-to-RMS noise ratio was also measured at each test range.

2.4.2 Tests Relating to the Study of Bit-Error Probabilities

As mentioned previously, there are three main sources of error in underwater data transmission systems - multipath interference, thermal inhomogeneities, and noise. The tests relating to the study of the bit-error probabilities were designed to provide information about the errors arising from these effects. In order to accomplish this objective, it was necessary to vary a number of system parameters and to investigate the effect of the variation on the bit-error probability.

The experimental investigation was carried out at all three test ranges over a period of five months beginning in mid-June 1974 and ending in mid-November 1974. By performing the tests over such an extensive period of time, any large changes in the prevailing climatic conditions could be covered fully in the experimental investigation and the results could be interpreted accordingly. In order to investigate the effects of the various sources of error, three test parameters were varied. The parameters varied were the data-rate, the data-pulse width, and the detection threshold level. By varying these three parameters, it was hoped that information relating to the way in which amplitude fluctuations affect the performance of the ASK system could be obtained. At each range, the following fixed test procedure was used:

1. A data signal was transmitted and the peak signal-to-RMS noise ratio was measured. By doing this, it was possible to set the detection threshold level as a fraction of the average peak signal amplitude.
2. A pulse width was selected.
3. A data-rate was then set for the particular data pulse width.
4. Data was then transmitted and the number of errors detected in transmission were counted. The total number of transmitted data pulses for each test was set at approximately 300,000. This

particular value was selected because a preliminary series of tests had shown that error-rates of between 10^{-2} and 10^{-4} frequently occurred. A value of approximately 300,000 was estimated to be sufficient to measure the short-term error probability accurately. The duration of each test varied from about four to twelve minutes, depending upon the data-rate.

5. A new data-rate was set and step 4 was repeated. In all, three data-rates were transmitted for each pulse width.
6. A new pulse width was selected and steps 3 to 5 were repeated.
7. The detection threshold level was changed and steps 2 to 6 were again carried out.

The above procedure was repeated many times at each test range over the five month test interval. In total, several hundred short-term tests were performed.

2.5 Data Analysis Techniques

2.5.1 Analysis of Tests Relating to the Study of Signal Amplitude Fluctuations

Three basic methods were used in the analysis of the tests relating to the study of signal amplitude fluctuations. The first method of analysis involved the computation of the probability density function (PDF) of the signal amplitude. The PDFs were determined by analysing the recorded data using a PDP-15 digital computer. The tape recordings of the demodulated pulses were played into the analogue-to-digital (A/D) converter of the computer and a programme was developed to sample the pulses at the appropriate instances in time. The programme was such that any number of samples could be taken and it was decided to carry out the analysis by considering two sample sizes of 400 and 4000 data pulses, which corresponded to respective time durations of 2.5 and 25 seconds.

By doing this, both the long-term and short-term fluctuations could be studied. In addition to computing the PDFs of the signal amplitude, a programme was also developed to perform a statistical analysis of each of the computed PDFs.

The statistics which were computed were based on the calculation of the various moments of the probability distributions. The values calculated were the mean (A), the standard deviation (δ), the coefficient of variation ($V = \delta/A$), the skew and the kurtosis of the distribution. These parameters were computed using the formulae,

$$A = \frac{1}{N}\sum_{i=1}^{N} x_i$$

$$\delta = \left[\frac{1}{N}\sum_{i=1}^{N} x_i^2 - A^2\right]^{1/2}$$

$$\text{skew} = \left[\frac{1}{N}\sum_{i=1}^{N} x_i^3 - \frac{3A}{N}\sum_{i=1}^{N} x_i^2 + 2A^3\right] \Big/ \delta^3 \qquad \ldots\ldots (2.17)$$

$$\text{kurtosis} = \left[\frac{1}{N}\sum_{i=1}^{N} x_i^4 - \frac{4A}{N}\sum_{i=1}^{N} x_i^3 + \frac{6A^3}{N}\sum_{i=1}^{N} x_i^2 - 3A^4\right] \Big/ \delta^4$$

where x_i = amplitude of i^{th} data sample

N = number of samples

These formulae are standard and have been used previously by MacKenzie (1962).

Two other parameters were determined when analysing the signal-plus-noise amplitude fluctuations. The parameters computed were the amplitude frequency spectra and the autocorrelation function of the signal-plus-noise* envelope. These parameters were determined in order to provide information about the spectral distribution of the amplitude fluctuations and about the rate of change of the fluctuations.

The tape recordings of the demodulated pulses were played into a

* In the remaining part of the thesis, the word 'signal' refers to the signal-plus-noise unless otherwise stated.

20 Hz sixth-order active low-pass filter. The resultant signal was then fed into the A/D converter of the computer where it was sampled and converted into a digital signal suitable for computer processing. A programme based on the fast Fourier transform (FFT) algorithm was developed to compute the amplitude frequency spectrum of the data signal. The autocorrelation function of the signal envelope was calculated by first computing the amplitude frequency spectrum of the signal. The spectrum was then squared, and the resultant signal, the power spectrum, was inverse-transformed, using the FFT routine, back to the time domain. This operation resulted in the formation of the autocorrelation function of the signal envelope.

2.5.2 Analysis of Tests Relating to the Study of Bit-Error Probabilities

The results of the several hundred 'short-term' tests relating to the study of the bit-error probability of the ASK data transmission system were used to compute 'long-term' or average bit-error probabilities. This provided information about the average performance of the ASK system.

During the testing of the system, three parameters were changed in order to study the effect of their variation on the performance of the system. These parameters were the data-pulse width, the data-rate, and the detection threshold level in the receiver. Because four data-pulse widths, three data-rates for each pulse width, and two detection threshold levels were used in the tests at each range, then it was possible to compute twenty-four average bit-error probabilities for each range tested.

In the presentation of the results of tests relating to the study of bit-error probabilities in Chapter 4, it will be shown that the average bit-error probabilities can be further sub-divided into two

groups which are related to the time of year during which the tests were carried out. As will be shown in Chapter 4, it is possible, by dividing the results in this way, to interpret them more easily and more meaningfully in terms of the prevailing climatic conditions at the test site.

CHAPTER THREE

A STUDY OF SIGNAL AMPLITUDE FLUCTUATIONS

Introduction

In this chapter, the amplitude fluctuations that result when pulses are transmitted through water are considered, and several aspects relating to these fluctuations are discussed. In particular, signal amplitude probability density functions (PDF) and the statistics which relate to the PDFs are examined. In addition, the signal envelope frequency spectra and the envelope autocorrelation functions are considered.

In the final part of the chapter, two models of the signal PDF are developed. The models, which are based on the consideration of the experimental investigation of the signal amplitude fluctuations, are developed in terms of two prevailing wind directions.

3.1 Amplitude Fluctuations and Their Relevance to Underwater Data Transmission

Signal level fluctuations can cause errors in the detection of pulses transmitted through water. If the detrimental effects of pulse amplitude fluctuations are to be overcome, then it is necessary to have detailed information about the fluctuations. There are various aspects of the amplitude fluctuations that are of importance in data transmission. Firstly, the probability density function of the signal amplitude is important since it provides information about the range of the fluctuations and about the most likely amplitudes which the signal can have. A knowledge of this information is useful when studying the way in which the variation of the detection threshold affects the error probability in a data transmission system.

There are two other aspects of amplitude fluctuations which can

provide additional information and that can be helpful in the design and implementation of optimum data receivers. These are the amplitude frequency spectrum of the envelope of the signal and the autocorrelation function of the envelope of the signal. These two parameters provide information about the spectral energy distribution of the signal fluctuations and information about the statistical properties of the signal amplitude fluctuations. From a knowledge of the amplitude frequency spectra and autocorrelation functions of the signal envelope fluctuations, it is possible to design automatic gain control and averaging detector circuits which are capable of reducing the effects of the fluctuations.

3.2 Measured Amplitude Frequency Spectra (Andrews and Turner, 1975)

The results presented in this section are based on measurements that were made when the prevailing wind direction was either approximately parallel to or approximately perpendicular to the direction of signal transmission. The results are presented in this way so that the relative significance of fluctuations due to both thermal inhomogeneities in the medium and surface waves on the water can be assessed. The geometry of the reservoir and the absorbent nature of the bottom were such that only a single surface-reflected path signal was consistantly observed at the receiver together with the direct-path signal at the ranges under test. It will be shown that, by considering the experimental data according the wind direction, it is possible to distinguish two sources of signal fluctuations.

Tests were carried out over the three transmission ranges of 150, 200 and 650 metres. In the experimental investigation, 0.8 msec duration raised-cosine pulses were transmitted every 6.4 msec at a carrier frequency of 150 kHz. In performing the tests, the peak signal-to-RMS noise ratio (measured at the demodulated output of the

receiver) was held at values of between 25 dB and 30 dB, depending upon the transmission range. This was accomplished by increasing the transmitter power as the range was increased. The received signal was demodulated and recorded on magnetic tape and the computation of the amplitude frequency spectra was carried out using the methods described previously in Section 2.5.1. The peak signal-to-RMS noise ratio was measured at each transmission range and in defining this parameter, 'peak signal' refers to only the signal and not the signal-plus-noise.

Recently, Urick (1974) has compared, favourably, signal amplitude fluctuation spectra in long range underwater transmissions with wave spectra curves based on the theory described by Neumann and Pierson (1966). Therefore, in the following presentation of experimentally determined amplitude frequency spectra which were computed from data measured under short-range transmission conditions, a similar comparison is made on the basis of Urick's results.

Some typical amplitude frequency spectra obtained from measurements made under the condition of a prevailing parallel-wind are shown in FIGURES 3.1 to 3.3, and corresponding perpendicular-wind spectra are illustrated in FIGURES 3.4 to 3.6. In each of the figures, the RMS noise voltage (measured in a 4.5 kHz band and normalised to the peak of the fluctuation spectrum) and the approximate noise spectrum* are also indicated. Additionally, amplitude wave frequency spectra computed using a formula derived by Marsh et al (1961) are shown in the figures. The wave spectra curves were computed using Marsh's equation in the form,

$$A(\omega) = \frac{c^{\frac{1}{2}}}{\omega^3} \exp(-g^2/\omega^2 s^2) \qquad \ldots\ldots (3.1)$$

where c = constant

ω = angular frequency

---

*For a discussion and derivation of the noise spectrum level, see APPENDIX D.

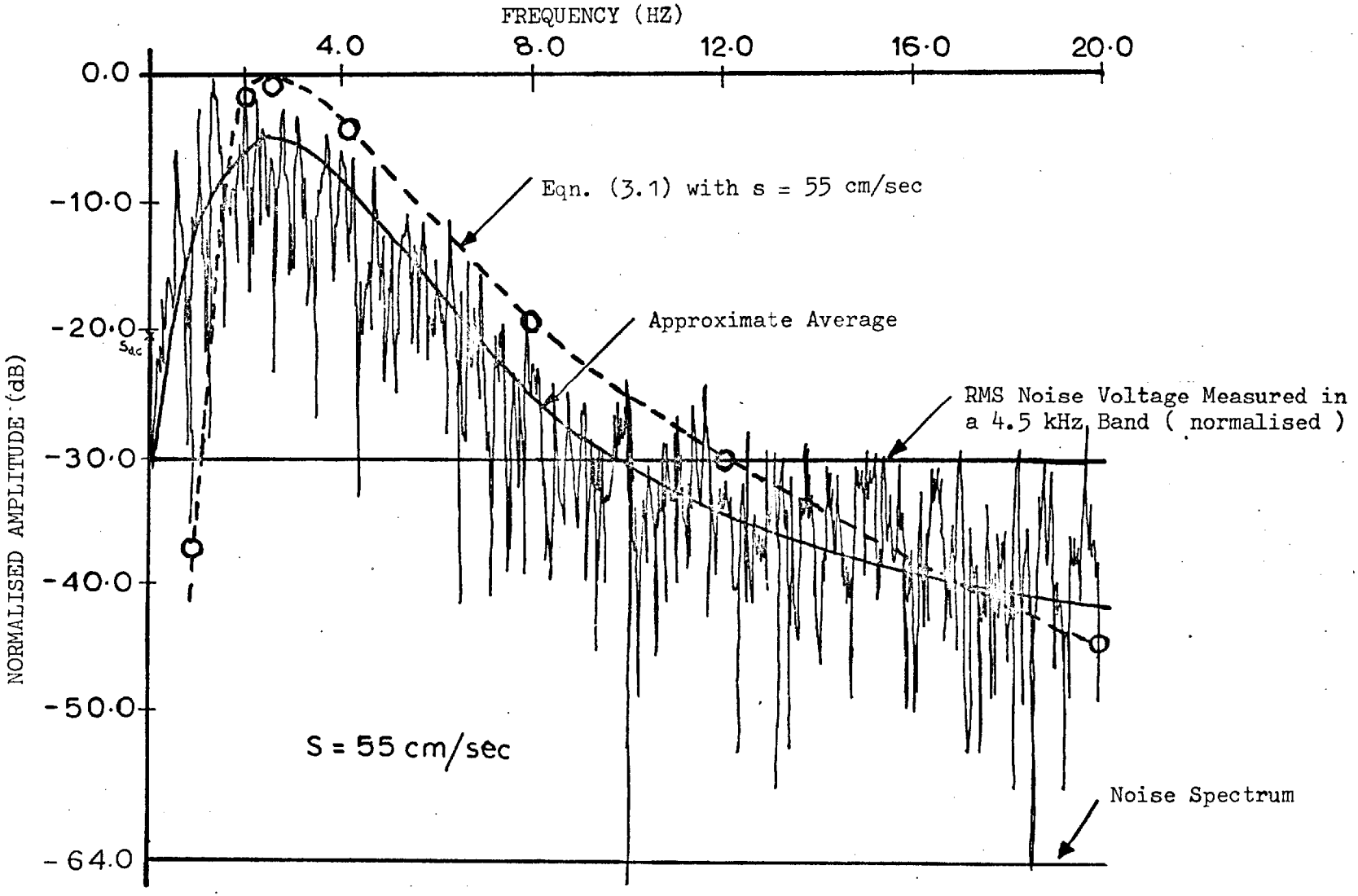


FIGURE 3.1 Measured Amplitude Frequency Spectrum at 150 metres with a Parallel-Wind Condition

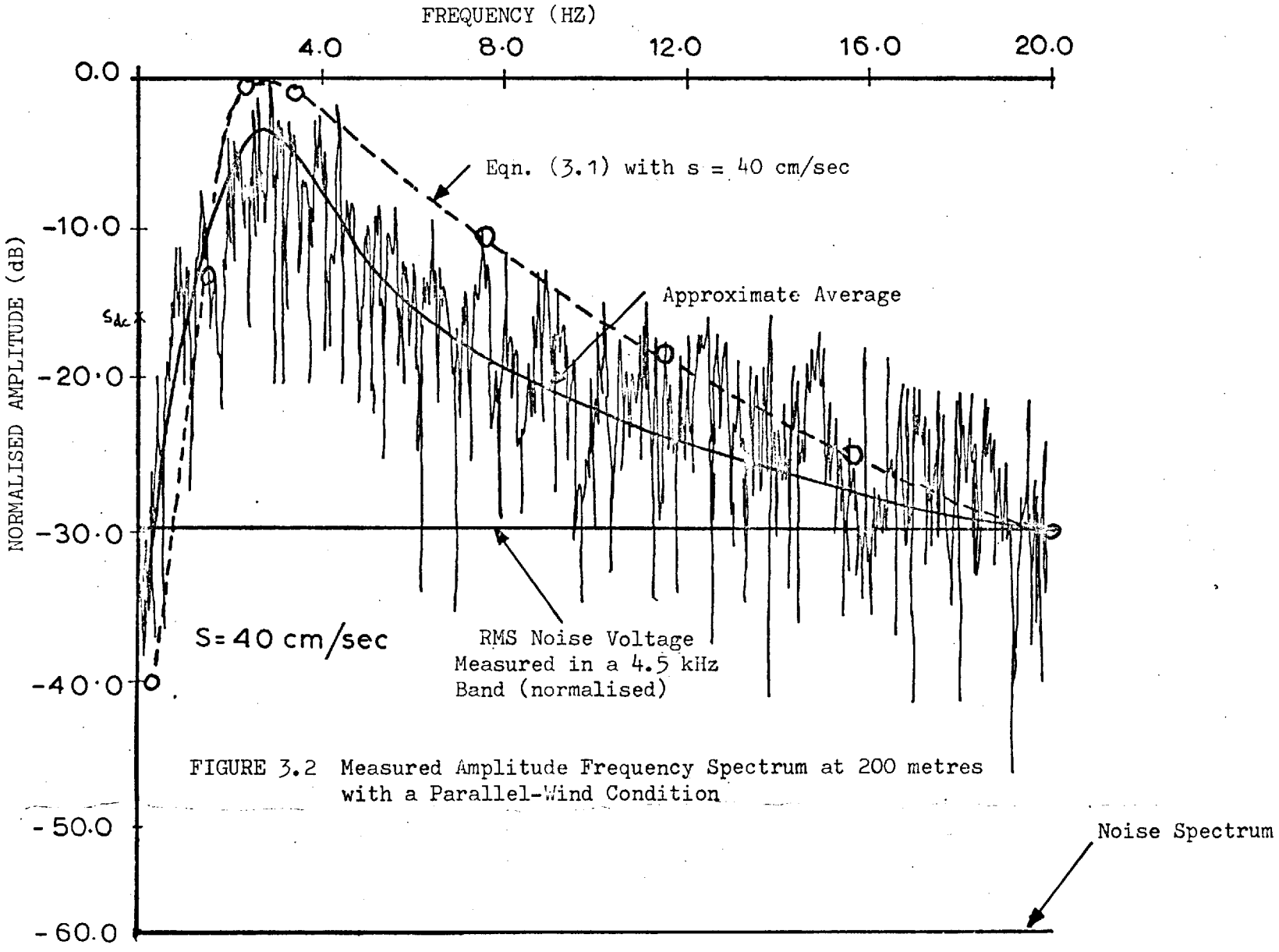


FIGURE 3.2 Measured Amplitude Frequency Spectrum at 200 metres with a Parallel-Wind Condition

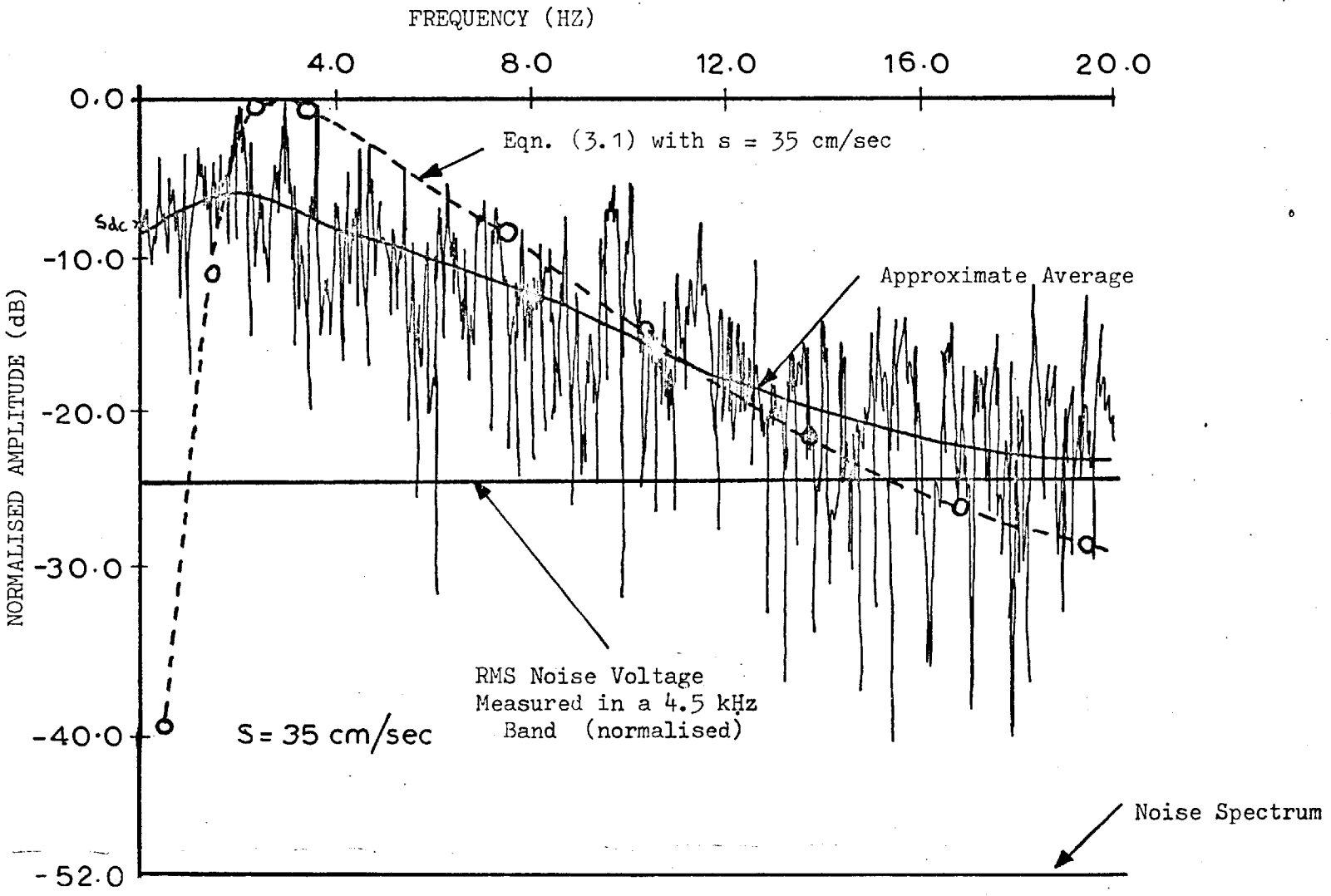


FIGURE 3.3 Measured Amplitude Frequency Spectrum at 650 metres with a Parallel-Wind Condition

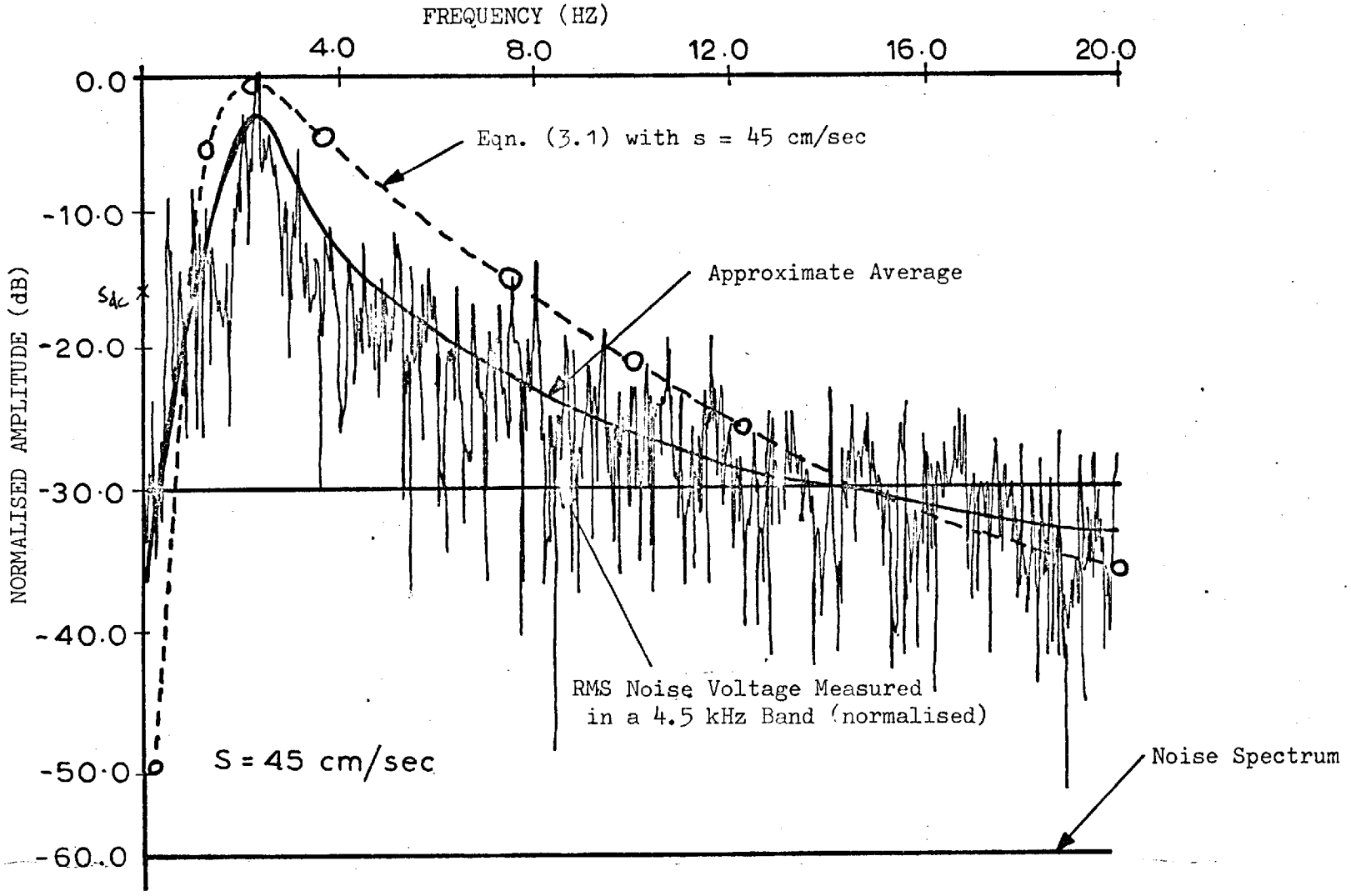


FIGURE 3.4 Measured Amplitude Frequency Spectrum at 150 metres with a Perpendicular-Wind Condition

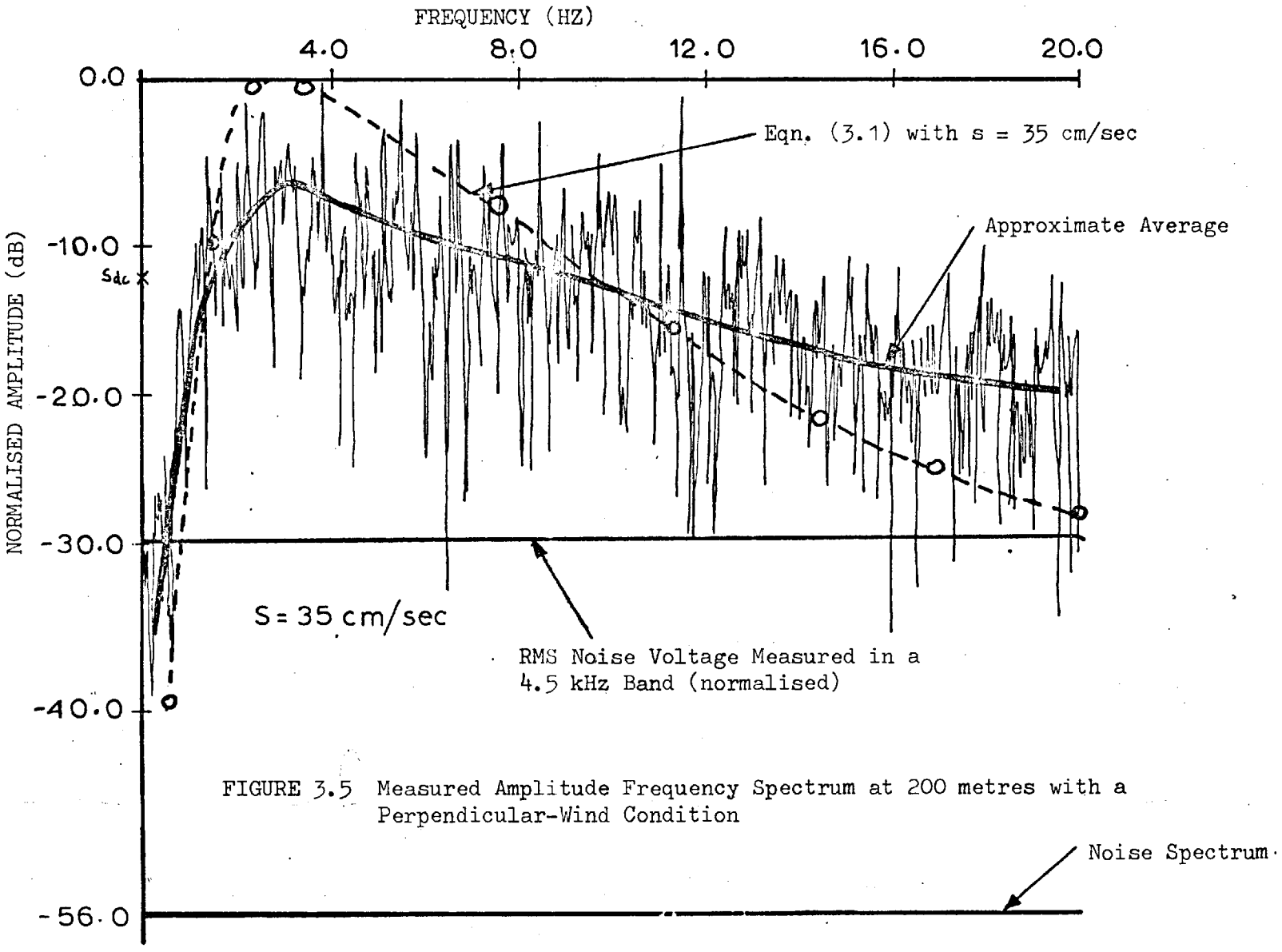


FIGURE 3.5 Measured Amplitude Frequency Spectrum at 200 metres with a Perpendicular-Wind Condition

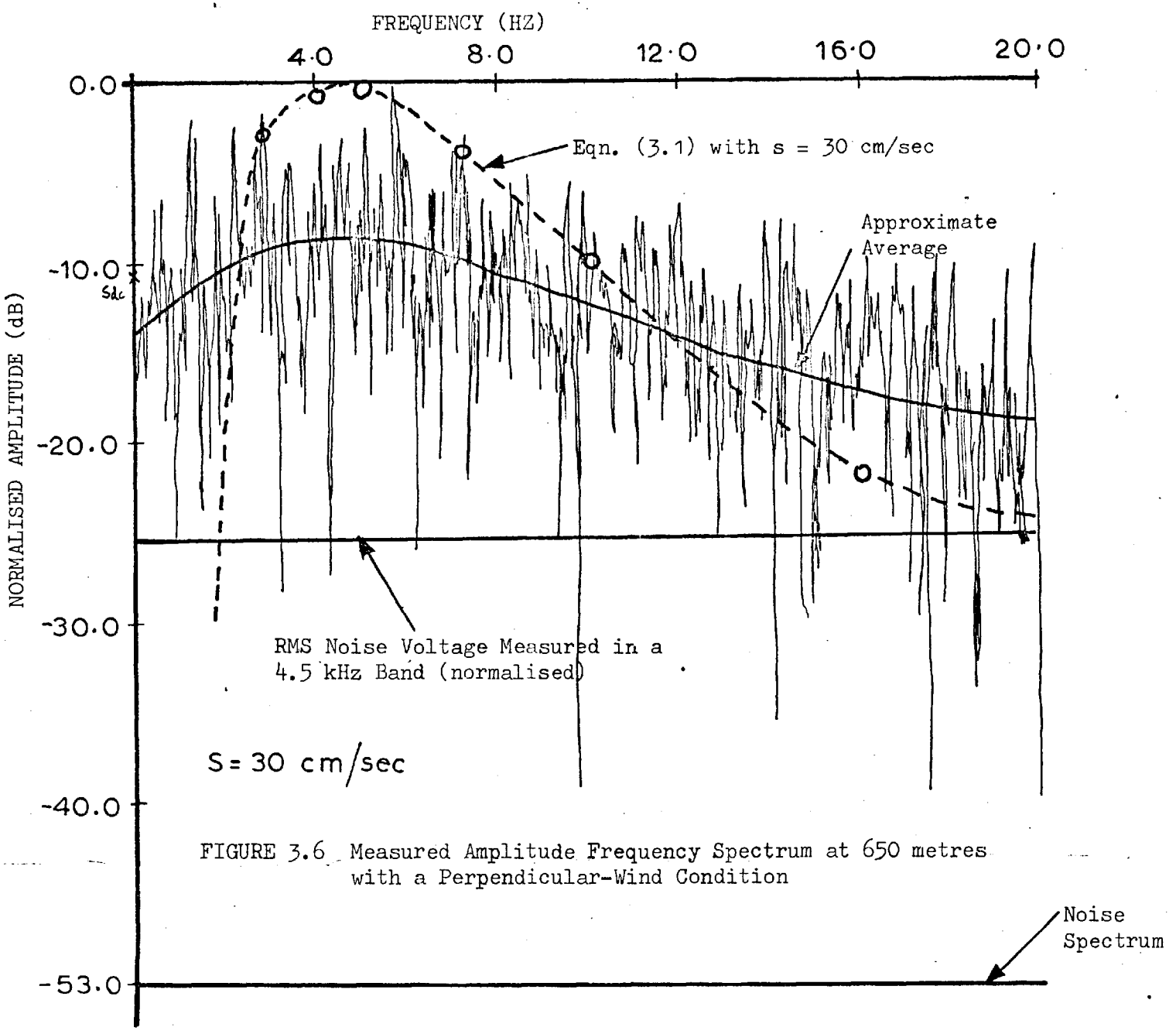


FIGURE 3.6 Measured Amplitude Frequency Spectrum at 650 metres with a Perpendicular-Wind Condition

g = acceleration due to gravity

and s = wind speed

The values of s which are indicated in each of the figures correspond to experimentally measured wave speeds, rather than to measured wind velocities.

An examination of FIGURES 3.1 to 3.3 shows that there is similarity between the experimentally determined amplitude frequency spectra and the wave frequency spectra computed from Equation (3.1). The results shown support the earlier results obtained by Urick (1974) and indicate that in the case of a prevailing parallel-wind, there is similarity between wave frequency spectra and amplitude frequency spectra.

The rapid fluctuations of the measured amplitude frequency spectra shown in FIGURES 3.1 to 3.3 can be explained in two ways. Firstly, the amplitude frequency spectra were determined from a single 512-bit time sample of data and the data sample was converted to its frequency domain representation by using a fast Fourier transform algorithm in which no averaging methods were used. Hence, the computed spectra are only estimates of the actual spectra and contain inherent fluctuations (see Oppenheim and Shafer, 1975 and APPENDIX B for a simple illustration). In order to reduce the fluctuations caused by a finite-length time sample of data, it would be necessary to use ensemble averaging techniques such as Bartlett's procedure (see Oppenheim and Shafer, 1975). However, in each of the figures, an approximate 'average' line has been drawn through the fluctuating spectra rather than using ensemble averaging.

A second explanation for the fluctuations in the measured amplitude frequency spectra when compared to the wave spectra given by Equation (3.1) is the limitation of the wave spectra model in the case of the experimental conditions encountered at the reservoir. The wave spectra model is derived under the condition of a fully developed open sea in

which there are asssumed to be an infinite number of simple harmonic progressive waves all travelling in the same direction on the water surface (Neumann and Pierson, 1966). This assumption is less valid in the case of a small bounded reservoir and hence, the actual spectra of the surface waves on the reservoir could be discrete, rather than continuous. When the fast Fourier transform of the amplitude fluctuations of the signal envelope is computed, therefore, it is possible to encounter frequencies in the spectrum at which there is little spectral energy caused by the effect of the surface waves. On conversion to a decibel scale, the small amounts of spectral energy at these frequencies would appear as large negative spikes or troughs, as illustrated in the figures.

From an analysis of FIGURES 3.1 to 3.3, the main difference between the measured amplitude frequency spectra and the computed wave spectra occurs in the frequency band below about 1 Hz. It is likely that this difference can be attributed partly to noise, partly to fluctuations arising from thermal inhomogeneities in the medium, and partly to slow movements of both the transmitting and receiving platforms.

In the perpendicular-wind case, as illustrated by FIGURES 3.4 to 3.6, the measured amplitude frequency spectra are more variable than in the parallel-wind case, and although the resemblance to the wave spectra phenomenon is still apparent, it is much less marked. It is conjectured that, in the case of a wind which is perpendicular to the line of signal transmission, the main cause of the signal amplitude fluctuations is the presence of thermal inhomogeneities in the medium. It will be shown later, in Section 3.4, that this conjecture is to some extent substantiated by values obtained for the coefficient of variation of the signal amplitude fluctuations.

3.3 Measured Autocorrelation Functions (Andrews and Turner, 1975)

The autocorrelation functions which are presented in this section were determined by using the methods outlined previously in Sections 2.4.1 and 2.5.1. Some typical autocorrelation functions computed from data obtained under the condition of a prevailing parallel-wind are shown in FIGURES 3.7 to 3.9. The figures relate, respectively, to transmission ranges of 150, 200 and 650 metres.

The autocorrelation functions shown in FIGURES 3.7 to 3.9 appear to resemble the form of the exponential-cosine autocorrelation function. This particular type of autocorrelation function is frequently encountered in many applications (Bendat, 1958), and the time of occurrance of the second zero-crossing of the autocorrelation function is indicative of a predominant frequency of the power spectrum of the autocorrelation function (Bendat, 1958). A more detailed discussion is given in APPENDIX C. In the case of FIGURES 3.7 to 3.9, the time of the second zero-crossing of the autocorrelation functions ranges from approximately 0.2 to 0.5 seconds, which corresponds to predominant frequencies of between 1.4 and 4 Hz (see APPENDIX C). These particular values are in agreement with the peaks of the amplitude frequency spectra shown in FIGURES 3.1 to 3.3, and thus, there is further indication that in the parallel-wind case, the time-varying nature of the pulse amplitudes is dependent strongly upon the effect of the surface-reflected path signal. A conclusion which can be drawn from the information contained in FIGURES 3.7 to 3.9 is that the statsitical properties of the signal amplitude fluctuations can change at rates of between about 1.4 and 4 Hz.

In addition to computing the autocorrelation functions for the parallel-wind case, autocorrelation functions were also computed for the perpendicular-wind case. It was found that, in general, when

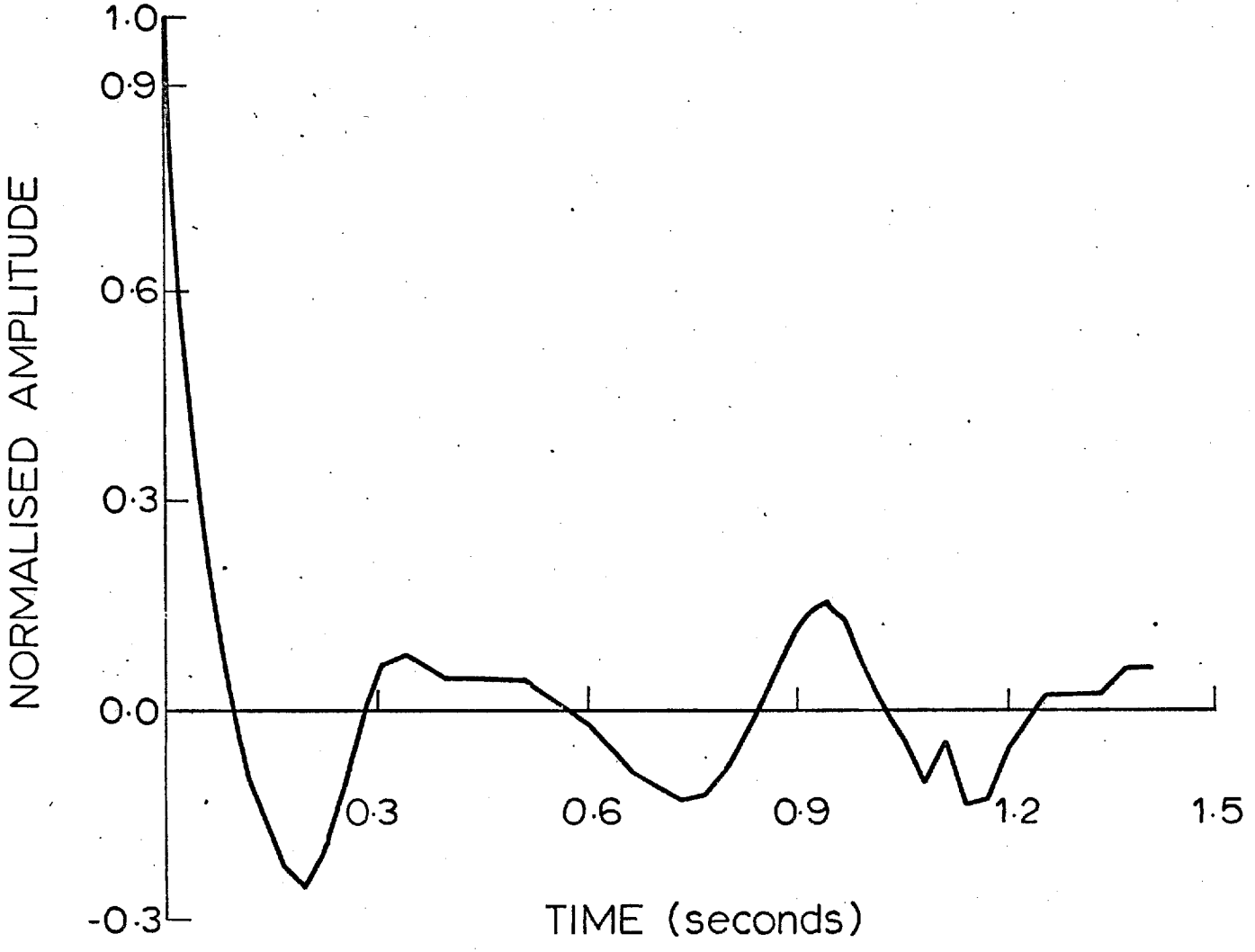


FIGURE 3.7 Computed Autocorrelation Function at 150 metres with a Parallel-Wind Condition

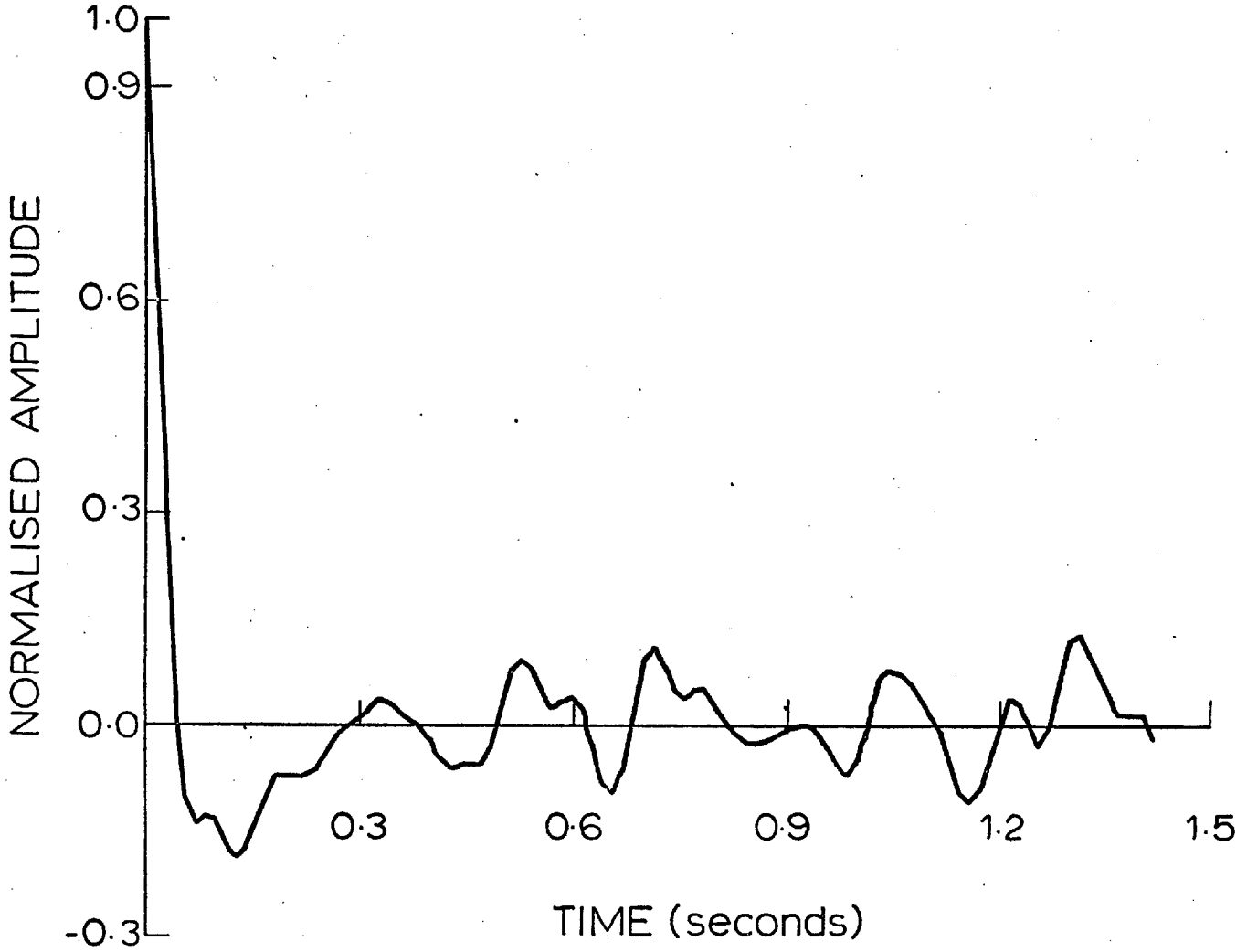


FIGURE 3.8 Computed Autocorrelation Function at 200 metres with a Parallel-Wind Condition

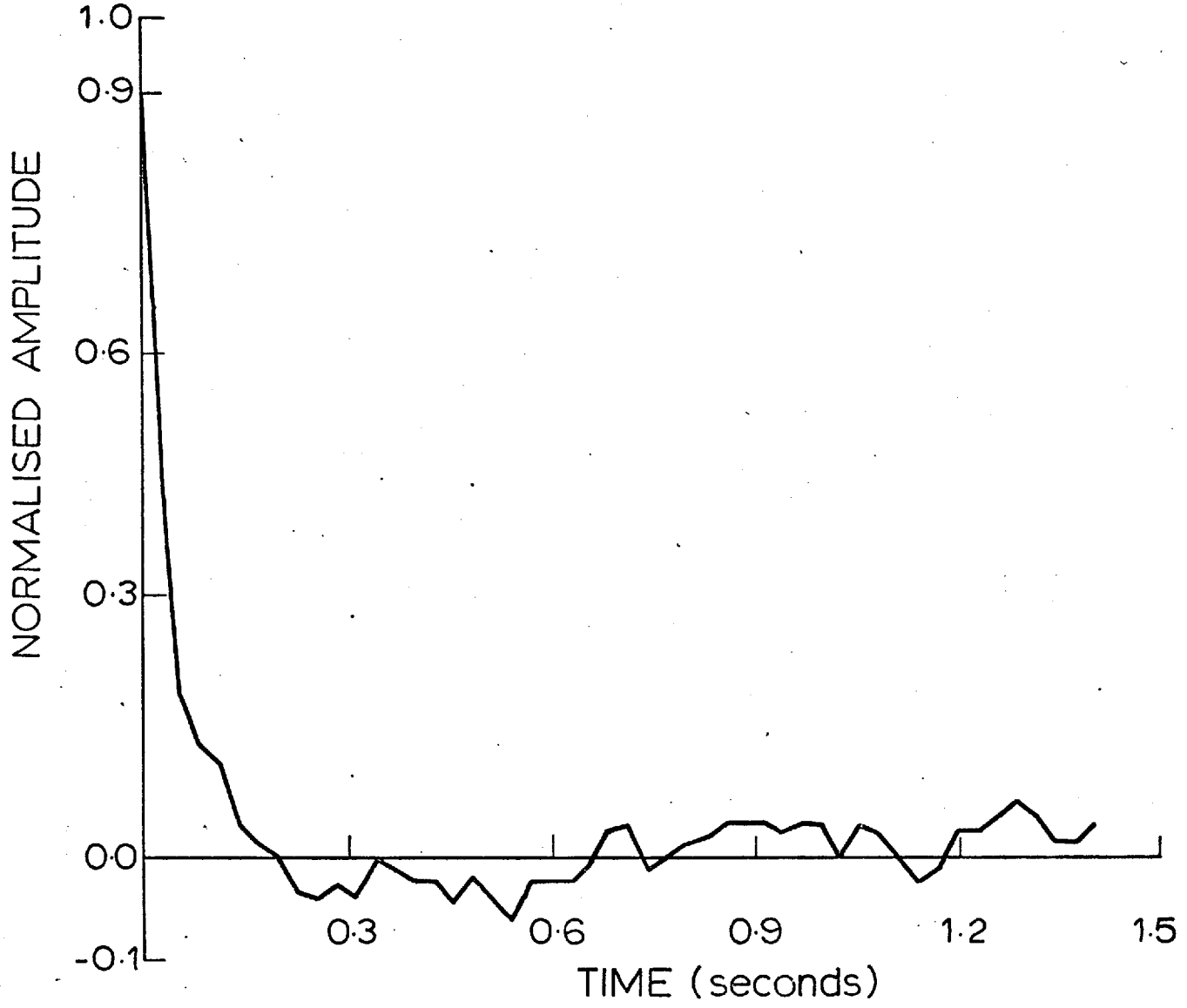


FIGURE 3.9 Measured Autocorrelation Function at 650 metres with a Parallel-Wind Condition

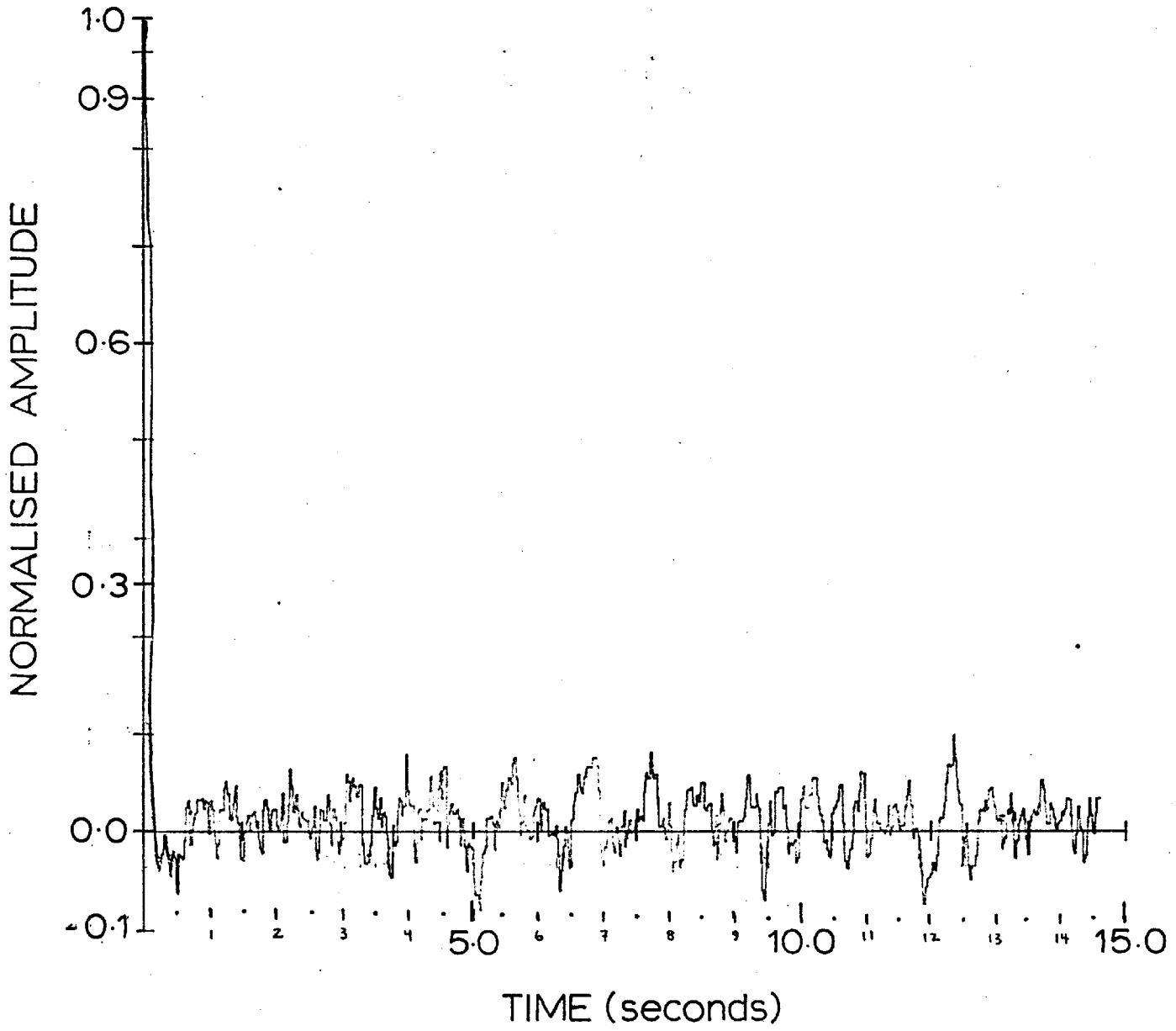


FIGURE 3.10 Computed Autocorrelation Function at 650 metres with a Perpendicular-Wind Condition

operating under perpendicular-wind conditions, the autocorrelation functions are more variable than in the parallel-wind case. This observation is to be expected from the fact that the apparent dependence of the received signal on the surface-reflected path signal is considerably less in the perpendicular-wind case than in the parallel-wind case. In order to investigate the autocorrelation functions for the perpendicular-wind case, a 30-second sample of data was analysed. By doing this, longer term fluctuations could be studied. A typical autocorrelation function for the perpendicular-wind condition at a range of 650 metres is shown in FIGURE 3.10. From this figure, it can be seen that beyond about 0.7 seconds, there is little correlation of the signal. The results appear to indicate that, although the dependence of the amplitude fluctuations on the surface-reflected path signal is reduced in the perpendicular-wind case when compared to the parallel-wind case, there is still a concentration of spectral energy in the frequency band around 2 Hz. This concentration of energy, which is mainly due to the surface-wave effect, still has a considerable effect on the autocorrelation function and on the statistical properties of the received signal.

3.4 Coefficient of Variation of the Amplitude Fluctuations (Andrews and Turner, 1975)

From the point of view of pulse detection in data transmission systems, the coefficient of variation, which is defined as the ratio of the standard deviation to the mean of the function, is a highly important parameter. The coefficient of variation was determined by analysing the computed probability density functions of the signal amplitude. The PDF's were computed, with the aid of a PDP-15 digital

computer, using the techniques described in Section 2.5.1. The data-pulse width used in the tests was 1.6 msec and two time sample lengths, of 2.5 seconds and 25.0 seconds containing 400 and 4000 data samples respectively, were used in the computation of the PDFs. The coefficients of variation presented in this section are average values obtained by taking account of more than 100 PDFs measured under the condition of an approximate constant peak signal-to-RMS noise ratio at the output of the receiver at all test ranges.

FIGURE 3.11, for example, shows the average coefficient of variation of 2.5 second and 25.0 second data sample lengths at the three test ranges for a wind which was perpendicular to the direction of signal transmission. The measured RMS noise level, normalised to the mean signal, is also indicated in the figure to illustrate the effect of the background noise on the experimental results. Because the results shown in FIGURE 3.11 are those obtained for the coefficient of variation of the signal-plus-noise, two additional modified curves have also been drawn in the figure. These latter curves refer to the signal-only case. It can be observed that at the short ranges (less than about 400 metres), the effect of the background noise is significant, particularly in the case of the 2.5 second samples. The effect of the noise is to reduce the values obtained for the signal-plus-noise case to those shown for the signal-only case as illustrated in the figure.

Also plotted in FIGURE 3.11 are two theoretical curves derived using the thermal fluctuation theory of Chernov (1967) with spacial correlation distances of 0.5 metres and 1.5 metres. The equation from which the theoretical curves were computed,, was,

$$\overline{\Delta V} = \left[\frac{\pi^{\frac{1}{2}}}{2} \overline{\mu}^2 \alpha R \right]^{\frac{1}{2}} k \qquad \ldots\ldots (3.2)$$

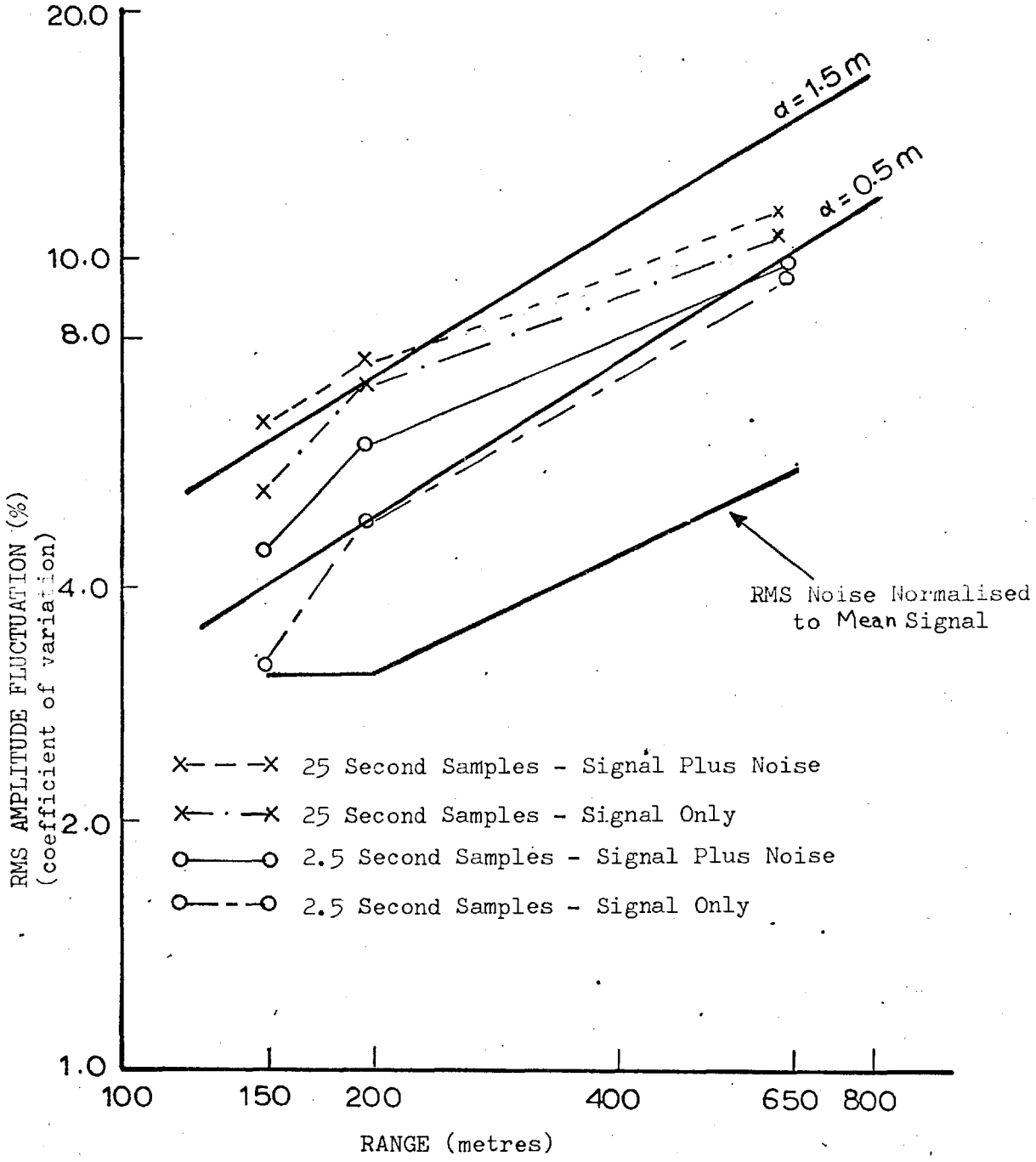


FIGURE 3.11 Average Coefficient of Variation For the Perpendicular-Wind Condition

where, $\overline{\Delta V}$ = RMS amplitude fluctuation (coefficient of variation)

$\overline{\mu^2}$ = mean-square fluctuation of the refractive index of water = 5.0×10^{-9}

α = spacial correlation distance

R = range

$k = 2\pi/\lambda$ = acoustic wavenumber

λ = acoustic wavelength in water

Equation (3.2) is derived from the general theory presented by Chernov (1967) under the assumption that the wave parameter, D, is large, and where D is defined as,

$$D = \frac{4\pi R}{k\alpha^2} \qquad \ldots\ldots (3.3)$$

From an analysis of FIGURE 3.11, it is clear that the measured coefficients of variation are in agreement with the RMS fluctuations predicted from Equation (3.2) . The difference between the experimental data and the two theoretical curves can be explained by the influence of the effect of the surface waves, even under the perpendicular-wind condition. The correlation distances used (0.5 and 1.5 metres) in the predicted curves are in agreement with those which would be expected from the theory of Tatarski (1967). The 25.0 second data shows a larger coefficient of variation than the corresponding 2.5 second data. This is to be expected since the longer time-samples include longer term fluctuations of the signal, and the coefficient of variation of the larger sample population should be greater than that of the smaller samples of the same data.

FIGURE 3.12 shows comparative results for a wind parallel to the line of transmission. The RMS noise level, normalised to the peak signal, is also indicated but is not of significance to the measured results. Because signal fluctuations due to both thermal inhomogeneities and the

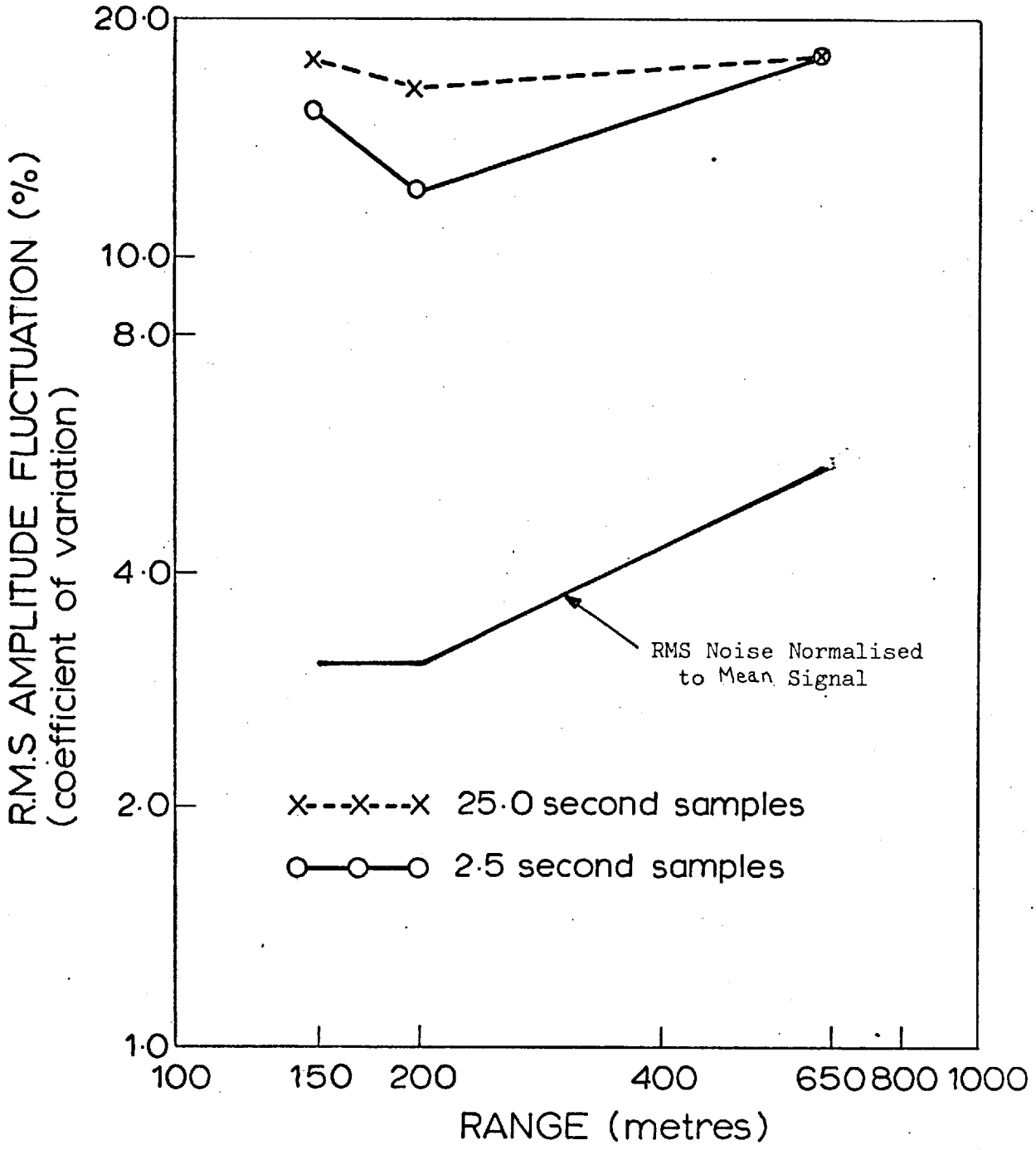


FIGURE 3.12 Average Coefficient of Variation for the Parallel-Wind Condition

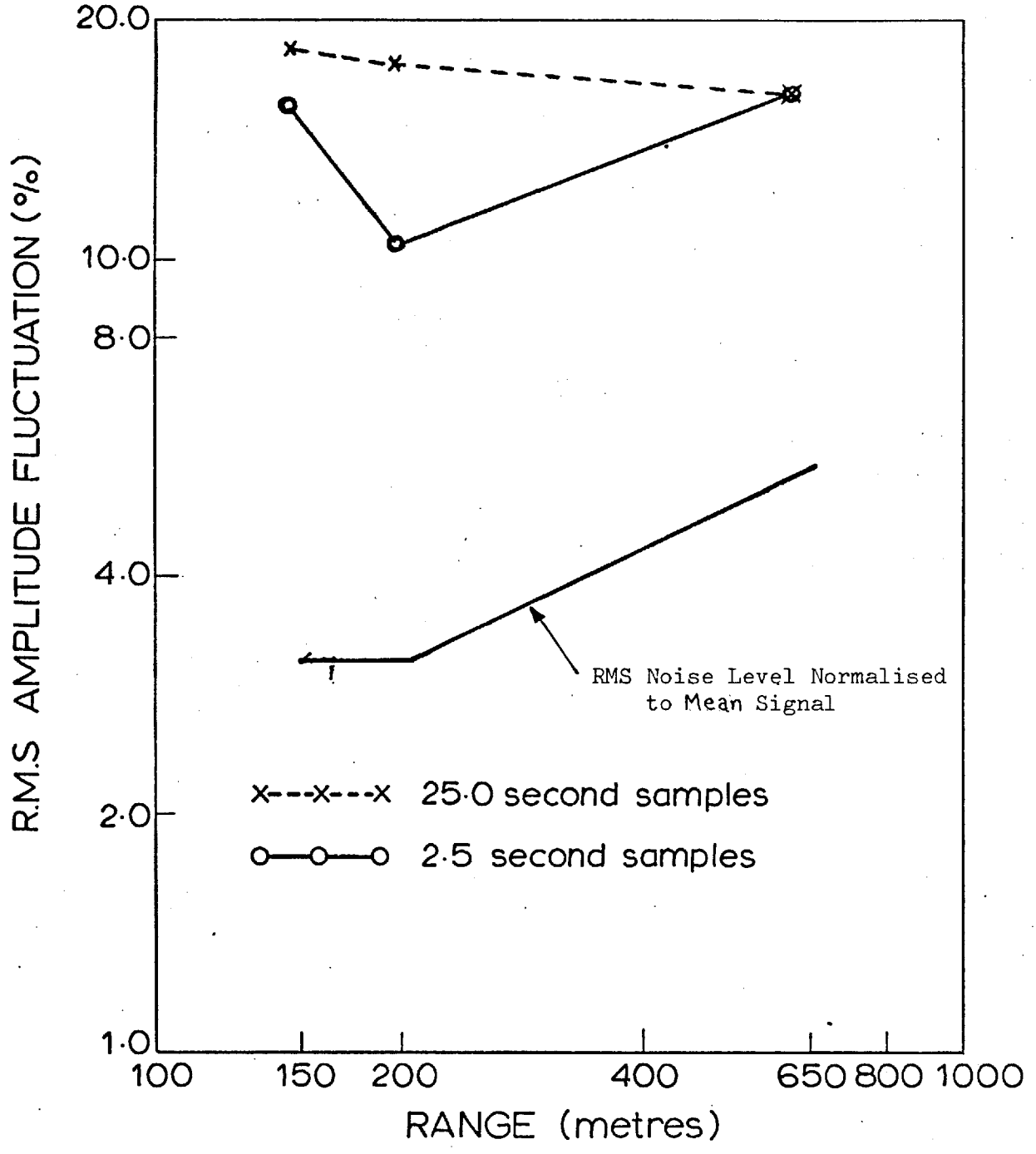


FIGURE 3.13 Average Coefficient of Variation of the Surface-Reflected Path Signal

the effect of surface waves are caused by two different phenomena, it is possible that these two sources can be considered statistically independent and separable. The separation of the two sources of fluctuations is based on the assumption that in the case of a perpendicular-wind, the fluctuations are caused, in the main, by thermal inhomogeneities in the medium. In the parallel-wind case, however, the signal amplitude fluctuations will be caused by both thermal inhomogeneities and the effect of surface waves (the noise is ignored in this case). Then, if this is true,

$$\overline{V}_{lw}^2 = \overline{V}_s^2 + \overline{V}_{ti}^2 \qquad \ldots\ldots (3.4)$$

and

$$\overline{V}_{pw} = \overline{V}_{ti}^2 \qquad \ldots\ldots (3.5)$$

where $\overline{V}_{lw}^2$ = parallel-wind coefficient of variation squared (mean-square amplitude fluctuation)

$\overline{V}_s^2$ = mean-square fluctuations due to the moving water surface

$\overline{V}_{ti}^2$ = mean-square fluctuations due to thermal inhomogeneities

$\overline{V}_{pw}^2$ = perpendicular-wind mean-square amplitude fluctuations

By consideration of FIGURES 3.11 and 3.12, and by using Equations (3.4) and (3.5), it is possible to calculate the coefficient of variation of the amplitude fluctuations caused by the moving water surface only. This has been done and the results are shown in FIGURE 3.13. The RMS noise level, normalised to the peak signal is also indicated in the figure. From FIGURE 3.13, it can be seen that the fluctuations due to the movement of waves on the water surface tends

to decrease with increasing range. This decrease with increasing range appears reasonable since the grazing angle of the signal incident on the water surface decreases as the range is increased, and the undulating nature of the surface thus tends to have a reduced effect on the incident signal as the grazing angle is decreased. The results shown in FIGURE 3.13 are in agreement with results obtained by Whitmarsh et al. (1957), although Whitmarsh's results were obtained at a much lower transmission frequency.

The main conclusion which can be drawn from the results contained in FIGURES 3.11 to 3.13 is that it appears that the effects of thermal inhomogeneities and surface waves on the signal amplitude fluctuations can be separated by using the simple technique of analysing the data in the basis of parallel-wind and perpendicular-wind experimental conditions. It will be shown in the following sections that because of the apparent large differences between the parallel-wind and perpendicular-wind data, it will be useful to develope PDF models based on these two different wind directions.

3.5 Analysis of the Signal Probability Density Functions

The results presented in this section are given in terms of

measurements made when the prevailing wind direction was approximately parallel to and approximately perpendicular to the direction of transmission. The results are presented in this way so that the effects of thermal inhomogeneities and of surface waves on the signal PDF can be observed. With the results of the previous section in mind, it was felt that the analysis of the PDFs according to the wind direction may reveal properties of the PDF which are not easily observable on a more general wind-direction basis.

The PDFs were determined from the analysis of demodulated 1.6 msec raised-cosine pulses. Two sample lengths, of 2.5 seconds and 25.0 seconds in duration, were analysed using the techniques described in Section 2.5.1.

At the 150-metre transmission range, the direction of the prevailing wind was found to have a considerable effect on the probability density function. This is illustrated in FIGURES 3.14 to 3.16. The PDF shown in FIGURE 3.14 was computed from data recorded when the prevailing wind direction was approximately perpendicular to the transmission path, while FIGURE 3.15 shows a comparative PDF under the parallel-wind condition. An approximate intermediate value between the parallel and perpendicular wind conditions is shown in FIGURE 3.16. A point to be noted immediately from the three figures is that as the prevailing wind changes from the perpendicular direction to the parallel direction, the skew of the resultant PDFs increase. This observation can be explained by the consideration of two important parameters.

Firstly, as shown in FIGURES 3.12 and 3.13, in the parallel-wind case, the fluctuations of the signal amplitude are mainly dependent on the effect of surface waves. Also, the effect of the surface waves is

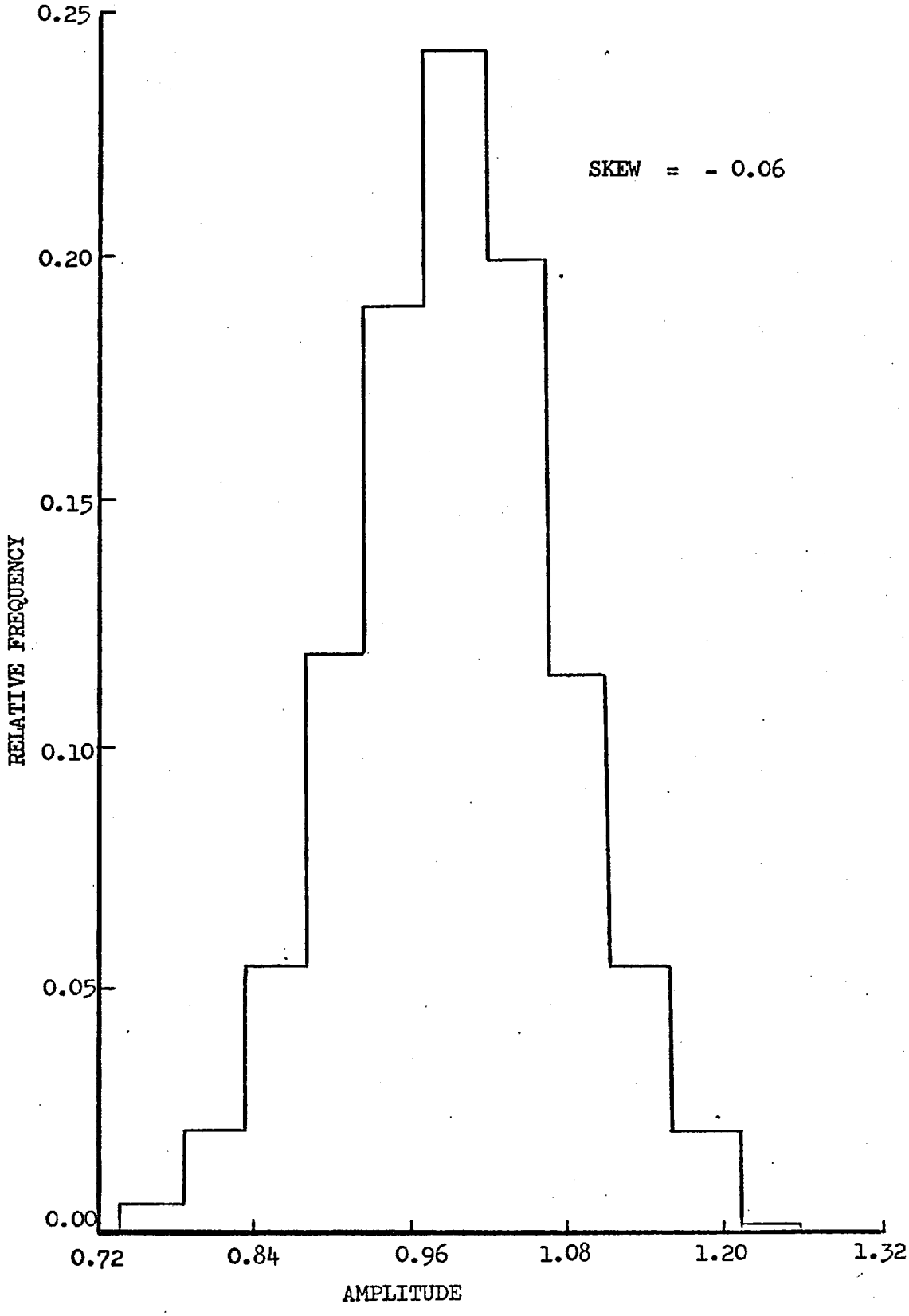


FIGURE 3.14 Typical PDF Measured at 150 metres with a Perpendicular-Wind

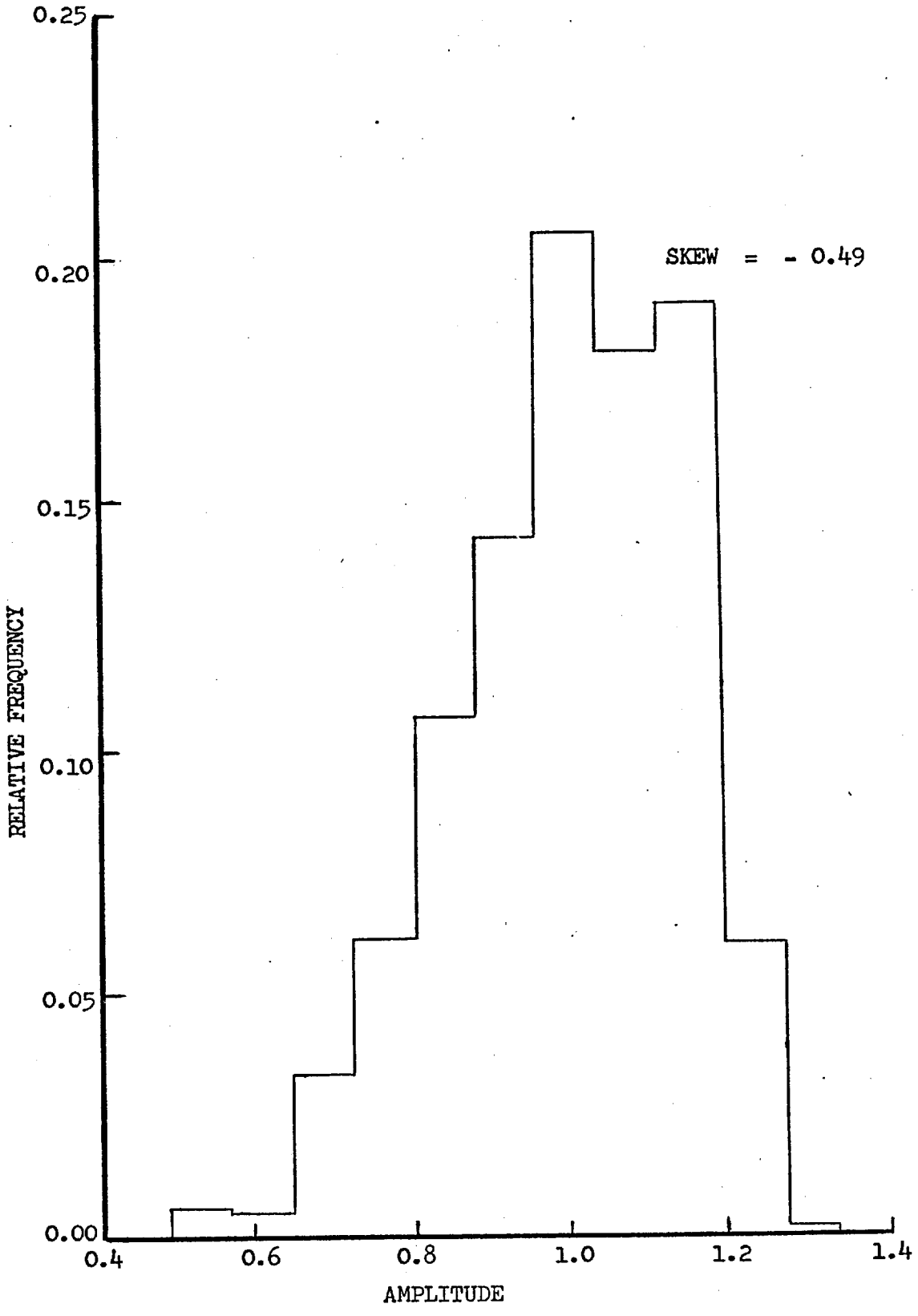


FIGURE 3.15 Typical PDF Measured at 150 metres with a Parallel-Wind

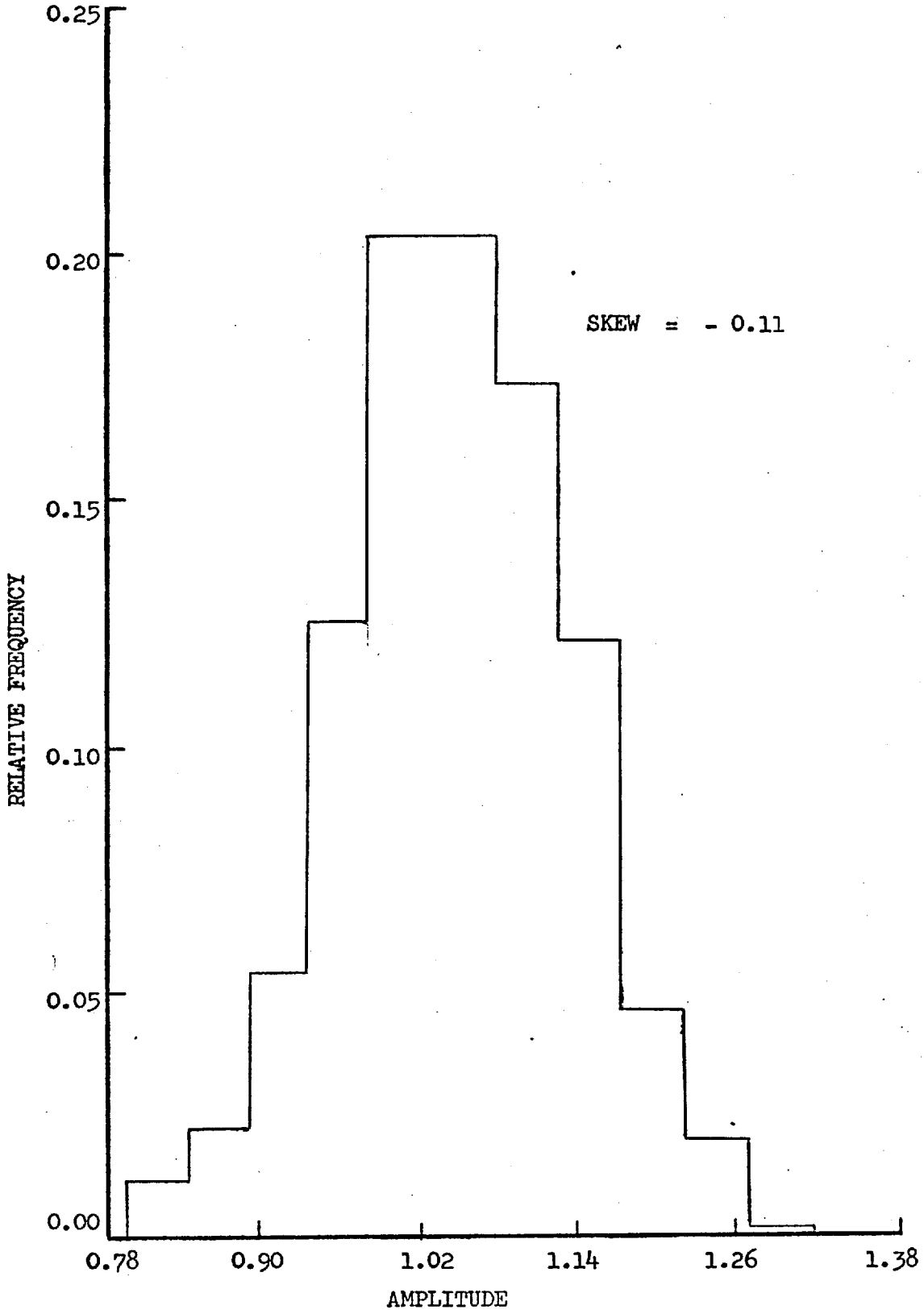


FIGURE 3.16 Typical PDF Measured at 150 metres - Intermediate Wind Direction

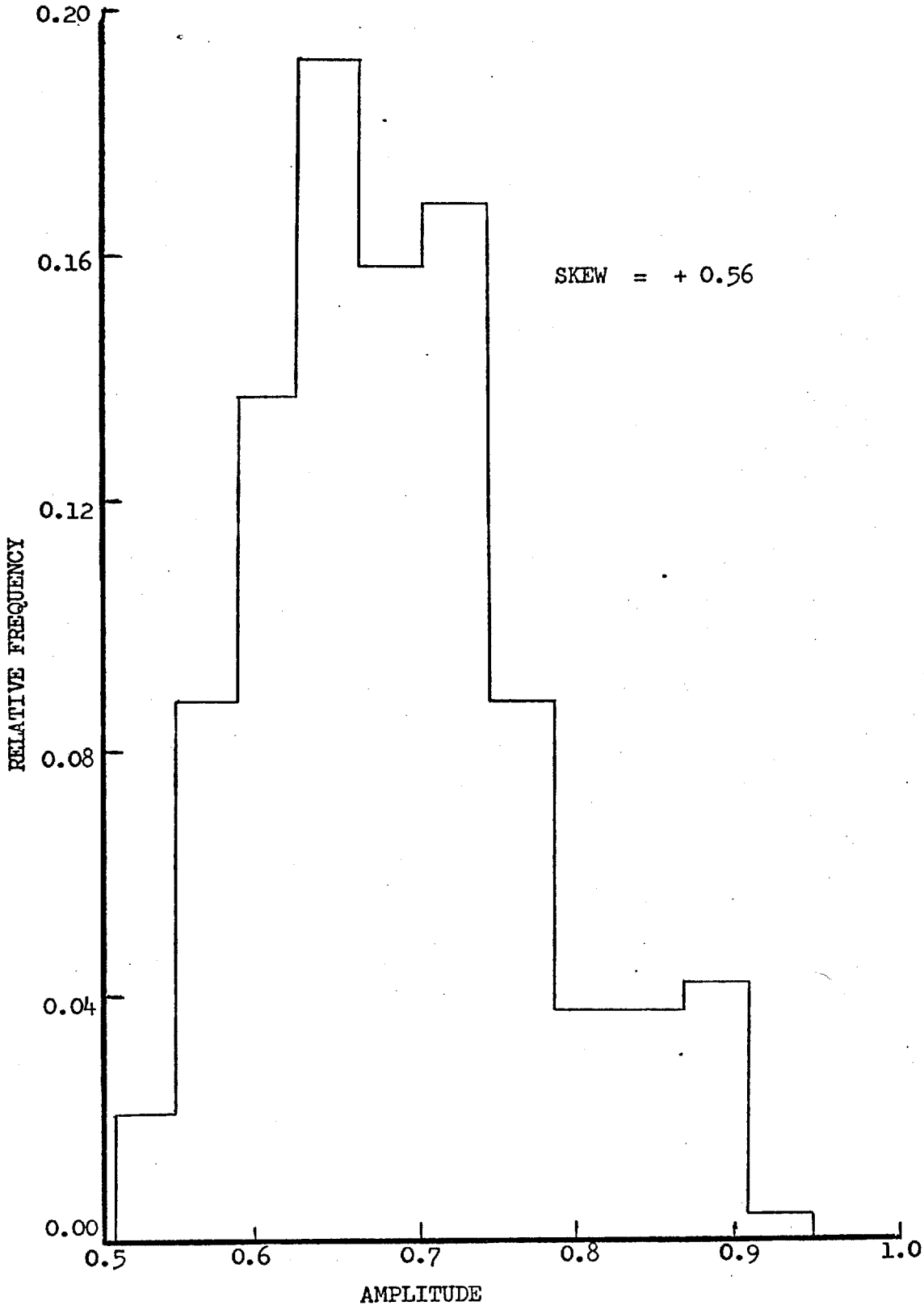


FIGURE 3.17 Typical PDF Measured at 150 metres under an Up-Wind Condition

strongest at the shorter ranges because the undulating nature of the surface has a particularly pronounced effect when the grazing angle is largest. This is a situation which occurs in the case of the 150-metre range. The second important fact which appears to be of value in explaining the results presented in FIGURES 3.14 to 3.16 is the effect of the slopes of the surface waves on the signal reflected from the water surface.

It has been shown (Medwin, 1967) that the specular scattering from the water surface is dependent mainly on the mean-square slope of the surface waves. A down-wind parallel to the direction of transmission can cause the mean-square slope of the surface waves to become negative. This phenomenon will therefore cause the PDF of the surface-reflected signal to become negatively skewed. Since the effect of the surface-reflected signal on the received signal PDF is strongest under the parallel-wind condition, it is to be expected that the largest skew should occur in the parallel-wind case. This has been observed at the 150-metre range, as illustrated by FIGURE 3.15. In the light of the above and a consideration of the information contained in FIGURES 3.12 and 3.13, it might be expected that the skew of the parallel-wind PDF should decrease with increasing range.

Although the results presented in FIGURES 3.14 to 3.16 apply to the down-wind propagation direction, it is possible, from the mean-square slope theory, to have a positive skew. A positive skew will result when signals are propagated under up-wind conditions. An experimentally measured PDF which illustrates a positive skew is shown in FIGURE 3.17. Overall, it is probably reasonable to assume that the long-term, or average, skew obtained under both up-wind and down-wind conditions would tend toward a value of approximately zero.

The statistical analysis of the computed probability density functions can provide further information about fluctuations of the received signal. The average statistics calculated from both perpendicular-wind and parallel-wind PDFs are listed in TABLES 3.1 and 3.2 respectively. The values given in the tables were obtained by finding the average value of the various parameters relating to more than fifteen PDFs at each range, for two data samples of 2.5 seconds and 25.0 seconds duration. An examination of the tables reveals several interesting trends.

The coefficient of variation, V, is always larger in the case of a parallel-wind than in the case of a perpendicular-wind, for all test ranges. Further information about the coefficient of variation can be found in the previous section. The skew and the kurtosis (amount of peakness) of the parallel-wind data are larger than those in the perpendicular-wind case, and the skew tends to decrease with increasing range. The latter observation is in agreement with the arguments presented earlier in this section.

From the tables, it can be seen that the skew, in the parallel-wind case, is positive, and not zero as conjectured previously. This can be explained simply in terms of the prevailing climatic conditions at the reservoir during the tests. It was found that the majority of the experimental results were obtained under up-wind propagation conditions, and this can almost certainly account for the positive skews shown in TABLE 3.2.

3.6 Derivation of Probability Density Function Models

The material of Sections 3.2 to 3.4 shows that when short-duration sound pulses are transmitted under shallow-water conditions the amplitude fluctuations of the pulses are related to the direction

TABLE 3.1

Perpendicular-Wind Statistics

2.5 Second Samples				25.0 Second Samples			
RANGE	V	SKEW	KURTOSIS	RANGE	V	SKEW	KURTOSIS
150m.	0.05	+0.17	2.81	150m.	0.07	+0.06	2.47
200m.	0.06	-0.05	2.80	200m.	0.08	-0.17	2.63
650m.	0.10	+0.07	2.65	650m.	0.13	+0.03	2.62

TABLE 3.2

Parallel-Wind Statistics

2.5 Second Samples				25.0 Second Samples			
RANGE	V	SKEW	KURTOSIS	RANGE	V	SKEW	KURTOSIS
150m.	0.14	+0.21	3.16	150m.	0.18	+0.41	2.45
200m.	0.11	+0.26	3.02	200m.	0.16	+0.20	2.71
650m.	0.14	+0.11	2.85	650m.	0.16	+0.08	2.83

of the prevailing surface wind. This suggests that the probability density functions might also depend on the wind direction and, further, that it might be possible to obtain theoretical models for the PDFs that are functions of wind direction. In order to test this hypothesis, a series of experiments were performed in which 0.8 msec duration raised-cosine pulses were transmitted under shallow-water conditions. The transmitter and receiver of the system were located so that the received signal was comprised of the direct-path signal and a single, essentially non-overlapping surface-reflected path signal. In setting up the system, care was taken in positioning the receiver to ensure that a minimum of interference occurred between the direct and surface-reflected path signals.

Using the test system, the PDFs of the envelopes of the direct-path and surface-reflected-path signals were measured for both perpendicular and parallel-wind conditions, and typical results are shown in FIGURES 3.18 and 3.19. Although FIGURES 3.18 and 3.19 show some 'within curve' fluctuation caused by the coarseness of the quantisation of the signal amplitude range, a comparison of FIGURES 3.18b and 3.19b shows that there is a considerable difference between the PDFs of the envelopes of the surface-reflected-path signals for the two different wind conditions. Under the perpendicular-wind condition, the PDF of the signal envelope appears to resemble a Rayleigh distribution, whereas under the parallel-wind condition, the PDF of the envelope of the surface-reflected-path signal appears to resemble a Rician distribution. These observations may be accounted for from a consideration of scattering theory.

The first point of importance concerns the dependence of the surface-reflected signal on the surface roughness. It has been shown (Beckmann and Spizzichino, 1963) that the PDF of the surface-reflected-

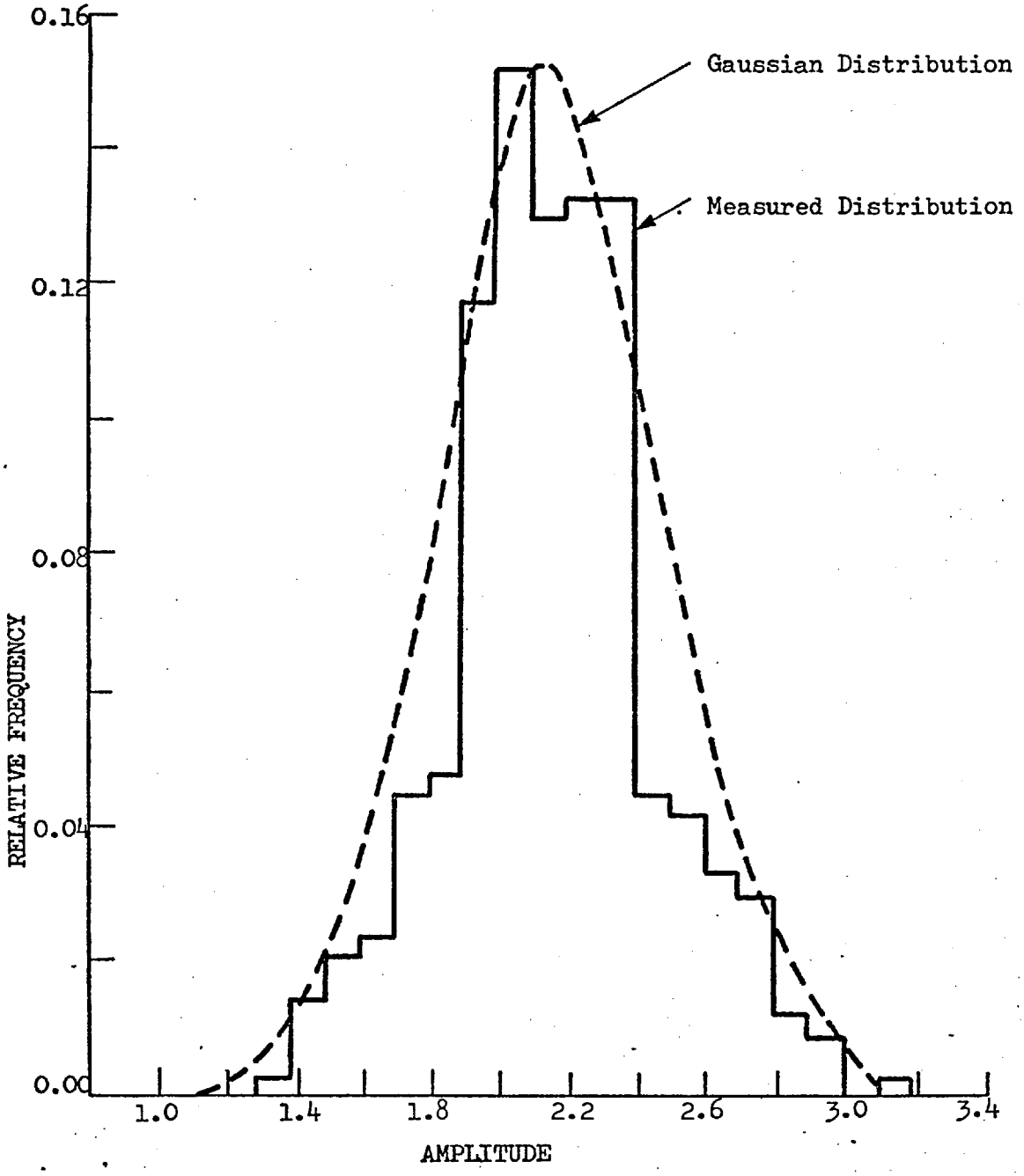


FIGURE 3.18a Direct-Path PDF at 150 metres with a Perpendicular-Wind

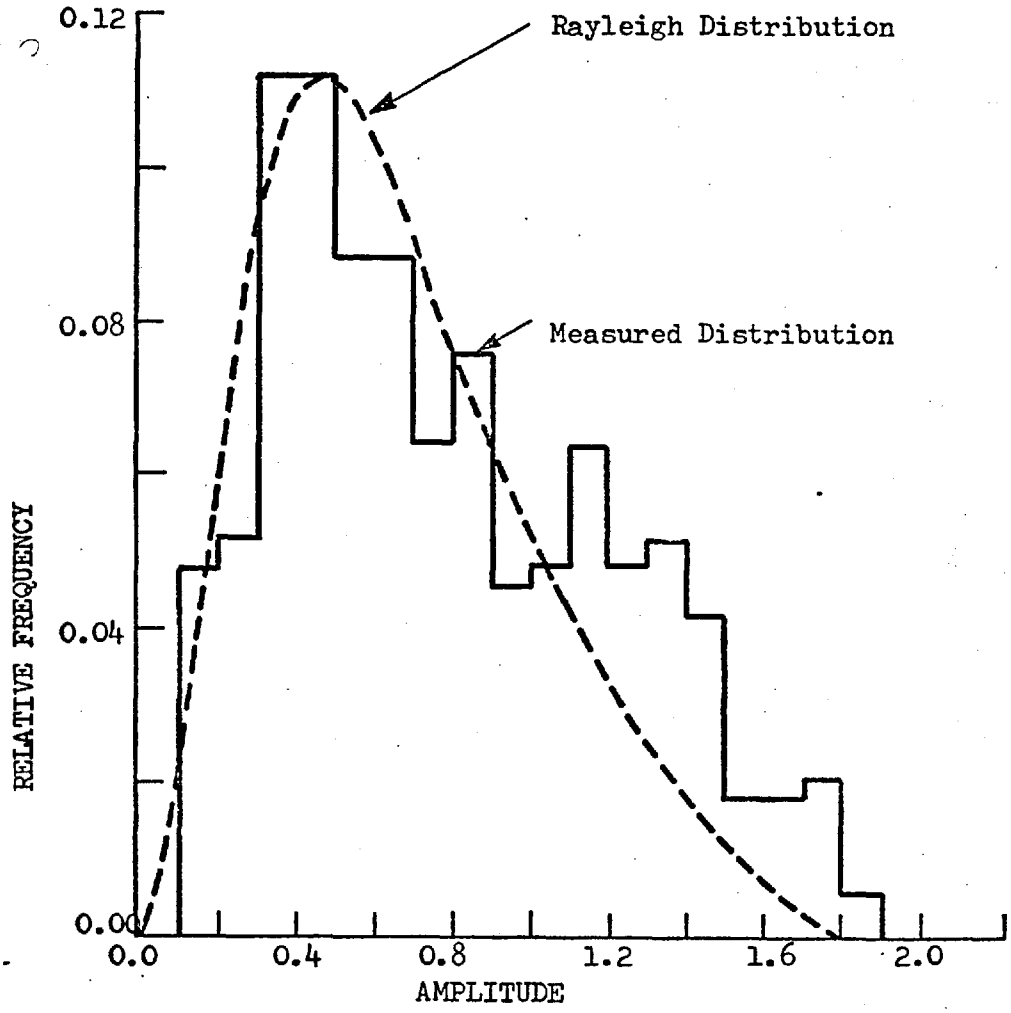


FIGURE 3.18b Surface-Reflected Path PDF at 150 metres with a Perpendicular Wind

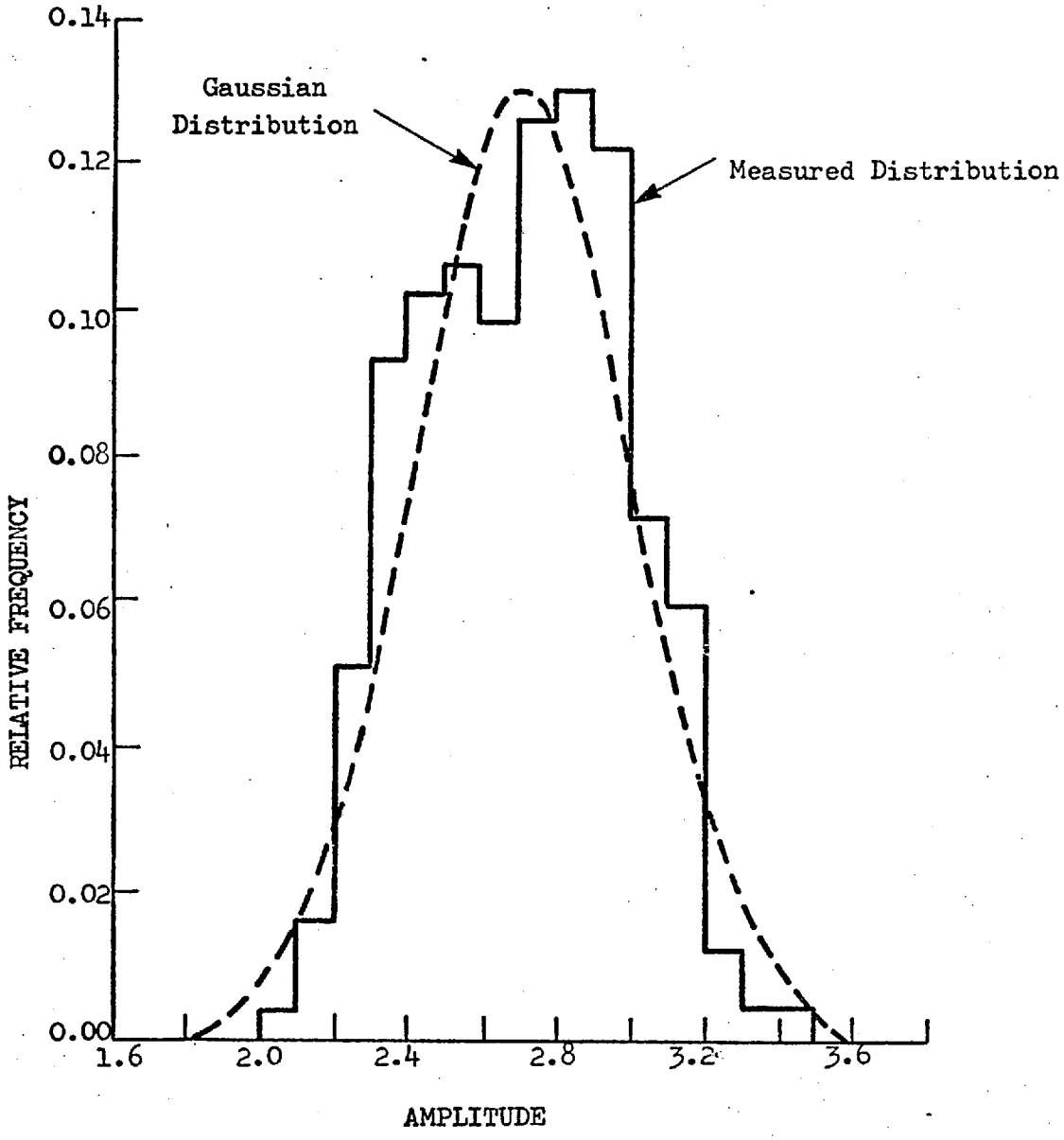


FIGURE 3.19a Direct-Path PDF at 150 metres with a Parallel-Wind

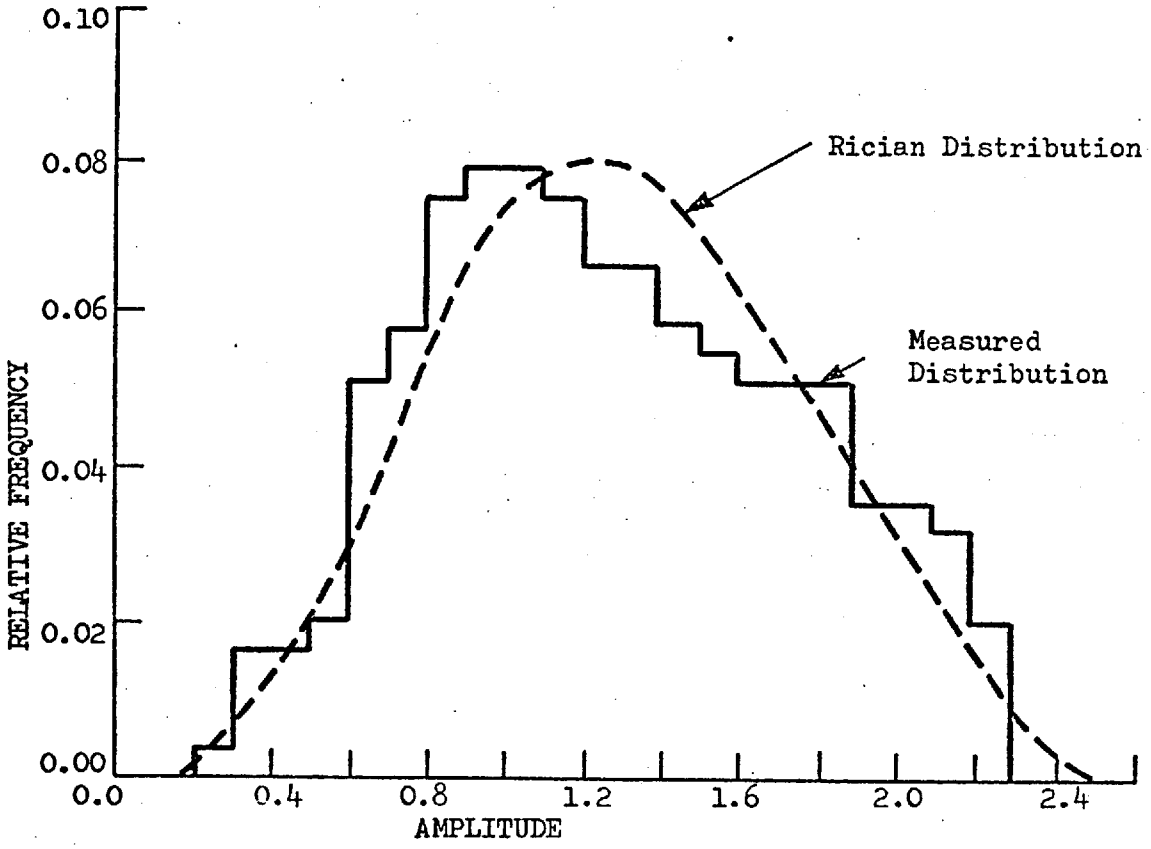


FIGURE 3.19b Surface-Reflected Path PDF at 150 metres with a Parallel-Wind

path signal is dependent upon the roughness of the reflecting surface and that if a roughness parameter, g, is defined to be,

$$g = 4\pi^2 \frac{h^2}{\lambda^2} (\cos\theta_1 + \cos\theta_2)^2 \qquad \ldots\ldots (3.6)$$

where h = r.m.s. wave height

λ = acoustic wavelength

θ_1 = angle of incidence with respect to the vertical

θ_2 = angle of reflection with respect to the vertical

then, for a 'rough' surface (i.e. $g \gg 1$), the scattered pressure in the specular direction ($\theta_1 = \theta_2$) has a zero-mean Gaussian distribution and a corresponding Rayleigh envelope distribution (see Beckmann and Spizzichino, 1963). It has also been shown (Beckmannn and Spizzichino, 1963) that in the case of a 'smooth' surface, in which $g \ll 1$, the scattered pressure consists of a steady component plus a zero-mean Gaussian distributed scattered component. The envelope of such a signal has been given by Rice (1954) and results in the so-called Rician distribution.

The second point of note in explaining the surface-reflected-path signal PDF concerns the dependence of the 'effective' roughness of the surface on wind direction. It has been shown (Medwin, 1967) that the wind direction has an effect on surface scattering and hence the parameter, g, may be influenced by the direction of the surface wind. In the test conditions reported on in this thesis, the angles of incidence and reflection were large. Under these conditions and with a wind parallel to the direction of propagation, the reflecting surface appears to be smooth because the effective scattering surface is reduced and shadowing (see Beckmann and Spizzichino, 1963) thus

occurs. However, under the perpendicular-wind condition, the shadowing effect is not present and the incident signal can therefore be reflected from any point on the surface waves and hence the surface appears to be less smooth than in the parallel-wind case. In short, the overall effect of this phenomenon is to reduce the effective r.m.s. wave height, h, in the parallel-wind case. These considerations indicate that under the prevailing test conditions, the water surface would appear, in effect, to be considerably more rough in the perpendicular-wind case than in the parallel-wind case. Thus, the measured PDFs of the envelope of the surface-reflected-path signals are in agreement with those which would be expected on the basis of scattering theory.

The PDFs of the envelope of the direct-path signals shown in FIGURES 3.18a and 3.19a appear to be Gaussian distributed. These observations can also be explained from a consideration of scattering theory. For the ranges and transmission frequency used in the tests, the direct-path signal, before detection, is comprised of a steady component plus a weakly scattered zero-mean Gaussian distributed component (Skudrzyk, 1957). The resulting envelope of this signal combination has been given, in another context, by Rice (1954), and for the pertaining test conditions, the envelope will approximate to a Gaussian distribution because of the large mean-to-standard deviation ratio (Schwartz, 1970).

If it is assumed that there is a strong interaction (overlap) between the direct-path and the surface-reflected-path signals, and that in fact the received signal is the sum of the constituent signals, then under the parallel-wind condition, the received signal before detection is the sum of two zero-mean independent Gaussian variables

plus two steady components. However, if the relative phase fluctuations between the two steady components are small, then the received signal can be considered as consisting of one steady component plus two zero-mean independent Gaussian variables. The envelope of such a signal results in a Rician distribution of the form,

$$f_1(r) = \frac{r}{\sigma_1^2} \exp\left[-\frac{(r^2+A_1^2)}{2\sigma_1^2}\right] I_o\left(\frac{rA_1}{\sigma_1^2}\right) \qquad \ldots\ldots (3.7)$$

where A_1 = average value of sampled signal envelope*

σ_1 = standard deviation of sampled signal envelope

r = amplitude of sampled signal envelope

$I_o(x)$ = hyperbolic Bessel function of x

If V_1, the coefficient of variation of the distribution, is defined to be,

$$V_1 = \frac{\sigma_1}{A_1} \qquad \ldots\ldots (3.8)$$

and if d_1, which can be regarded as the normalised amplitude, is given by,

$$d_1 = \frac{r}{A_1} \qquad \ldots\ldots (3.9)$$

then the Rician distribution given by Equation (3.7) can be written in the form,

---

* A_1 will be the average value of the Rician distribution under certain conditions. In the experimental tests reported on in this thesis, A_1 is the average value. A detailed discussion is given in APPENDIX A.

$$f_1(d_1)\ f_1(r) = \frac{d_1}{V_1^2 A_1} \exp\left[-\frac{(1+d_1^2)}{2V_1^2}\right] I_o\left(\frac{d_1}{V_1^2}\right) \quad \ldots\ldots (3.10)$$

In the situation in which the wind direction is perpendicular to the direction of signal transmission, the resultant signal, prior to detection, is the sum of two zero-mean independent Gaussian variables plus a steady component. The envelope of this signal is Rician but because of the large mean-to-standard deviation ratios encountered in the perpendicular-wind case (see TABLES 3.1 and 3.2), the PDF of the envelope of the signal can be approximated by a Gaussian distribution (Schwartz, 1970) of the form,

$$f_2(r) = \frac{1}{\sigma_2\sqrt{2\pi}} \exp\left[-\frac{(r-A_2)^2}{2\sigma_2^2}\right] \quad \ldots\ldots (3.11)$$

where A_2 = average value of sampled signal envelope

σ_2 = standard deviation of sampled signal envelope

If, as before, V_2 is defined as,

$$V_2 = \frac{\sigma_2}{A_2} \quad \ldots\ldots (3.12)$$

and d_2 as,

$$d_2 = \frac{r}{A_2} \quad \ldots\ldots (3.13)$$

then Equation (3.11) can be written in the form,

$$f_2(d_2) = f_2(r) = \frac{1}{V_2 A_2\sqrt{2\pi}} \exp\left[-\frac{(d_2-1)^2}{2V_2^2}\right] \quad \ldots\ldots (3.14)$$

To test the accuracy of the PDF models given by Equations (3.10)

and (3.14), a series of tests were carried out at the reservoir over a range of 650 metres. The PDFs of the sampled signal envelope were measured with surface-winds approximately parallel to and perpendicular to the direction of signal transmission. Typical results of the tests are shown in FIGURES 3.20 and 3.21. Also shown on these figures are the respective computed PDFs obtained from Equations (3.10) and (3.14). The computed values were obtained by using the appropriate measured coefficients of variation and mean values. In FIGURE 3.20, a Gaussian distribution of the same mean and standard deviation as the Rician prediction from Equation (3.10) is also indicated. It can be seen that the Rician distribution provides a better fit to the experimental data than does the Gaussian distribution.

The PDF models given by Equations (3.10) and (3.14) have been derived, respectively, for wind directions which were approximately parallel to and approximately perpendicular to the direction of signal transmission. However, in practice, these particular conditions occur relatively infrequently and thus, it is important to know whether the PDF models can be used in the more general situation in which the wind direction is at any angle to the line of transmission. In the next chapter, this question is dealt with by examining system performance in terms of bit-error probabilities. The validity of the proposed PDF models will then be examined in terms of a comparison between the predicted and measured error probabilities.

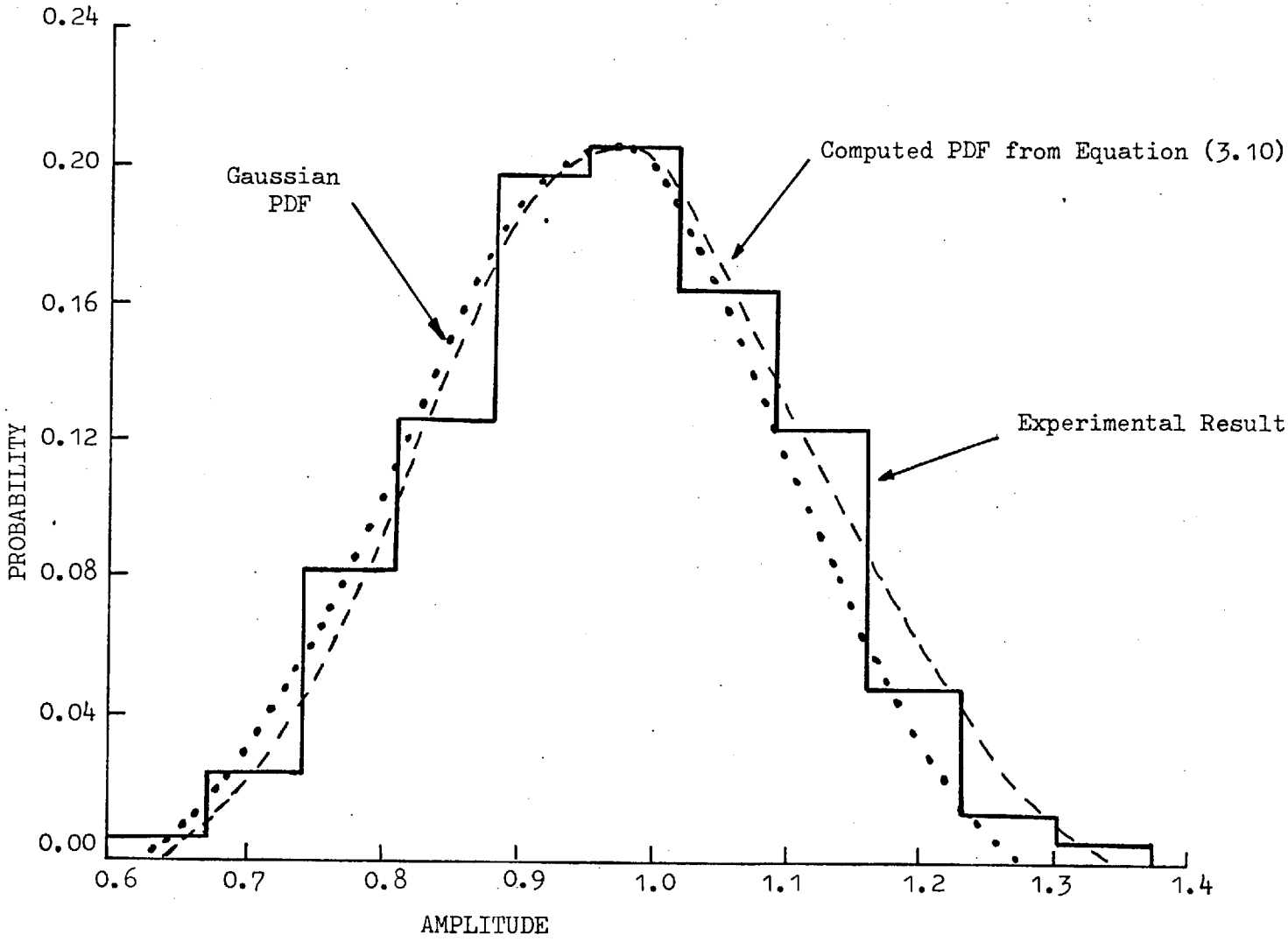


FIGURE 3.20 Comparison ofPredicted and Measured PDFs for the Parallel-Wind Condition

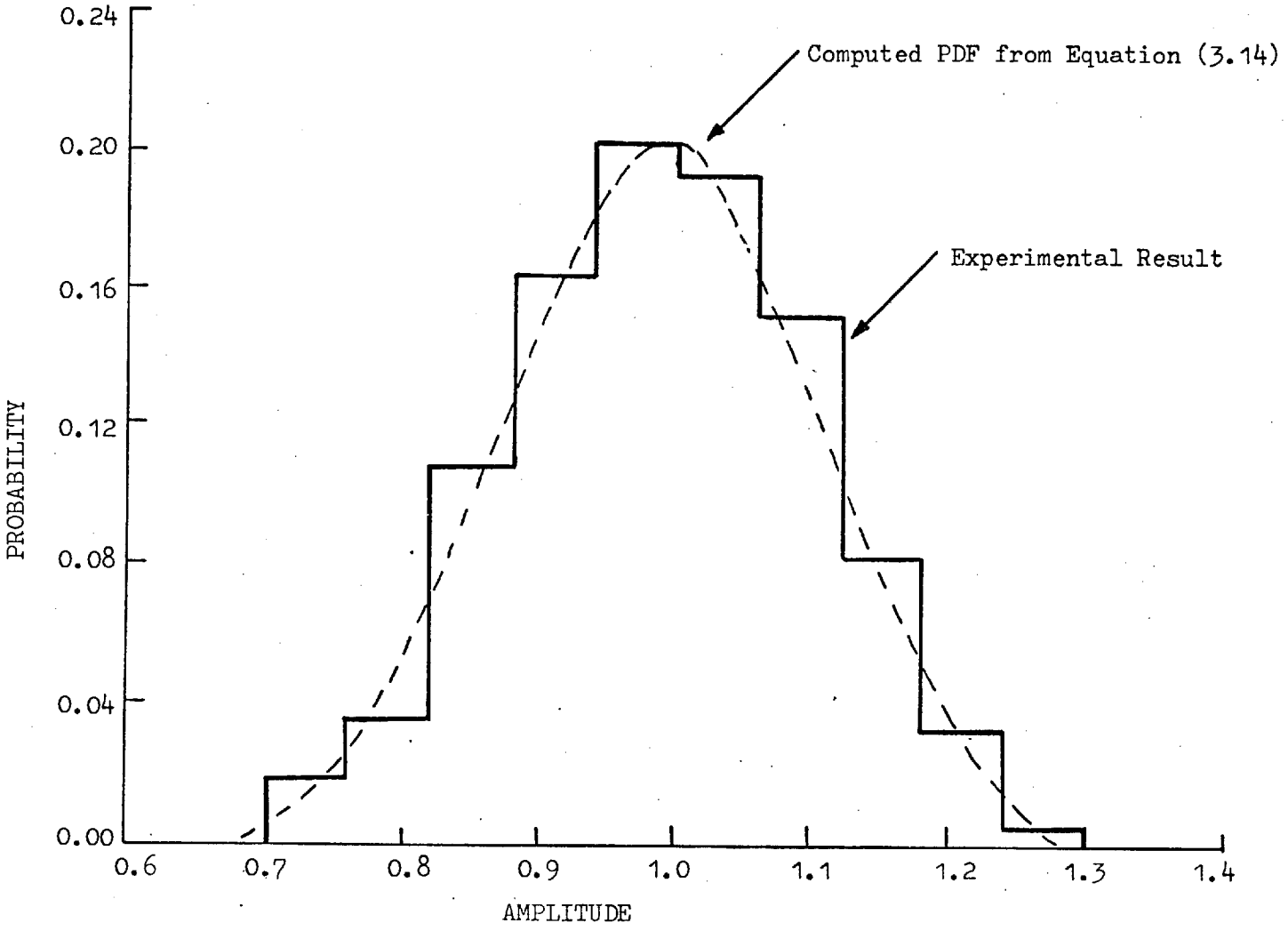


FIGURE 3.21 Comparison of Predicted and Measured PDFs for the Perpendicular-Wind Condition

CHAPTER FOUR

A STUDY OF BIT-ERROR PROBABILITIES

Introduction

In this chapter, the question of the bit-error probability in an underwater data transmission system is considered. Specifically, the results of an extensive series of tests with a data communication system using 'on-off' ASK techniques are presented and analysed. Also, the PDF models developed in Chapter 3 are used in the prediction of bit-error probabilities, and the predicted results are compared with the experimentally measured results. In the last part of the chapter, optimum fixed detection threshold levels are computed from a consideration of the PDF models presented in Chapter 3.

4.1 Test Procedure and Presentation of Results (Andrews and Turner, 1976)

The main sources of error in underwater data communication systems are multipath, signal fluctuations arising from thermal inhomogeneities in the medium, and background thermal noise. The tests reported on in this chapter were designed to provide information about the errors arising from these sources and to provide information about the effects on the bit-error probabilities of such factors as transmitted power, data-pulse width, transmission range, data-rate, and climatic conditions.

The system was tested in the reservoir at Staines during the period from early June 1974 to mid-November 1974. The tests were performed during this period in order to obtain results under a variety of climatic conditions ranging from the warm summer conditions to the much colder, and more constant, water temperature conditions of autumn. In the following presentation of the results of the tests, the experimental data will be divided into two groups - those obtained

during the summer (June to September) and those obtained during the autumn (October and November). The experimental data was grouped in this way on account of the manner in which the temperature-depth profile in the reservoir varied during the test period. During the summer, the temperature-depth profile was observed, from time-to-time, to change considerably within two or three days because of the heating effects of both the sun and the surrounding warm air on the water. However, during the autumn, the water temperature varied little with depth and remained quite constant over a period of several days. An illustration of the variability of the temperature-depth profile measured during the summer is shown in FIGURE 4.1, and results obtained over a similar period during the autumn are shown in FIGURE 4.2. From the figures, it can be seen that there can be considerable change in the temperature-depth profile over a three-day interval in the summer, but little change over a similar period during the autumn. By separating the experimental data into autumn and summer results, it was hoped to obtain more information about the effect of a change in climatic conditions on the measured bit-error probabilities.

A series of tests were carried out at ranges of 150, 200 and 650 metres. The test procedure has been described previously in Chapter 2 and the results which are presented in this chapter are average values obtained by using the methods described in Chapter 2. In obtaining the complete set of results presented in this chapter, the transmitter power was held fixed. The power used in the tests was set at 50 milli-Watts peak. The major results of the tests are shown in FIGURES 4.3 to 4.11. The material of FIGURES 4.3 to 4.6 contains the results of the summer (June to September) tests, and FIGURES 4.7 to 4.11 relate to measurements made during the autumn (October and November)

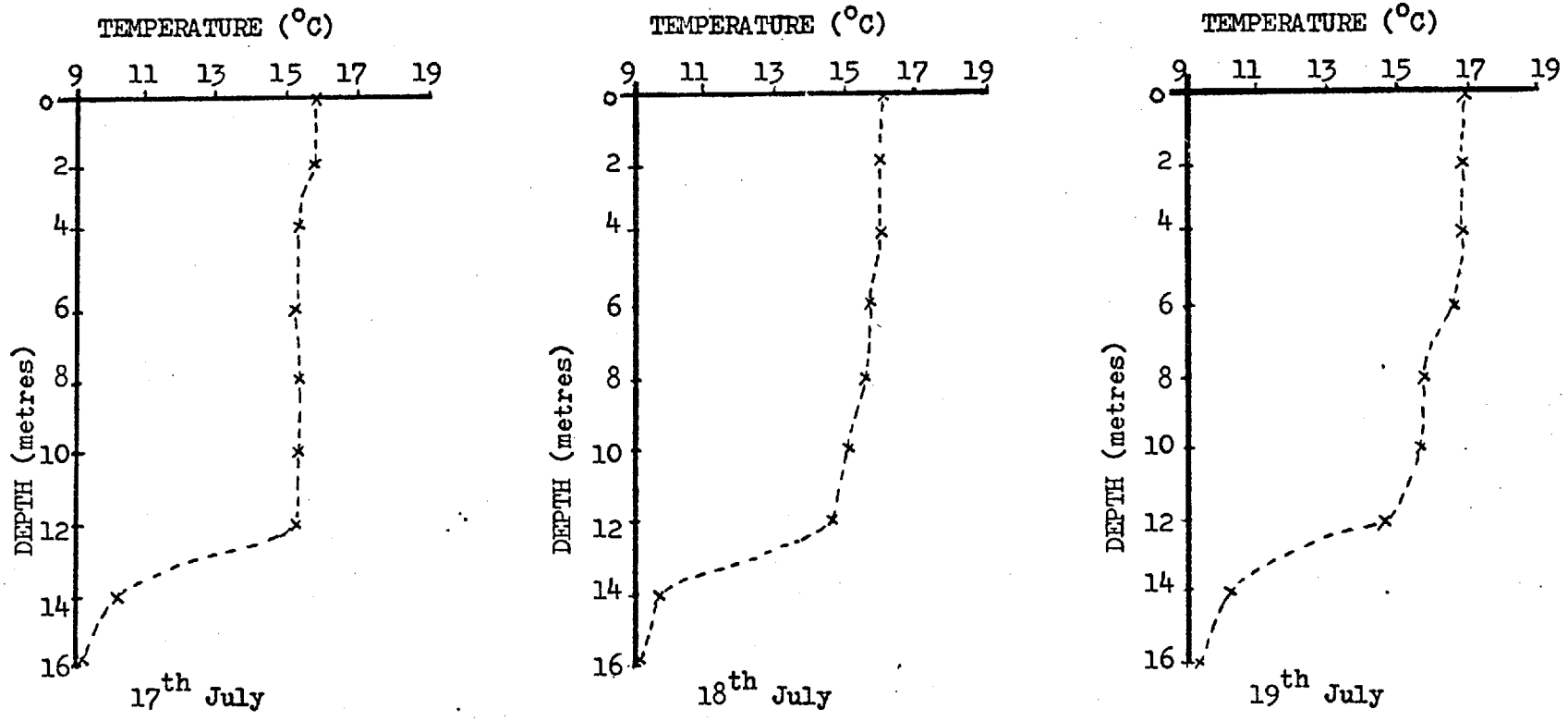


FIGURE 4.1 Typical 3-Day Variation in the Temperature-Depth Profile Measured During Summer

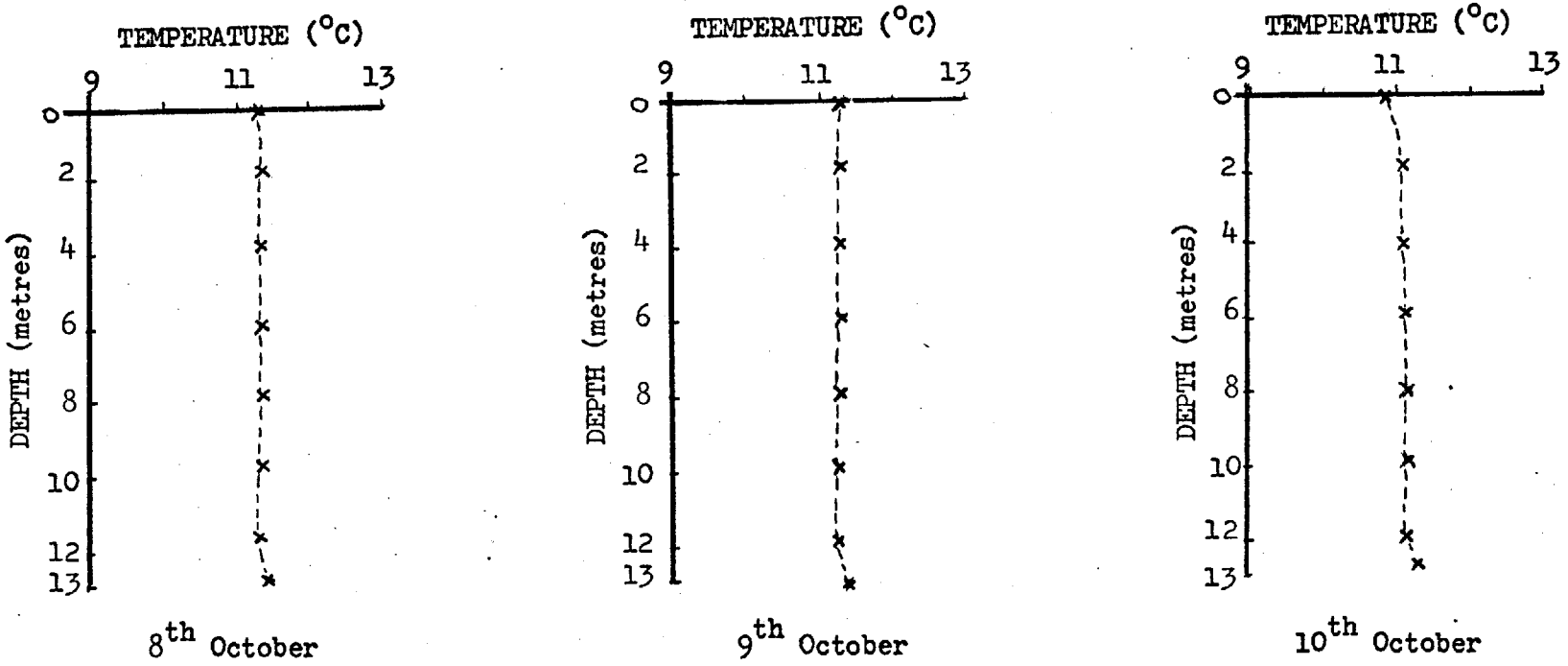


FIGURE 4.2 Typical 3-Day Variation in the Temperature-Depth Profile Measured During Autumn

period.

In FIGURES 4.3 to 4.5, the average probability of bit-error is given as a function of range for data-pulse widths of 0.8, 1.0 and 1.6 msec. The figures provide some indication of the effect of the data-rate on the average error probability. The results contained in FIGURE 4.3 were obtained when information was transmitted with a gap of two data-pulse widths between each data pulse. The results in FIGURE 4.4 were obtained when the gap between adjacent data-pulses was reduced to one pulse width, and the results in FIGURE 4.5 relate to the situation in which there was no gap between adjacent data-pulses. A comparison of FIGURES 4.3 to 4.5 therefore provides some information relating to the effects of pulse dispersion and multipath on the probability of error. More direct information regarding this aspect is to be found in FIGURE 4.6. In the figure, the average probability of bit-error is given as a function of data-rate for various data-pulse widths at a range of 650 metres and with a detection threshold level of $\frac{1}{2}$ of the average received signal level.

The autumn results, which correspond to the summer results contained in FIGURES 4.3 to 4.6, are presented in FIGURES 4.7 to 4.10. In FIGURE 4.11, the average probability of error is given as a function of range for various data-rates while the detection threshold level was held constant at one absolute value for all ranges. In the tests which relate to FIGURE 4.11, the threshold level was held constant at its 650-metre range value.

4.2 Interpretation and Analysis of the Summer Results

From the results contained in FIGURES 4.3 to 4.6, it can be seen that during the summer period, the performance of the data transmission system was somewhat variable. The variability of the system

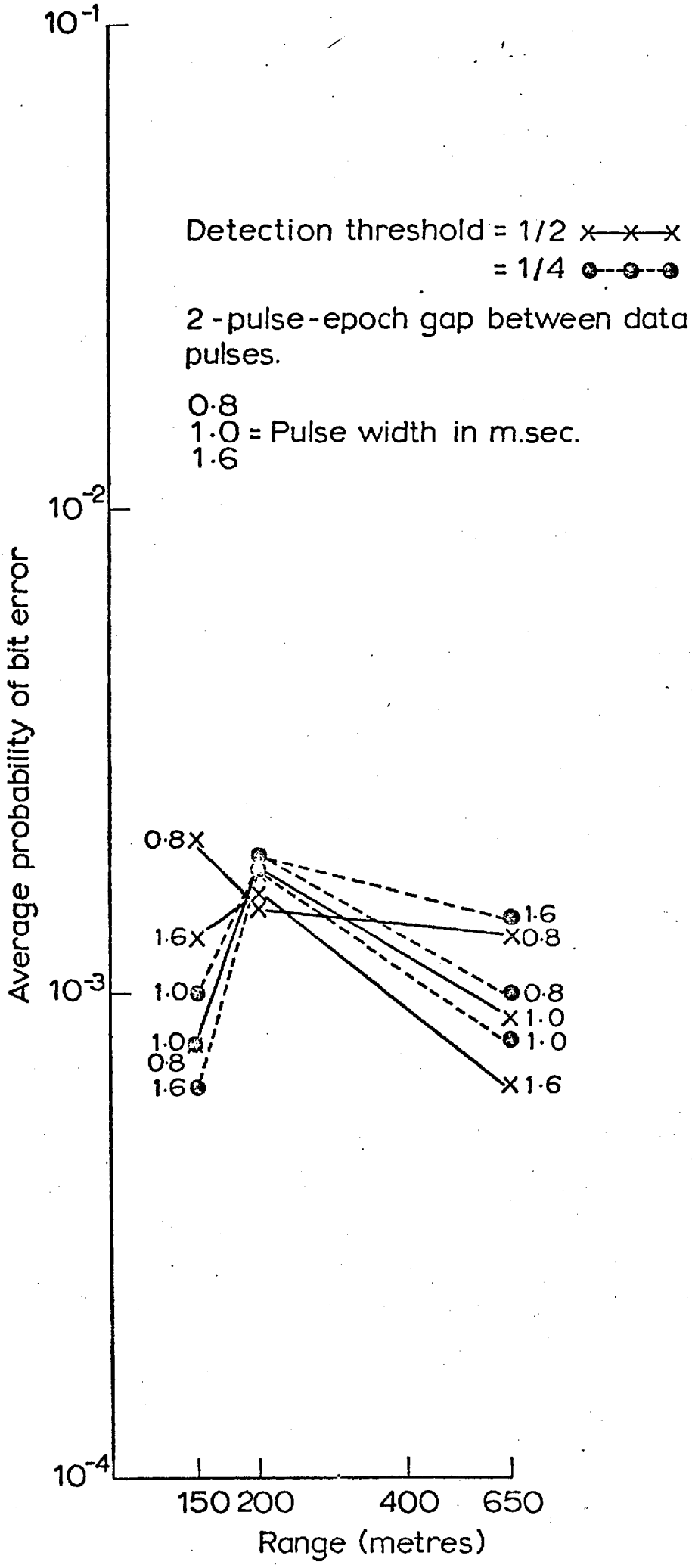


FIGURE 4.3 Average Probability of Bit-Error vs Range During Summer

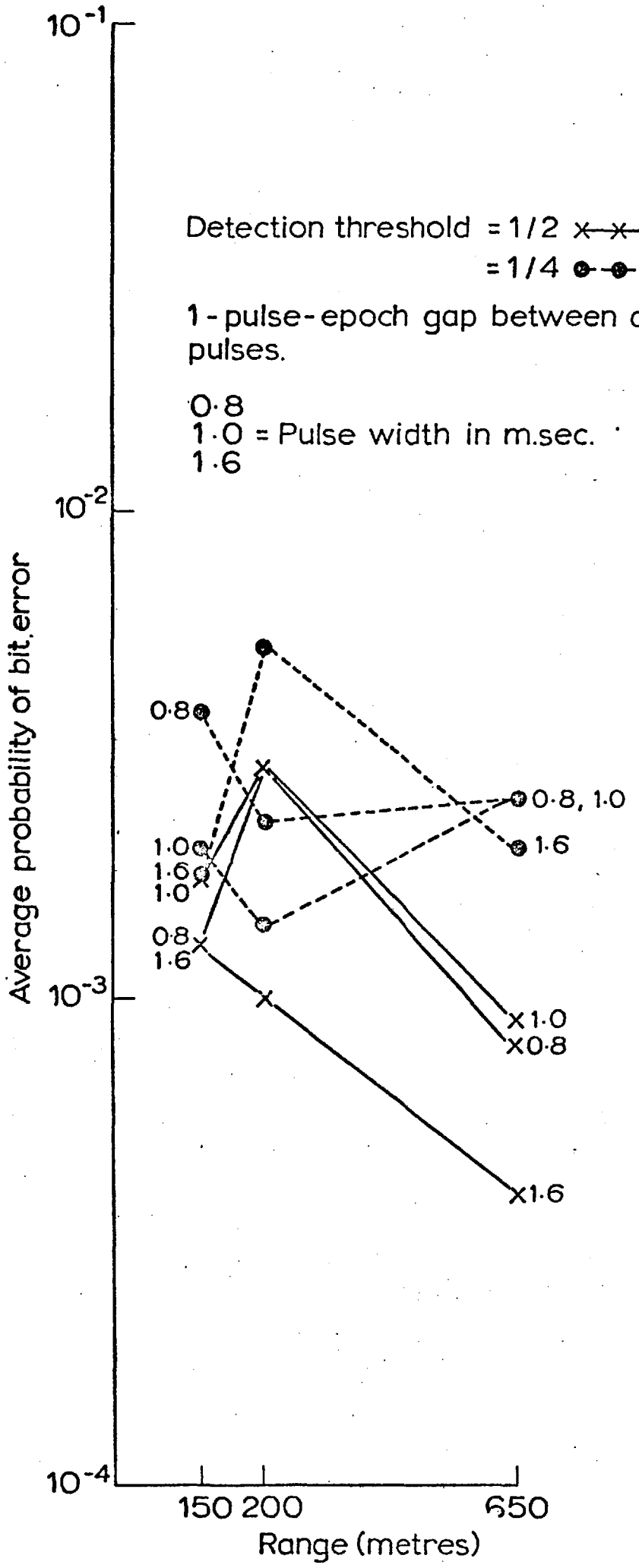


FIGURE 4.4 Average Probability of Bit-Error vs Range During Summer

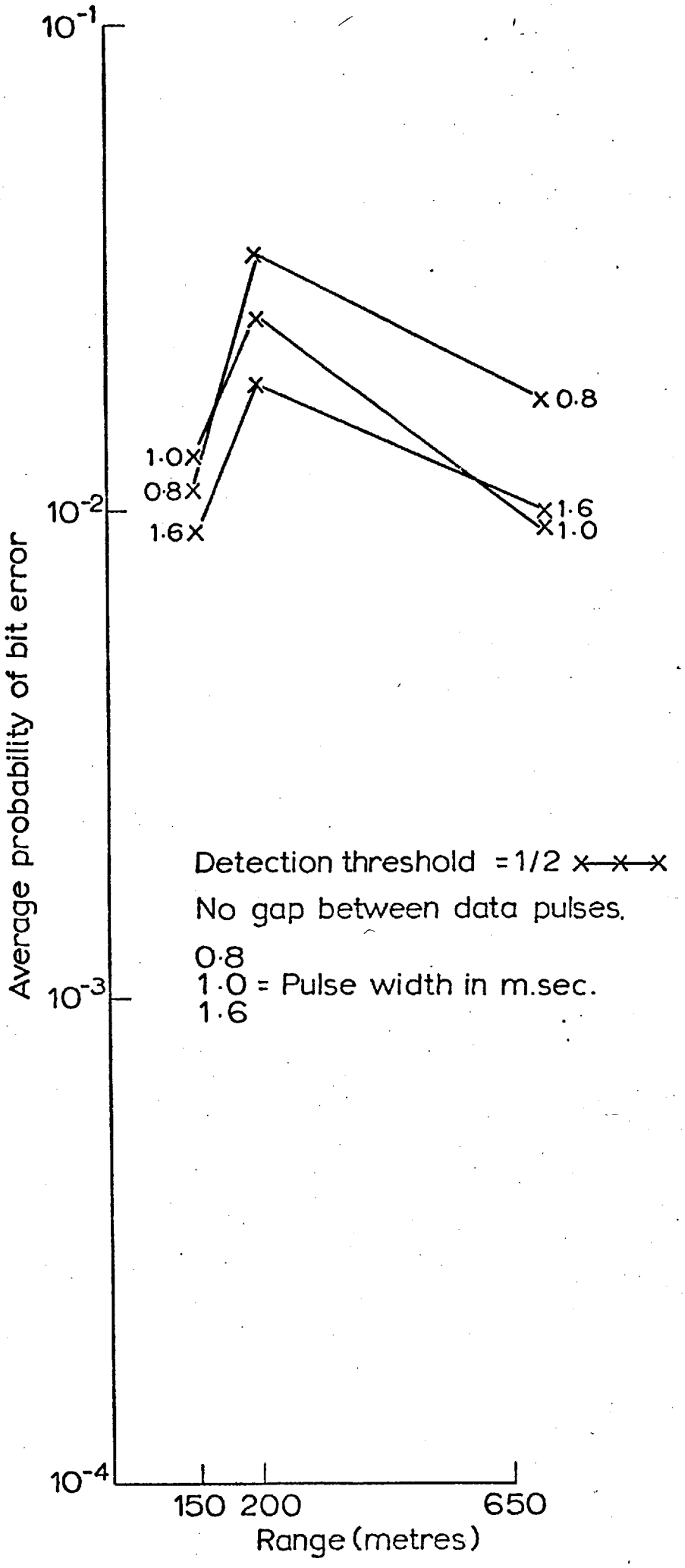


FIGURE 4.5 Average Probability of Bit-Error vs Range During Summer

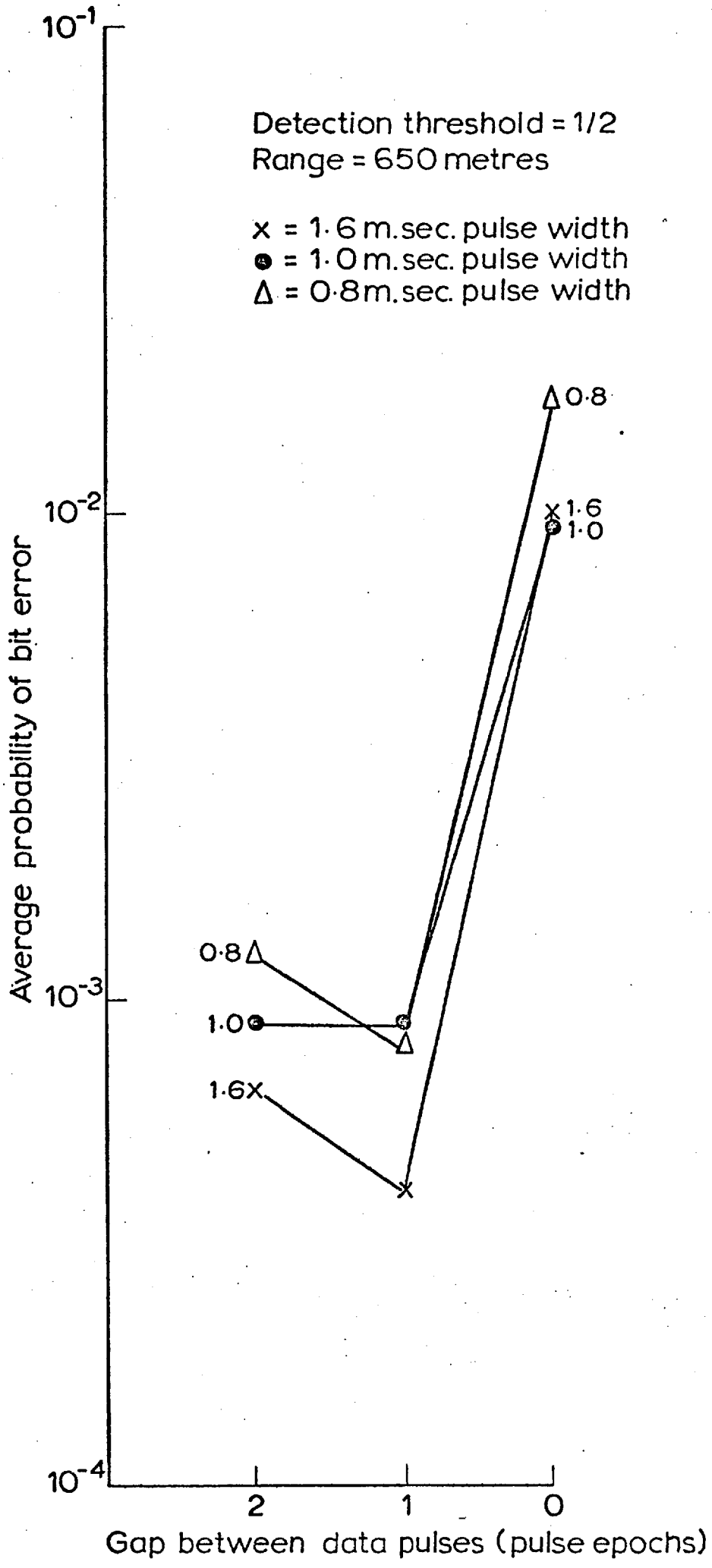


FIGURE 4.6 Average Probability of Bit-Error as a Function of Data-Rate During Summer

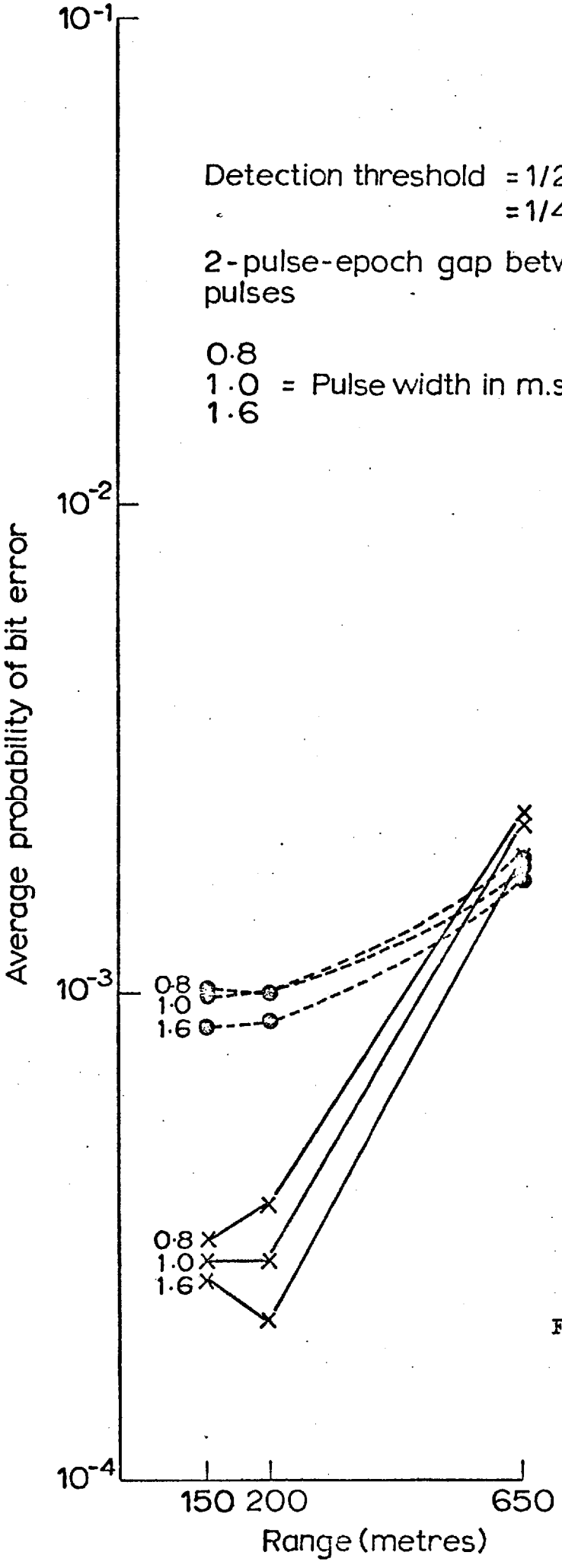


FIGURE 4.7 Average Probability of Bit-Error vs Range During Autumn

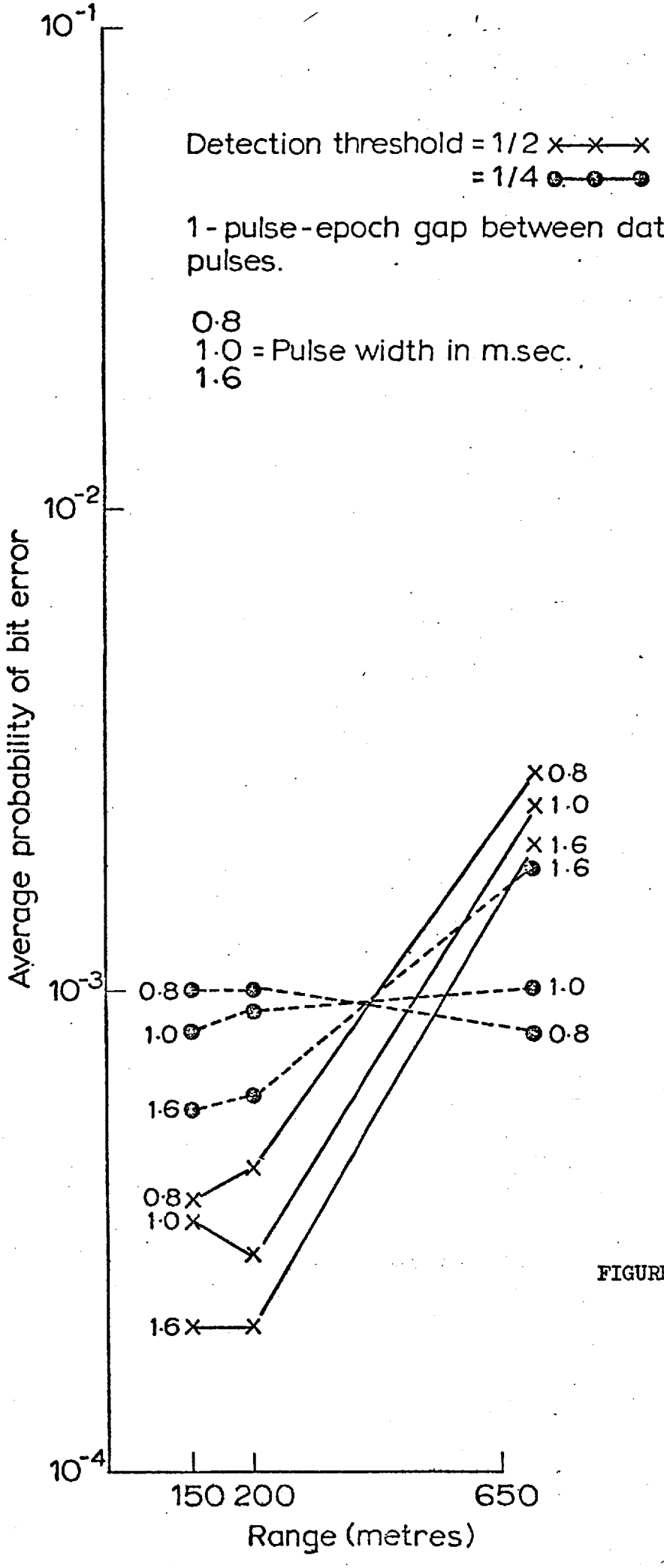


FIGURE 4.8 Average Probability of Bit-Error vs Range During Autumn

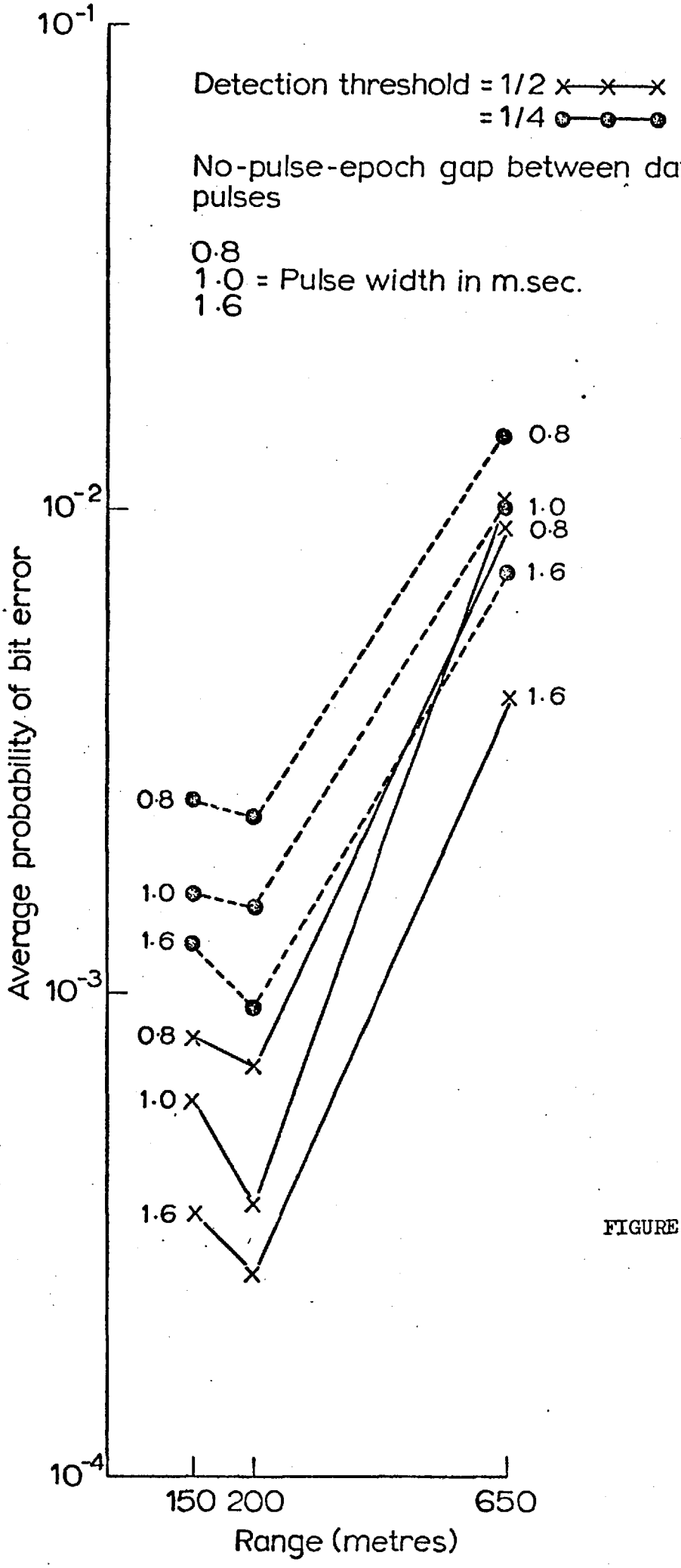


FIGURE 4.9 Average Probability of Bit-Error vs Range During Autumn

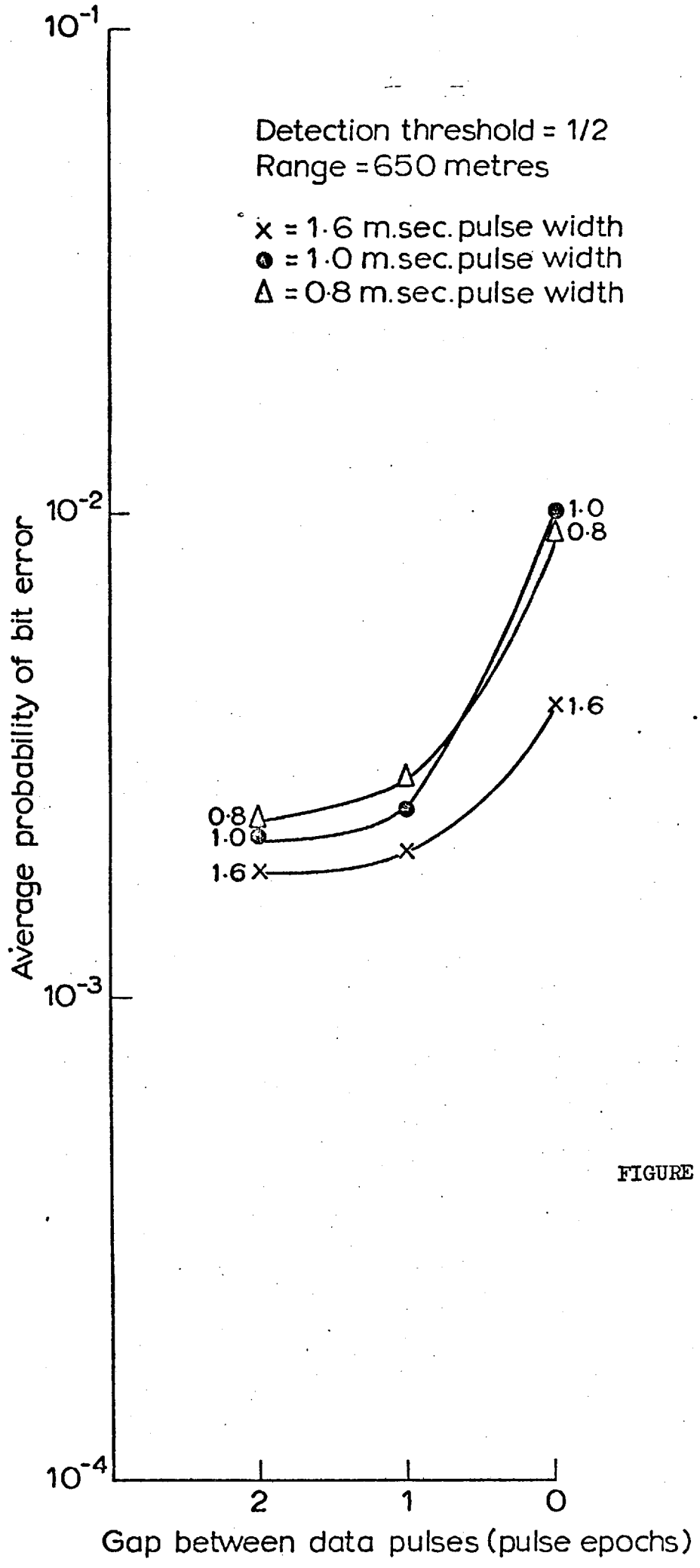


FIGURE 4.10 Average Probability of Bit-Error as a Function of Data-Rate During Autumn

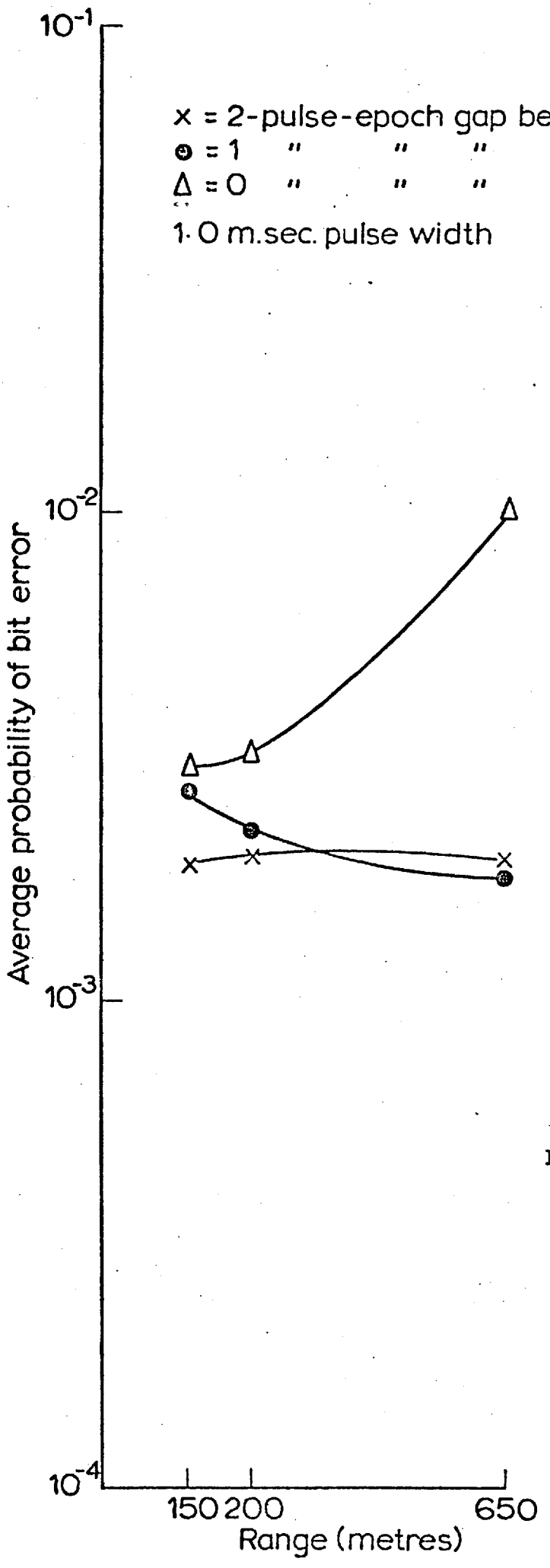


FIGURE 4.11 Average Probability of Bit-Error During Autumn with an Absolute Fixed Threshold

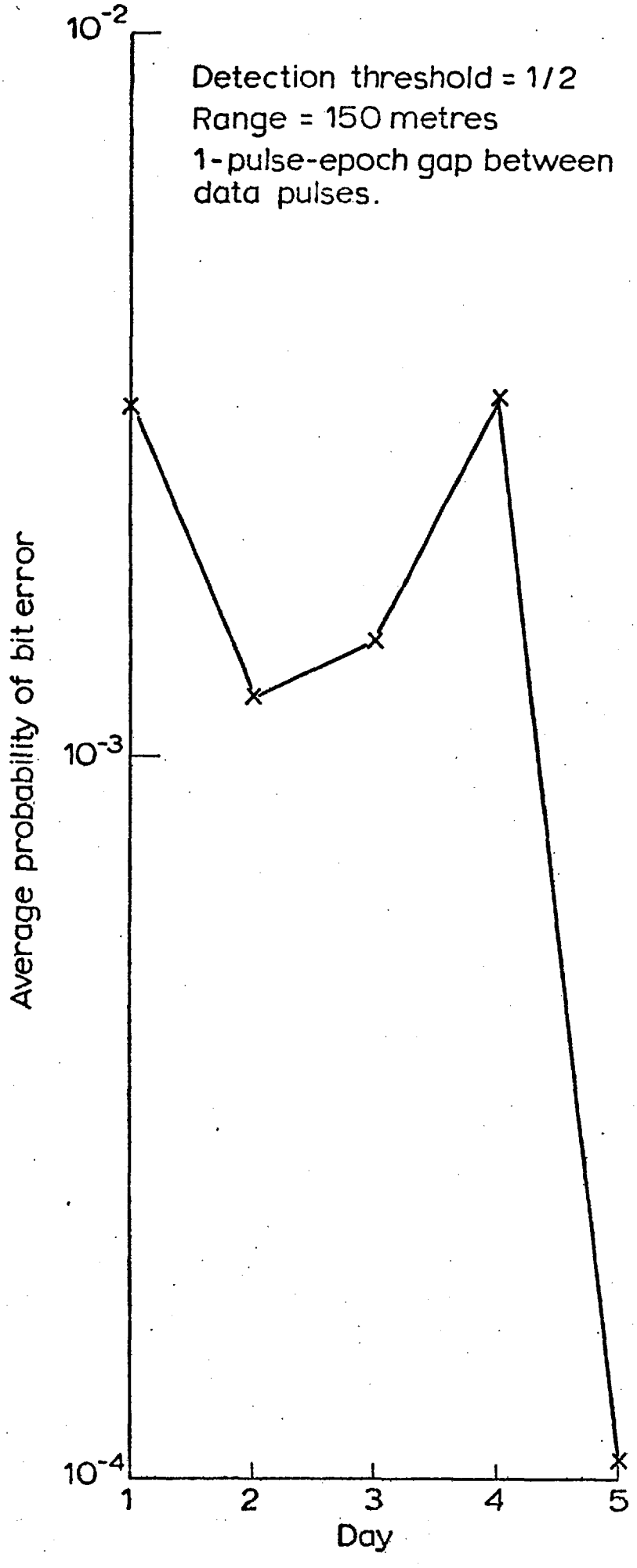


FIGURE 4.12 Daily Variation in System Performance During Summer

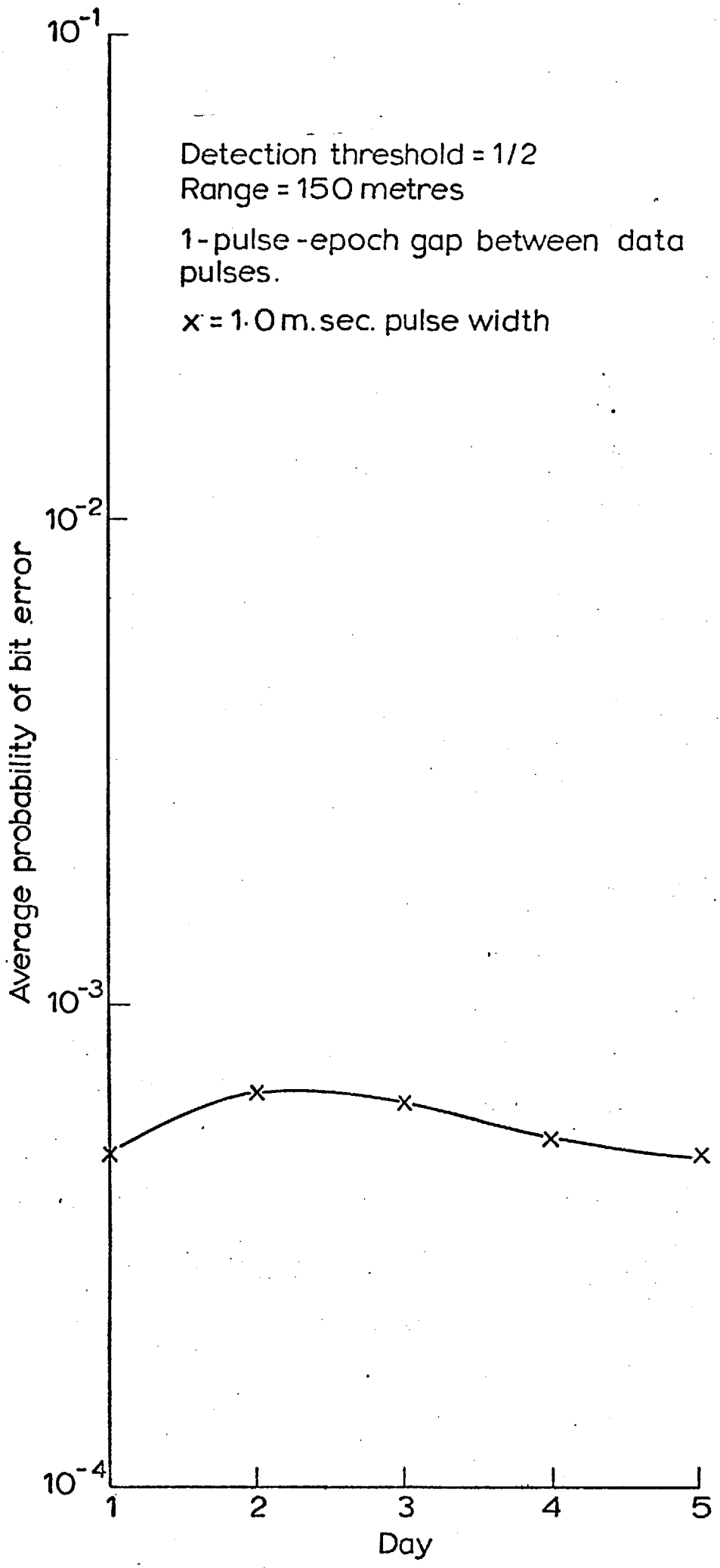


FIGURE 4.13 Daily Variation in System Performance During Autumn

performance during the summer period was found to be associated mainly with the rapidly changing thermal conditions within the reservoir and with the fact that a large mechanical pump was used during the summer to stir the water in the reservoir. Because the thermal characteristics of the reservoir could change considerably within the space of twenty-four hours, marked changes in the refractive index of the medium could result. This would lead to significant changes in the fluctuations of the received signals and thus, a considerable variability in system performance could result. To investigate this aspect further, a study of the performance of the system was examined during an arbitrarily chosen five-day period, and the results of the examination are shown in FIGURE 4.12. From the figure, it can be seen that the measured bit-error probability changed quite significantly during the five-day period.

The material contained in FIGURES 4.3 to 4.5, and more particularly, in FIGURE 4.6, provides information about the way in which the probability of bit-error varies as a function of range and data-pulse width. The figures show that if the gap between data-pulses is increased from one pulse width to two pulse widths, there is virtually no change in the probability of error, but if the gap is reduced to zero, then the probability of bit-error is increased significantly. This increase in the error probability is due to intersymbol interference in the form of multipath propagation. The geometry of the reservoir and the absorbent nature of its bottom were such that the multipath took the form of a single echo from the water surface with the echo spreading into the immediately adjacent pulse epoch.

4.3 Interpretation and Analysis of the Autumn Results

The results contained in FIGURES 4.7 to 4.11 indicate that during

the autumn period, the performance of the data transmission system remained relatively constant, and in many respects, the performance is easier to predict and understand than in the case of the summer results. During the autumn, the thermal conditions within the reservoir changed very little from day to day, and the transmission characteristics of the medium were found to remain correspondingly constant. To investigate the system performance further, as in the summer case, a study of the performance of the system during an arbitrary five-day period was carried out. The results are shown in FIGURE 4.13. The figure reveals that, during the autumn period, the system performance changes very little from day-to-day.

From FIGURES 4.7 to 4.9, it can be seen that in most cases, the bit-error probability tends to increase with increasing range for all data pulse widths and detection thresholds. This trend is to be expected because of the fact that, for a constant transmitter power, the signal-to-noise ratio decreases for increasing range.

The effect of intersymbol interference on the average bit-error probability can be seen in FIGURES 4.7 to 4.9, and more particularly in FIGURE 4.10. A comparison of FIGURES 4.6 and 4.10 shows that during both the summer and autumn periods, there is a sharp increase in the bit-error probability when the gap between adjacent data-pulses is decreased from one pulse width to zero.

An examination of FIGURE 4.11 provides further insight into the performance of the ASK data transmission system. The results shown in the figure were obtained under the condition of a fixed absolute threshold level for all test ranges. In the tests, the threshold level was set at $\frac{1}{2}$ of the received average signal amplitude at the 650-metre range and held constant at this value for all other ranges.

From the figure, it can be seen that the average probability of bit-error remains relatively constant for all ranges. Although the reasons for this fact are not immediately obvious, a consideration of the probability density functions of the background noise and the signal amplitude throw some light on the matter. It will be shown (see Section 4.5) that the optimum detection threshold level varies from approximately 0.45 at 650 metres to about 0.15 at 150 metres, and that the PDFs of the received signal amplitude vary in a manner illustrated in FIGURE 4.14. It has been found, experimentally, that the errors due to false dismissals tend to remain fairly constant for all test ranges. This is illustrated by areas A and B in the example PDFs shown in FIGURE 4.14.

The effect of the receiver detection threshold on the average bit-error probability can be observed from FIGURES 4.7 to 4.9. From the figures, it can be seen that at the 150-metre range, a threshold of $\frac{1}{2}$ produces a lower bit-error probability than does a threshold level of $\frac{1}{4}$, but at the 650-metre range, the opposite tends to be true. It is not clear, at this time, why this should be so. The difference in results obtained with the two thresholds is quite small for each range and it does not appear possible to draw any firm conclusions from the measurements. Similar types of rather inconclusive results have been obtained during the summer period, as illustrated in FIGURES 4.3 to 4.6.

The autumn results presented in FIGURES 4.7 to 4.11 show that, irrespective of the range, the data-rate, and the detection threshold, the probability of bit-error decreases slightly with increasing data-pulse width. However, further tests have shown that if the data-pulse width is increased beyond 1.6 msec to 2.0 msec, then there is no further reduction in the bit-error probability. The slight improvement resulting from the use of wide pulse widths can be explained in terms

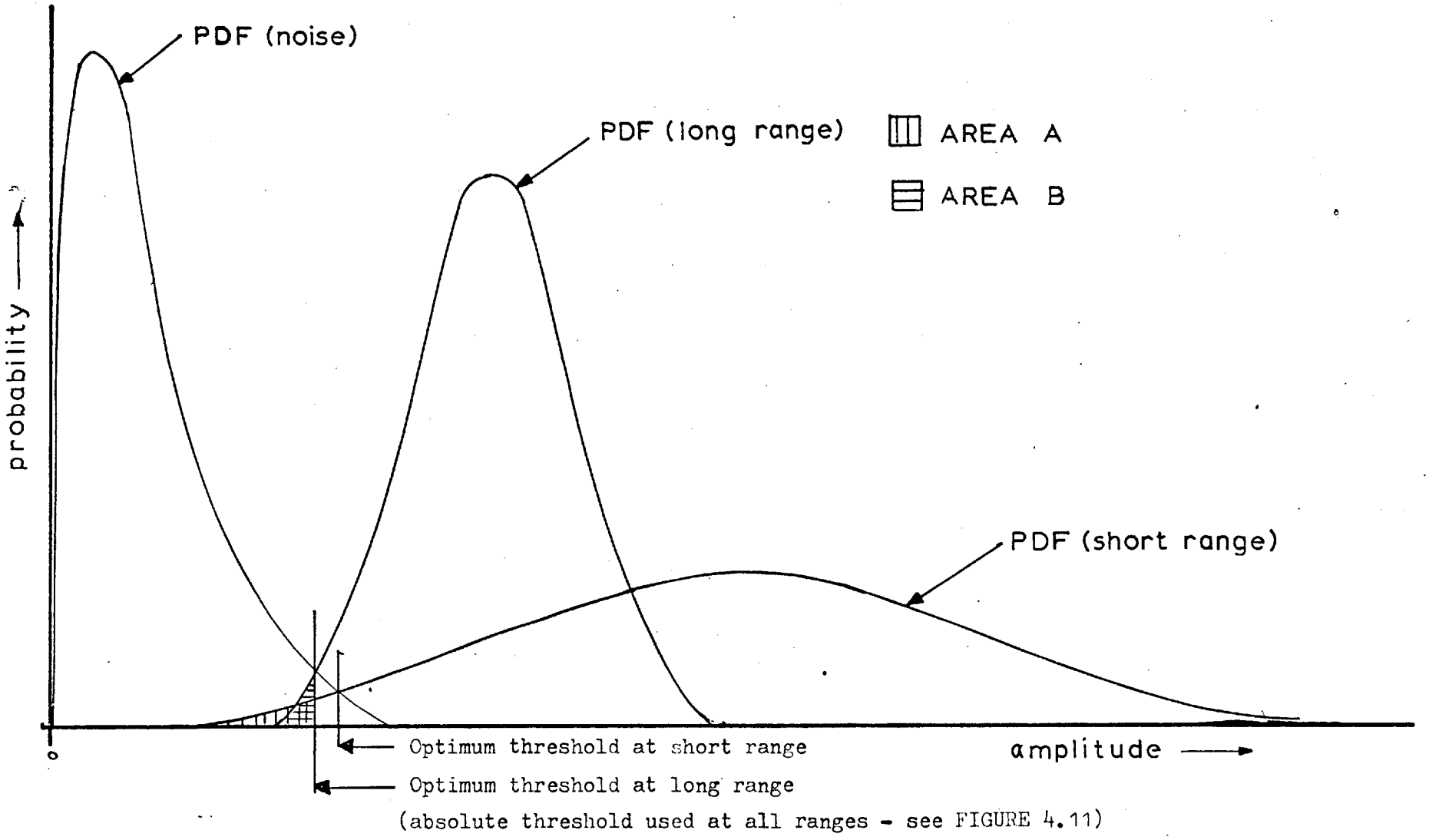


FIGURE 4.14 Illustration of the Variation of the Signal PDFs with Range

of the slight timing jitter and pulse amplitude fluctuations that were observed during the tests. The operation of the sampling pulse in the error-counting section of the receiver was governed by the bit-synchroniser circuit. The synchroniser was capable of adjusting the receiver clock in 50 μsec increments and this resulted in a timing jitter in the sampling operation. Narrow pulse-width systems, in which the decisions are taken by sampling the received data pulse and comparing the sample amplitude with a threshold, are more sensitive to the combination of timing jitter and amplitude fluctuations than are systems using wider pulses. It will be observed from FIGURES 4.7 to 4.11 that the improvement resulting from increasing the data-pulse width is only slight, and the reduction in data-rate that results from increasing the data-pulse width would be hard to justify in a practical data transmission system.

4.4 A Comparison of Predicted and Measured Bit-Error Probabilities

It is useful to be able to predict, theoretically, the performance of the underwater data transmission system in terms of the average bit-error probability. In order to do so, a knowledge of both the noise PDF and the signal-plus-noise PDF is required. In Chapter 3, two PDF models of the sampled signal amplitude fluctuations were derived based on wind directions which were approximately perpendicular and parallel to the direction of transmission. Since these specific conditions will occur relatively infrequently, it is important to know whether the PDF models derived in Chapter 3 can be used in the more general situation in which the wind direction is at any angle to the line of transmission. In this section, the performance of the ASK system is examined in terms of the predicted and measured average bit-error probabilities.

If the data transmission rate is sufficiently slow, then inter-

symbol interference effects can be avoided. In the test system, which is described in Chapter 2, a form of envelope detection was used in the data receiver. The average probability of error in a binary communication system in which envelope detection is used in the receiver can be written in the form,

$$P(e) = P_{fa}(e) + P_{fd}(e)$$

$$= P_o \int_T^{\infty} f_n(r)dr + P_1 \int_0^T f_s(r)dr \qquad \ldots\ldots (4.1)$$

where $P_{fa}(e)$ and $P_{fd}(e)$ are the false alarm and false dismissal probabilities respectively; P_1 and P_o are the a priori probabilities of a binary 'one' and a binary 'zero' respectively; $f_n(r)$ is the PDF of the demodulated noise; $f_s(r)$ is the PDF of the signal-plus-noise; and T is the detection threshold level.

For envelope detection, the demodulated noise PDF will be a Rayleigh distribution.* In the underwater data transmission system used in the tests, a 5% carrier was transmitted when a binary 'zero' was sent. The resulting demodulated output of the receiver in this case would not be Rayleigh distributed but Rician distributed (Rice, 1954). However, the amount of carrier present when a binary 'zero' is transmitted is small and the resulting PDF can be approximated by a Rayleigh distribution of the form,

$$f_n(r) = \frac{r}{N_o^2} \exp\left[-\frac{r^2}{2N_o^2}\right] \qquad \ldots\ldots (4.2)$$

where N_o^2 is the noise power.

* This is the case for true 'ON/OFF' ASK systems.

In the case of a perpendicular, or cross wind condition, the PDF of the envelope of the received signal is a Gaussian distribution of the form given by Equation (3.11). If Equations (3.11) and (4.2) are substituted into (4.1), then the cross-wind error probability can be written in the form,

$$P_{cw}(e) = P_o \int_{r=T}^{\infty} \frac{r}{N_o^2} \exp\left[-\frac{r^2}{2N_o^2}\right] dr + P_1 \int_{o}^{T} \frac{1}{\sigma_2\sqrt{2\pi}} \exp\left[-\frac{(r-A_2)^2}{2\sigma_2^2}\right] dr \quad \ldots\ldots (4.3)$$

It is helpful in evaluating Equation (4.3) to normalise the coordinate r by setting

$$x = \frac{r}{N_o} \quad \ldots\ldots (4.4)$$

If this is done, then Equation (4.3) can be re-written as,

$$P_{cw}(e) = P_o \int_{x=T/N_o}^{\infty} x \exp\left[-\frac{x^2}{2}\right] dx + P_1 \int_{o}^{T/N_o} \frac{N_o}{\sigma_2\sqrt{2\pi}} \exp\left[-\frac{(xN_o - A_2)^2}{2\sigma_2^2}\right] dx \quad \ldots\ldots (4.5)$$

Consider next, that part of Equation (4.5) which constitutes the false alarm probability, $P_{fa}(e)$, where

$$P_{fa}(e) = P_o \int_{x=T/N_o}^{\infty} x \exp\left[-\frac{x^2}{2}\right] dx \quad \ldots\ldots (4.6)$$

The integral given by Equation (4.6) can be solved as follows:

$$P_{fa}(e) = -P_o \exp\left(-\frac{x^2}{2}\right)\Bigg|_{T/N_o}^{\infty}$$

$$= -P_o\left[0 - \exp\left(-\frac{T^2}{2N_o^2}\right)\right]$$

$$= P_o \exp\left[-\frac{T^2}{2N_o^2}\right] \qquad \ldots\ldots (4.7)$$

If the peak signal-to-RMS noise ratio is defined as,

$$\beta = \frac{A_2^2}{N_o^2} \qquad \ldots\ldots (4.8)$$

and if d_2, the normalised threshold, is defined as,

$$d_2 = \frac{T}{A_2} \qquad \ldots\ldots (4.9)$$

then Equation (4.7) can be written in the form

$$P_{fa}(e) = P_o \exp\left[-\beta\frac{d_2^2}{2}\right] \qquad \ldots\ldots (4.10)$$

The false dismissal probability, $P_{fd}(e)$, which is the part of Equation (4.5) given by,

$$P_{fd}(e) = P_1\int_{x=o}^{x=T/N_o} \frac{N_o}{\sigma_2\sqrt{2\pi}} \exp\left[-\frac{(xN_o - A_2)^2}{2\sigma_2^2}\right]dx \qquad \ldots\ldots (4.11)$$

can also be further simplified. If y is defined as,

$$y = \frac{(xN_o - A_2)}{\sigma_2\sqrt{2}} \qquad \ldots\ldots (4.12)$$

then by substitution of (4.12) into (4.11), $P_{fd}(e)$ becomes,

$$P_{fd}(e) = P_1 \int_{y=\frac{-A_2}{\sigma_2\sqrt{2}}}^{y=\frac{T-A_2}{\sigma_2\sqrt{2}}} \frac{1}{\sqrt{\pi}} \exp(-y^2)\, dy \qquad \ldots\ldots (4.13)$$

Equation (4.13) may be further simplified by the consideration of the symmetry properties of a Gaussian distribution. If ARG is defined to be,

$$ARG = \frac{1}{\sqrt{\pi}} \exp(-y^2) \qquad \ldots\ldots (4.14)$$

then,

$$P_{fd}(e) = P_1 \int_{y=\frac{-A_2}{\sigma_2\sqrt{2}}}^{y=\frac{T-A_2}{\sigma_2\sqrt{2}}} ARG\, dy \qquad \ldots\ldots (4.15)$$

The total area under a normalised Gaussian distribution is, therefore,

$$\int_{-\infty}^{\frac{-A_2}{\sigma_2\sqrt{2}}} ARG\, dy + \int_{\frac{-A_2}{\sigma_2\sqrt{2}}}^{\frac{T-A_2}{\sigma_2\sqrt{2}}} ARG\, dy + \int_{\frac{T-A_2}{\sigma_2\sqrt{2}}}^{+\infty} ARG\, dy = 1 \qquad \ldots\ldots (4.16)$$

If the complementary error function is defined as,

$$erfc(w) = \frac{2}{\sqrt{\pi}} \int_{w}^{\infty} \exp(-t^2)\, dt \qquad \ldots\ldots (4.17)$$

then Equation (4.16) can be expressed as,

$$\int_{y=\frac{-A_2}{\sigma_2\sqrt{2}}}^{y=\frac{T-A_2}{\sigma_2\sqrt{2}}} \text{ARG} \;=\; 1 - \tfrac{1}{2}\text{erfc}\left(\frac{T - A_2}{\sigma_2\sqrt{2}}\right) - \int_{-\infty}^{y=\frac{-A_2}{\sigma_2\sqrt{2}}} \text{ARG} \qquad \ldots\ldots (4.18)$$

Moreover, if the value of $-A_2/\sigma_2\sqrt{2}$ is sufficiently large (i.e. a high signal-to-noise ratio), then the last integral in Equation (4.18) becomes very small, or in other words,

$$\int_{-\infty}^{y=\frac{-A_2}{\sigma_2\sqrt{2}}} \text{ARG} \longrightarrow 0 \qquad \ldots\ldots (4.19)$$

By using the identity,

$$\text{erfc}(-x) \;=\; 2 - \text{erfc}(x) \qquad \ldots\ldots (4.20)$$

the false dismissal probability can be written in the form,

$$P_{fd}(e) \;=\; P_1\left[\tfrac{1}{2}\text{erfc}\left(\frac{(A_2-T)}{\sigma_2\sqrt{2}}\right)\right] \qquad \ldots\ldots (4.21)$$

On setting $T = A_2 d_2$ and $V_2 = \sigma_2/A_2$, it follows that

$$P_{fd}(e) \;=\; P_1\left[\tfrac{1}{2}\text{erfc}\left(\frac{(1-d_2)}{V_2\sqrt{2}}\right)\right] \qquad \ldots\ldots (4.22)$$

Thus, the average probability of error in the perpendicular-wind case can be given as,

$$P_{cw}(e) \;=\; P_o\left[\exp\left(-\frac{d_2^2}{2}\beta\right)\right] \;+\; P_1\left[\tfrac{1}{2}\text{erfc}\left(\frac{(1-d_2)}{V_2\sqrt{2}}\right)\right] \ldots\ldots (4.23)$$

In the case of a wind which is parallel to the direction of transmission, the PDF of the envelope of the signal is a Rician distribution as given by Equation (3.7). By substitution, the parallel-wind bit-error probability, $P_{pw}(e)$, is

$$P_{pw}(e) = P_o \int_{r=T}^{\infty} \frac{r}{N_o^2} \exp\left[-\frac{r^2}{2N_o^2}\right] dr + P_1 \int_{o}^{r=T} \frac{r}{\sigma_1^2} \exp\left[-\frac{(r^2+A_1^2)}{2\sigma_1^2}\right] I_o\left(\frac{rA_1}{\sigma_1^2}\right) dr \quad \ldots\ldots (4.24)$$

The false alarm probability, which is given by the first integral in Equation (4.24), is of the form similar to Equation (4.10) and can be expressed as,

$$P_{fa}(e) = P_o \exp\left[-\frac{\beta}{2} d_1^2\right] \quad \ldots\ldots (4.25)$$

where $d_1 = T/A_1$.

The false dismissal probability can be expressed in the form of the Q-function (Marcum, 1950), where the Q-function is defined as,

$$Q\{a,b\} = \int_{b}^{\infty} v \exp\left[-\frac{(a^2+v^2)}{2}\right] I_o(av)\, dv \quad \ldots\ldots (4.26)$$

If $$v = \frac{r}{\sigma_1}$$

and $$a = \frac{A_1}{\sigma_1} \quad \ldots\ldots (4.27)$$

then the false dismissal probability, which is the second integral in Equation (4.24), can be expressed in the form,

$$P_{fd}(e) = P_1 \int_0^{V=\frac{T}{\sigma_1}} v \exp\left[-\frac{(a^2+v^2)}{2}\right] I_o(av)\, dv \qquad \ldots\ldots (4.28)$$

Equation (4.28) is simply $\left(1 - Q\left\{a, T/\sigma_1\right\}\right)$ and hence,

$$P_{fd}(e) = P_1\left[1 - Q\left\{a, \frac{T}{\sigma_1}\right\}\right] \qquad \ldots\ldots (4.29)$$

If $V_1 = \sigma_1/A_1$ and $d_1 = T/A_1$, then

$$P_{fd}(e) = P_1\left[1 - Q\left\{\frac{1}{V_1}, \frac{d_1}{V_1}\right\}\right] \qquad \ldots\ldots (4.30)$$

Thus, the average probability of bit-error in the parallel-wind case is given by,

$$P_{pw}(e) = P_o\left[\exp\left(-\frac{\beta}{2} d_1^2\right)\right] + P_1\left[1 - Q\left\{\frac{1}{V_1}, \frac{d_1}{V_1}\right\}\right] \qquad \ldots\ldots (4.31)$$

The perpendicular-wind and parallel-wind error probabilities (Equations (4.23) and (4.31) are expressed in terms of the peak signal-to-r.m.s. noise ratio, β, the coefficients of variation, V_1 and V_2, and the normalised detection thresholds, d_1 and d_2. By using suitable values for these parameters, it is possible to compute average bit-error probabilities for both the perpendicular-wind and parallel-wind propagation conditions. Since $T = dA$, a particular value of d represents the detection threshold normalised to the average signal amplitude, A. In the results which follow, a value of $d_1 = d_2 = 0.5$ was used in the computation of Equations (4.23) and (4.31). This particular value of d was also the value of the threshold level used at the reservoir during the experimental tests.

The values for V_1 and V_2 have been given previously in FIGURES 3.11 and 3.12 and in TABLES 3.1 and 3.2. The computation of Equations (4.23) and (4.31) was based on values of V_2 and V_1 which were determined over a 25.0 second time interval. These 'long-term' values were used, rather than the 2.5 second 'short-term' values, because the longer term values are more representative when comparing the measured average bit-error probabilities with the predicted error probabilities. This is on account of the fact that the measured error probabilities were determined over a period of several minutes for each error test.

Values of the peak signal-to-RMS noise ratio, β, were measured at the reservoir for all test ranges and these measured values are shown in FIGURE 4.15. Also shown in this figure are computed values of S/N * ratios based on the measured value at the 150-metre range. The computed values for the 200 and 650-metre ranges were then calculated from a consideration of spherical divergence and losses due to absorption (see Chapter 2). From FIGURE 4.15, it can be seen that the measured values of β are in close agreement with the computed values.

By using the appropriate values of V_1, V_2 and β in Equations (4.23) and (4.31), it is possible to compute error probabilities for both the perpendicular-wind and parallel-wind cases respectively. The computed bit-error probabilities, with $P_o = P_1 = 0.5$, and the experimentally determined values are shown as a function of β in FIGURE 4.16. The measured values shown in the figure were obtained from tests carried out during both the summer and autumn periods. From FIGURE 4.16, it can be observed that at S/N ratios above 17 dB, the parallel and perpendicular-wind model predictions appear to be upper and lower bounds to the measured bit-error probabilities, but that the

* S/N is used as an abbreviation for peak signal-to-RMS noise

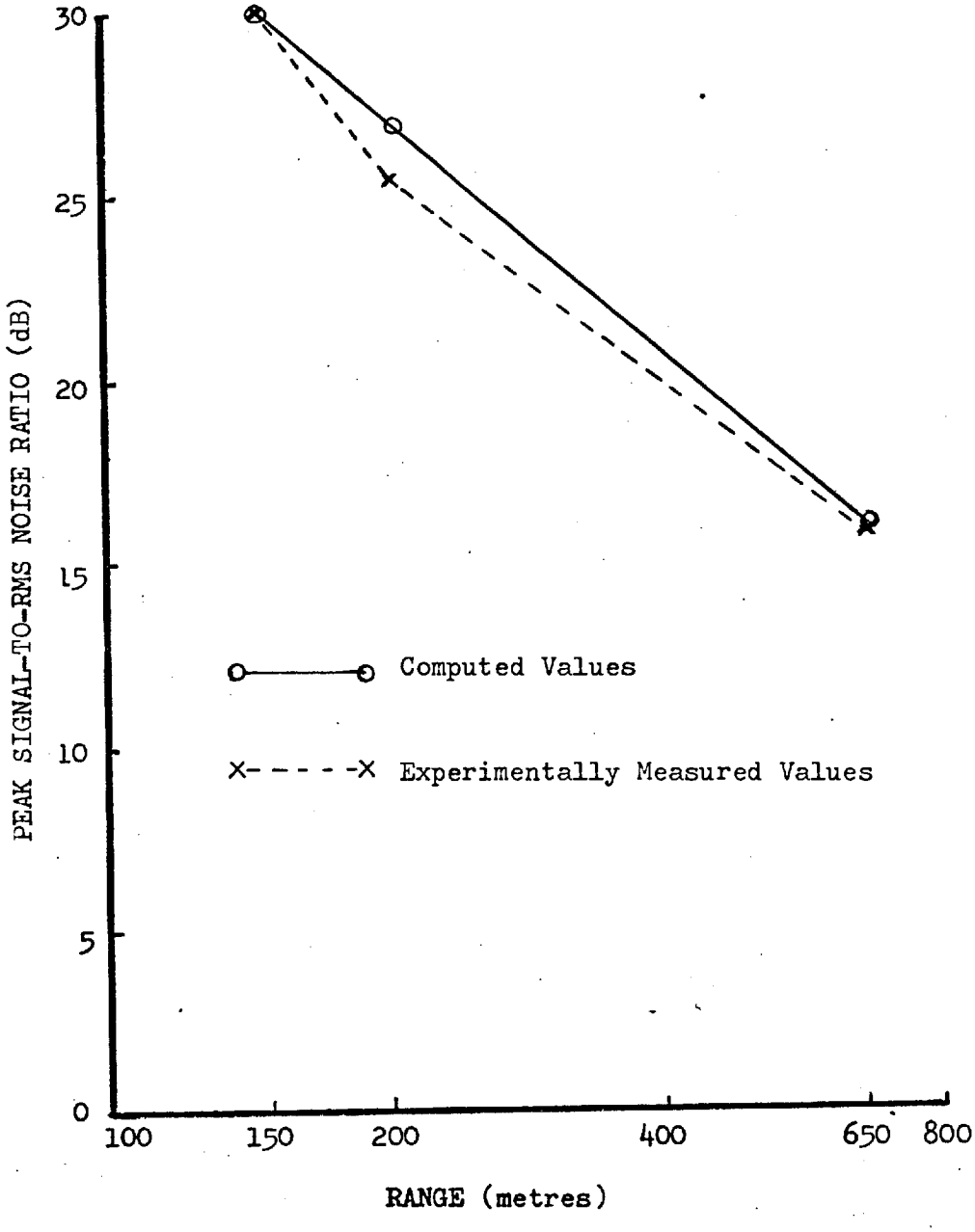


FIGURE 4.15 Measured and Computed Peak Signal-to- RMS Noise Ratios

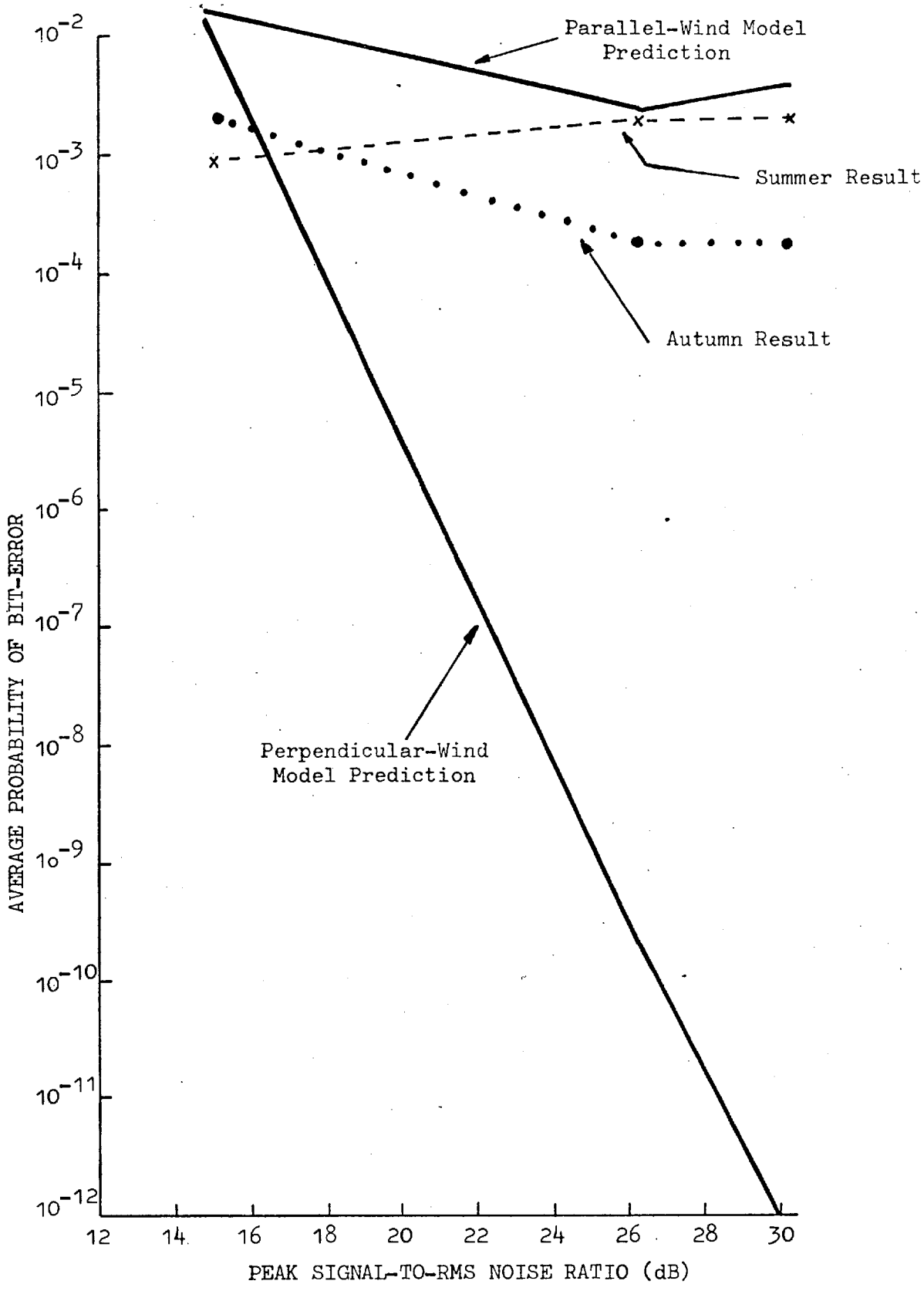


FIGURE 4.16 Computed and Measured Error Probabilities

measured data lies closer to the upper bound than to the lower bound, particularly at the high values of signal-to-noise ratio. There are two main facts which may account for this trend.

Firstly, the derivation of the PDF models used in the computation of the bounds was based on the assumption that there was no time delay between the direct-path and surface-reflected-path signals. However, at the 150-metre range, this assumption is of somewhat limited validity because of the significant time delay between the two signal paths. This time delay would affect the parameter, V. This parameter was determined from the received signal PDFs which were obtained by sampling the received data-pulses at the centre of each data-pulse. If the two signals arriving from the direct-path and surface-reflected-paths were not coincident in time, then the measured value of V would not be totally representative of the actual value. It is thought that, particularly at the 150-metre range, the measured values of V are somewhat lower than the values which would be obtained if the two signals were coincident.

A second factor which can explain the results shown in FIGURE 4.16 is the effect of the prevailing wind direction on the average bit-error probabilities. Although the measured results were obtained under a variety of wind directions, it was found that the majority of the experimental tests were recorded under a prevailing parallel-wind condition. Thus, the measured results would tend to be 'biased' towards the upper bound, as illustrated in FIGURE 4.16.

It can also be seen that at S/N ratios less than 17 dB, the measured results are not bounded by the values computed from the perpendicular-wind model prediction. A possible explanation for this is that at the long ranges, which are associated with the lower values of signal-to-noise ratio shown in FIGURE 4.16, multiple reflections may have

occurred and the Gaussian model may be of somewhat limited validity. However, the Rician model, as used in the parallel-wind case, would still be applicable provided the relative phase fluctuations between the various steady components of the reflected paths were small.

4.5 Optimum Fixed Detection Threshold Level

Further information about the way in which the signal PDF changes with wind direction and range can be obtained by an analysis of the optimum fixed detection threshold level which minimises the average probability of bit-error. It is possible to compute the optimum fixed threshold from an analysis of both the noise PDF and the signal-plus-noise PDF. If the a priori probabilities, P_o and P_1, are equal, then by using the Bayes decision strategy, the optimum fixed threshold can be found by determining the point at which the value of the signal-plus-noise PDF is equal to the value of the noise-only PDF. To be more explicit, the optimum threshold, r_o, can be found when (see Schwartz, Bennett and Stein, 1966),

$$\frac{f_s(r_o)}{f_n(r_o)} = \frac{P_o}{P_1} = 1 \qquad \ldots\ldots (4.32)$$

where $f_s(r_o)$ and $f_n(r_o)$ are the signal-plus-noise and noise PDFs respectively, and r_o is the optimum fixed detection threshold level.

In the case of a wind which is perpendicular to the direction of transmission, the minimum probability of error can be found by setting Equation (4.2) equal to Equation (3.11); that is when,

$$\frac{r_o}{N_o^2} \exp\left[-\frac{r_o^2}{2N_o^2}\right] = \frac{1}{\sigma_2\sqrt{2\pi}} \exp\left[-\frac{(r_o-A_2)^2}{2\sigma_2^2}\right] \qquad \ldots\ldots (4.33)$$

If, $r_o = d_o A_2$, $\beta = A_2^2/N_o^2$, and $V_2 = \sigma_2/A_2$, then Equation (4.33) can be written in the form,

$$\sqrt{2\pi}\, V_2 \beta d_o = \exp\left[-\frac{(d_o-1)^2}{2V_2^2} + \frac{d_o^2}{2}\beta\right] \qquad \ldots\ldots (4.34)$$

After taking natural logarithms, it is found that,

$$2V_2^2\left[\ln(\sqrt{2\pi}\, V_2 \beta d_o)\right] = -(d_o-1)^2 + d_o^2 \beta V_2^2 \qquad \ldots\ldots (4.35)$$

Because of the complexity of the form of Equation (4.35), it is necessary to use iterative computations to evaluate the equation to obtain values for d_o.

In the case of a parallel-wind, the minimum probability of bit-error can be found by setting Equation (4.2) equal to Equation (3.7); that is when,

$$\frac{r_o}{N_o^2}\exp\left[-\frac{r_o^2}{2N_o^2}\right] = \frac{r_o}{\sigma_1^2}\exp\left[-\frac{(r_o^2+A_1^2)}{2\sigma_1^2}\right] I_o\left(\frac{r_o A_1}{\sigma_1^2}\right) \qquad \ldots\ldots (4.36)$$

On setting $r_o = d_o A_1$, $\beta = A_1^2/N_o^2$, and $V_1 = \sigma_1/A_1$, Equation (4.36) can be written as,

$$\beta V_1^2 \exp\left[-\frac{d_o^2}{2}\beta\right] = \exp\left[-\frac{(d_o^2+1)}{2V_1^2}\right] I_o\left(\frac{d_o}{V_1^2}\right) \qquad \ldots\ldots (4.37)$$

It is also necessary to solve Equation (4.37) by using iterative compuations because of the hyperbolic Bessel function.

By using suitable values of β, V_2 and V_1 in Equations (4.35) and (4.37), the optimum fixed detection threshold, d_o, can be computed as a function of the transmission range. This has been

done and the results are shown in FIGURE 4.17. In the figure, the computed threshold levels are shown for both the perpendicular and parallel-wind cases.

From an analysis of FIGURE 4.17, it can be seen that for both the perpendicular and parallel-wind cases, the optimum fixed detection threshold level increases with increasing range. This phenomenon can be explained in terms of the peak signal-to-RMS noise ratio and the variances of the probability density functions of the signal-plus-noise and noise amplitudes. At the shorter transmission ranges, the peak signal-to-RMS noise ratio, β, was high, typically 25 to 30 dB. However, it was found that the variances of the signal-plus-noise PDF was considerably larger than the variance of the noise-only PDF, as illustrated in FIGURE 4.14. This implies that in order to minimise the bit-error probability, it is necessary to reduce the detection threshold setting to a value of less than one-half of the average peak signal amplitude. However, at the long range (650 metres), the difference between the variances of the two PDFs was found to be less than at the shorter ranges and hence, the optimum threshold level is increased toward the relative value of 0.5 as illustrated in FIGURE 4.17.

A further point that can be made from the information contained in FIGURE 4.17 is that for all transmission ranges, the relative optimum threshold level is lower in the parallel-wind case than in the corresponding perpendicular-wind case. This can be explained in terms of the coefficients of variation of the signal-plus-noise PDF information that was presented in TABLES 3.1 and 3.2. In these tables, it was shown that at all test ranges, the coefficient of variation was larger in the parallel-wind case than in the perpendicular-wind case. By taking account of the previous analysis

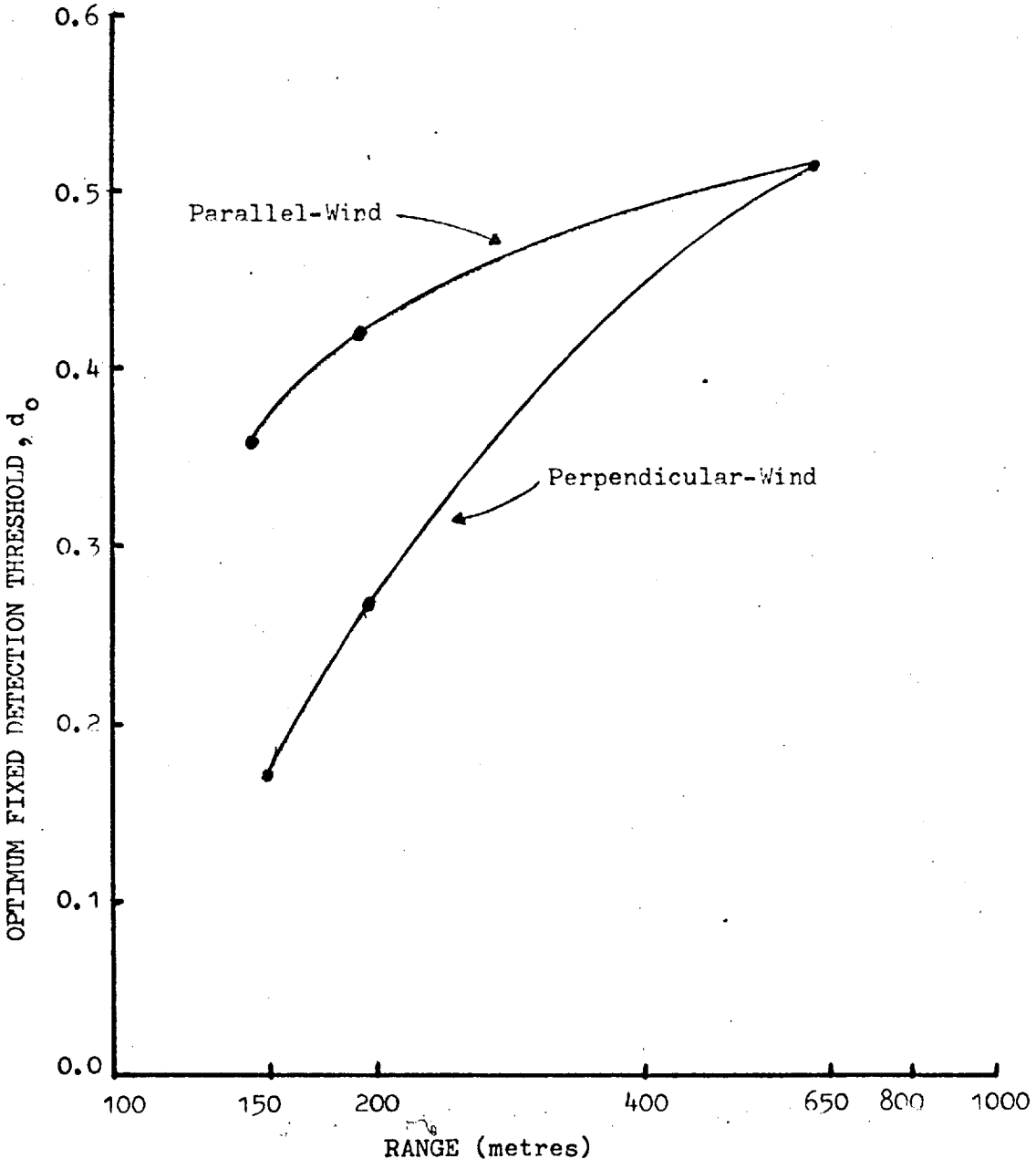


FIGURE 4.17 Computed Optimum Fixed Threshold Levels

relating to the increasing detection threshold with increasing range, then it is possible to explain the fact that the optimum threshold will be lower in the parallel-wind case than in the corresponding perpendicular-wind case.

The measured bit-error probabilities, in general, provide rather inconclusive information about the effect of the detection threshold level on the average bit-error probability. However, the data shown in FIGURE 4.11 clearly supports the hypothesis that the optimum threshold level increases with increasing range. The results shown in FIGURE 4.11 were obtained under the condition of an absolute fixed threshold level at all test ranges. The threshold was set at one-half of the average peak signal amplitude at the 650-metre range and was then held constant at this level for subsequent tests carried out at the 200 and 150-metre ranges. FIGURE 4.11 shows that the average bit-error probability remains relatively constant for all the test ranges when using the fixed absolute threshold level. Thus, as the transmission range was decreased, and hence the peak signal-to-RMS noise ratio was increased, the receiver detection threshold level, in terms of the average peak signal amplitude, was decreased. More explicitly, the actual threshold level changed from approximately 0.5 to 0.1 as the transmission range was decreased from 650 metres down to 150 metres. Thus, if the actual fixed detection threshold level used in this particular series of tests was approximately equal to the optimum threshold level at each range, then it is possible that the average bit-error probability would remain relatively constant, as illustrated in FIGURE 4.11.

Although some of the experimental results have been in agreement with the theory presented in this section, the majority of the results

obtained with threshold settings of 0.5 and 0.25 of the average peak signal amplitude at each test range do not provide any conclusive evidence of the effect of the threshold level on the average bit-error probability. It is clear that more work is required in the investigation of the effect of the detection threshold level on the bit-error probability and in the relationship between the measured data and computed results.

CHAPTER FIVE

BASEBAND PULSE RESPONSE

Introduction

The baseband pulse response of a communication system is a parameter that is highly important in system design. A detailed knowledge of the pulse response, and the way it varies as a function of time, are essential if the effects of pulse dispersion are to be understood and neutralised. In this chapter, the baseband pulse response of the ASK underwater data transmission system is considered and the results of a preliminary practical investigation into some of the properties of the response are presented.

5.1 Practical Derivation of the Baseband Pulse Response

There are two main methods which can be used to investigate the properties of the communication channel. The first method, which is well-established, involves the determination of the impulse response of the channel. From an analysis of the impulse response, it is possible to determine both the time and the frequency response of the channel. Also, additional information about multipath interference and pulse dispersion can be obtained.

Although the impulse response is perhaps the most convenient method of expressing the properties of a channel, there are several difficulties associated with its use. In practice, it is not possible to generate ideal impulse signals and it is necessary, therefore, to use finite-width pulses. As finite-width pulses have to be used, it is necessary to apply deconvolution methods in order to obtain the impulse response. The channel impulse response can be deconvolved from the received signal in two ways, both of which can be implemented with the aid of a digital computer. The first method involves the division, in

the frequency, of the received signal spectrum by a replica of the transmitted signal spectrum. Although this can be accomplished using fast Fourier transform (FFT) programmes, the method requires exact phase synchronisation between the transmitted and received signals. If, for example, both the transmitted signal and received signal are recorded on magnetic tape, then the phase information required in the computation of the desired impulse response can be lost. This can be explained as follows.

A signal, x(t), is transmitted through a linear network (or channel), which has an associated impulse response, h(t). The received signal, y(t), will therefore be the convolution of x(t) and h(t), or,

$$y(t) = h(t) \circledast x(t) \qquad \ldots\ldots (5.1)$$

where $\circledast$ denotes convolution.

If, however, x(t) and y(t) are recorded separately on magnetic tape and then played into a digital computer through an analogue-to-digital converter, then although y(t) is still the convolution of x(t) and h(t), the recording of x(t) will be time-shifted when compared to y(t), unless x(t) is exactly synchronised to y(t). Thus, x(t) becomes x(t+T), where T is the time shift due to the absence of synchronisation. If $X(\omega)$, $H(\omega)$, and $Y(\omega)$ are the Fourier transforms of x(t), h(t) and y(t), respectively, then the desired frequency response of the channel can be given by $H(\omega)$, where $H(\omega)$ is

$$H(\omega) = Y(\omega)/X(\omega) \qquad \ldots\ldots (5.2)$$

If x(t) becomes x(t+T), then $X(\omega)$ will be $X(\omega)e^{-j\omega T}$, and therefore

the new frequency response of the channel is,

$$H'(\omega) = H(\omega)e^{-j\omega T} \qquad \ldots\ldots (5.3)$$

It can be seen from Equation (5.3) that although the magnitude frequency spectrum, $|H(\omega)|$, is unchanged, or

$$|H'(\omega)| = |H(\omega)| \qquad \ldots\ldots (5.4)$$

the phase spectrum has been altered by an amount equal to $-\omega T$. In order to compute $h(t)$ from $H(\omega)$, both the phase and amplitude spectra information are required. However, if the phase information of $H(\omega)$ is incorrect, as illustrated in Equation (5.3), then the desired, or true response, $h(t)$, cannot be computed.

A second method of deconvolving the channel impulse response from the received signal is the use of complex cepstrum analysis (Gold and Rader, 1969). This method does not require phase synchronisation between the transmitted and received signals and it is therefore advantageous when compared with the previously mentioned method of analysis. However, the cepstrum method is somewhat complex and involves the use of a considerable amount of computer time.

In addition to the two main methods of analysing the channel response, there is another method which can be used. This method involves the use of the pulse response to determine information about some of the properties of the channel. As in the case of impulse response testing, an analysis of the pulse response can provide information about multipath interference and pulse dispersion. The pulse response method is very simple and requires little computer time or programming. However, is does suffer from the disadvantage that the overall time and frequency response of the channel cannot be determined as easily.

The preliminary practical investigation into the pulse response of

the ASK underwater system that is presented in this chapter is based on the measurements of the pulse response of the system. In the investigation, narrow-width raised-cosine pulses were transmitted and the received pulse wave-forms were recorded and analysed. The results obtained provide some fairly simple information relating to effects such as multipath and pulse dispersion. It should be emphasised, however, that the results are only provisional and that a much more extensive investigation and analysis is required in order to take in a wider range of operational and climatic conditions. It is necessary that this should be done if general, wide-ranging, conclusions are to be drawn.

5.2 Presentation of Experimental Results

The results in this section are presented on the basis of measurements taken when the prevailing wind direction was approximately parallel and approximately perpendicular to the direction of transmission. Because of the effect that the prevailing wind direction has on other factors such as the PDF and the amplitude frequency spectrum of the signal, it was hoped that the analysis of the pulse response on a similar basis would result in a deeper understanding of the behaviour of the channel.

The tests were carried out at the reservoir over a period of several months in order that measurements could be made under a variety of climatic conditions. A sequence of 0.8 msec duration raised-cosine pulses was transmitted at each range tested. The pulses were transmitted with a repetition rate of one pulse every 6.4 msec and throughout the test period, the transmitter power was held fixed at 50 milli-Watts peak. When transmitting data pulses at a rate of 156 pulses per second,

the effects of intersymbol interference and pulse dispersion on the adjacent transmitted data pulses were observed to be negligible.

In order to obtain information relating to the time variation of the pulse response, the experimental results are divided into three groups. The groups are formed on the basis of observation, or sampling, intervals. The first group is related to an observation interval of 6.4 msec, which corresponds to observing each data-pulse in the transmitted sequence. The second group relates to an observation interval of 320 msec, which corresponds to sampling every 50th data-pulse, and the third group is associated with an interval of 960 msec, or every 150th data-pulse. Each of the figures presented in the chapter shows six consecutive pulses obtained from either of the three sampling intervals. Thus, on the pulse-to-pulse basis, the figure shows an overall time interval of 38.4 msec. When considering every 50th pulse, the time interval shown in the figure is 1920 msec, while in the case of sampling every 150th pulse, the total time shown in the figure is 5760 msec.

The material contained in FIGURES 5.1 to 5.6 was obtained by sampling the received data every 6.4 msec and each figure shows six consecutive pulses on this basis. FIGURES 5.1 to 5.3 show, for each range tested, typical results obtained under the condition of a wind which was approximately perpendicular to the direction of transmission, while FIGURES 5.4 to 5.6 show corresponding results obtained under the parallel-wind condition. In FIGURES 5.7 to 5.12, typical results obtained when considering every 50th received data pulse are illustrated, and FIGURES 5.13 to 5.18 show results obtained on the basis of considering every 150th data pulse. In all of the figures, the horizontal axis corresponds to a time duration of 5.0 msec.

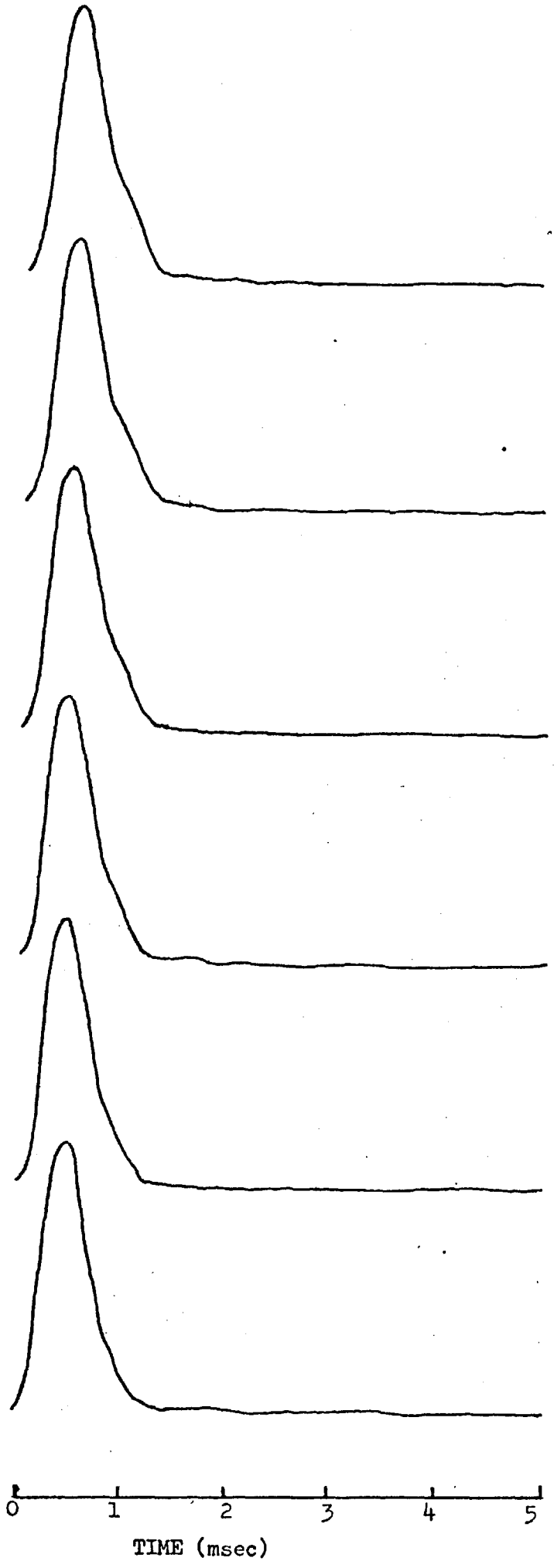


FIGURE 5.1 Perpendicular-Wind Pulse Response at 150 metres (every consecutive pulse)

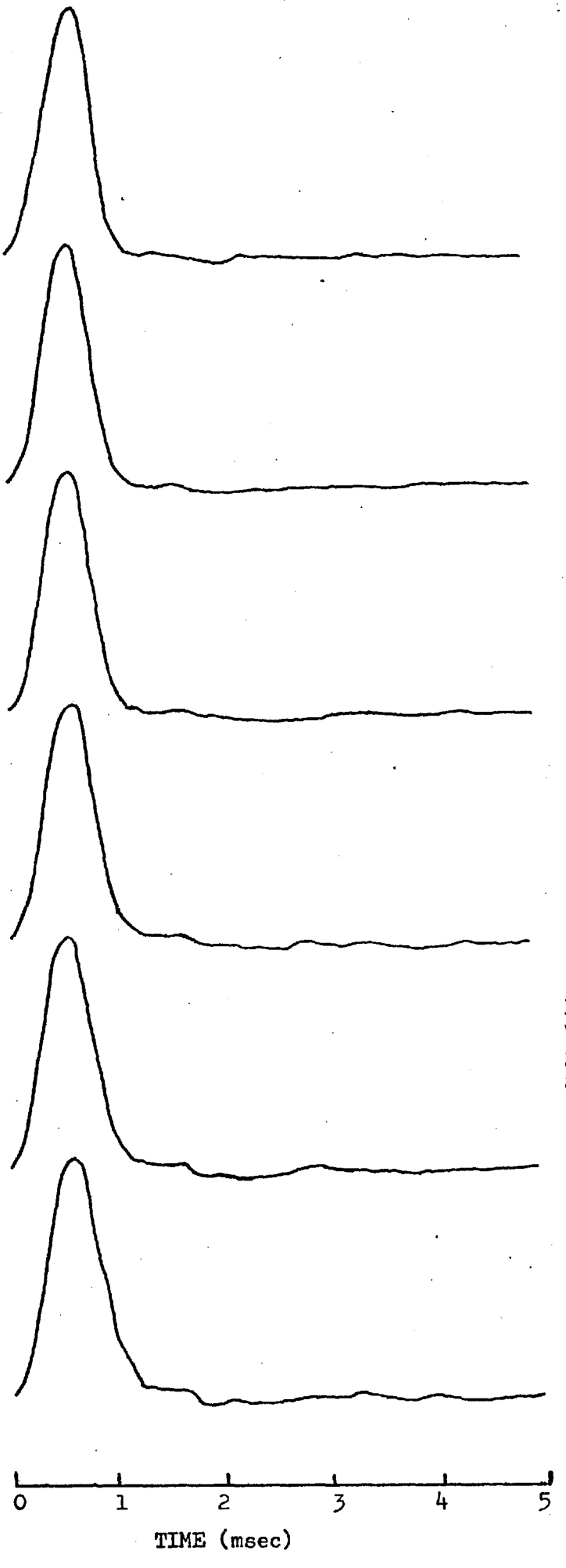


FIGURE 5.2 Perpendicular Wind Pulse Response at 200 metres (every consecutive pulse)

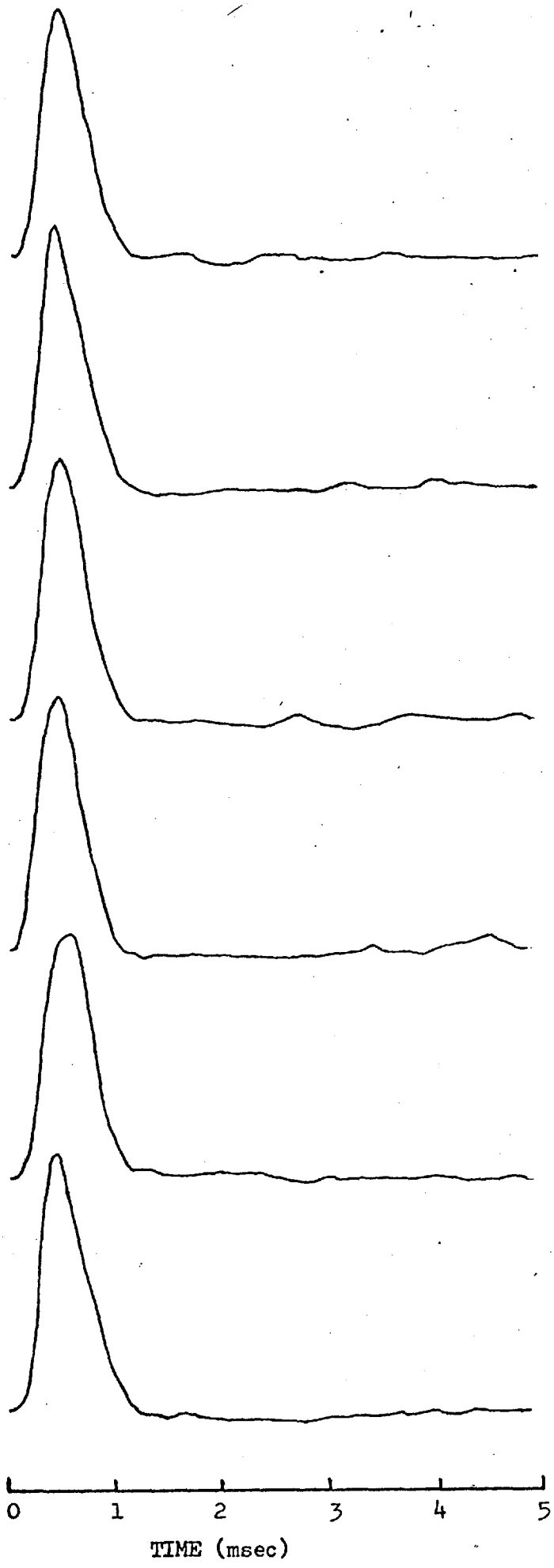


FIGURE 5.3 Perpendicular-Wind Pulse Response at 650 metres (every consecutive pulse)

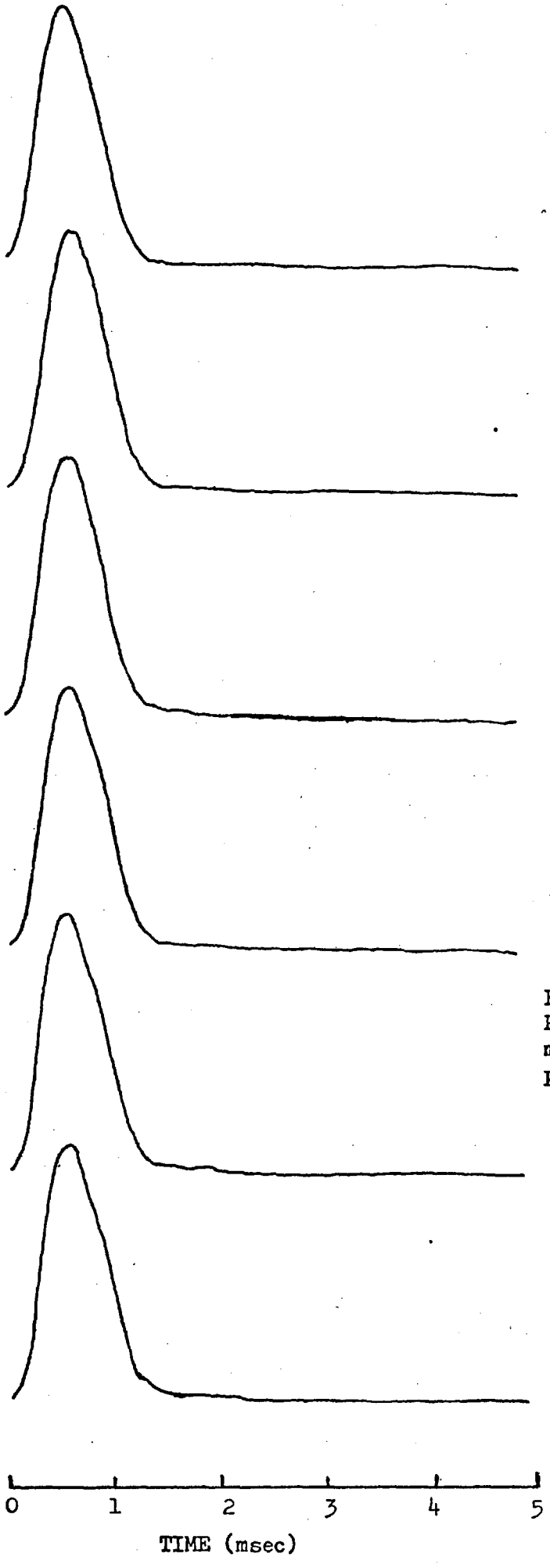


FIGURE 5.4 Parallel-Wind Pulse Response at 150 metres (every consecutive pulse)

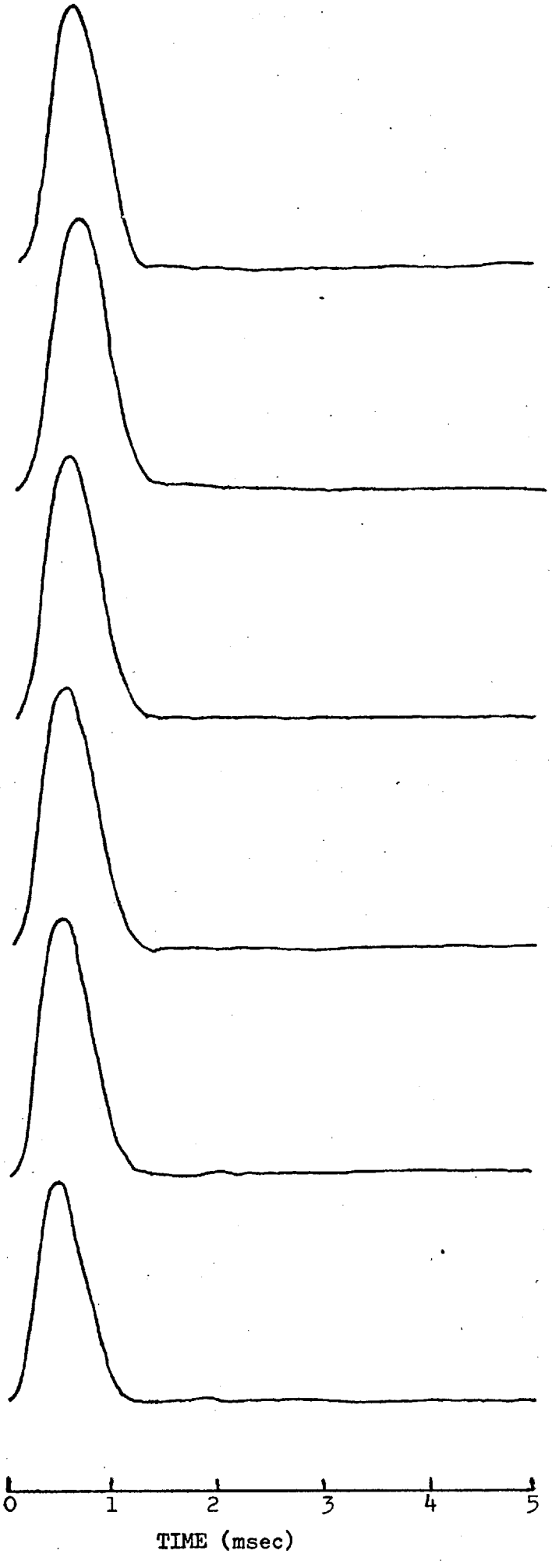


FIGURE 5.5 Parallel-Wind Pulse Response at 200 metres (every consecutive pulse)

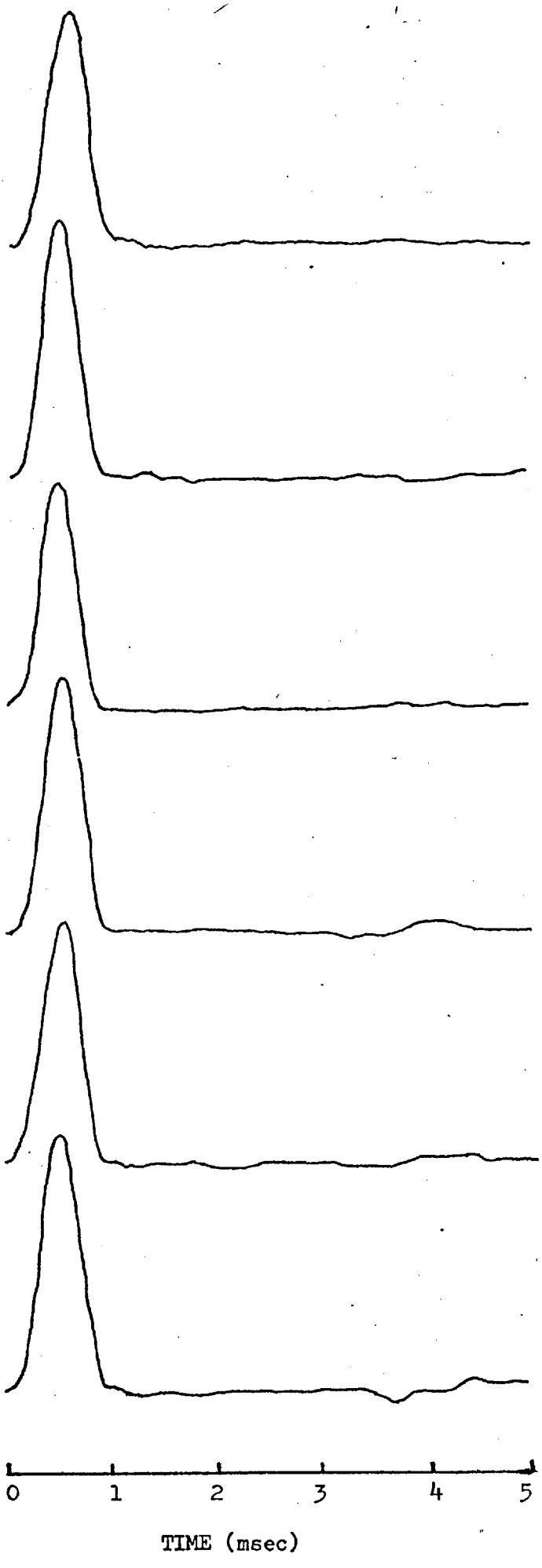


FIGURE 5.6 Parallel-Wind Pulse Response at 650 metres (every consecutive pulse)

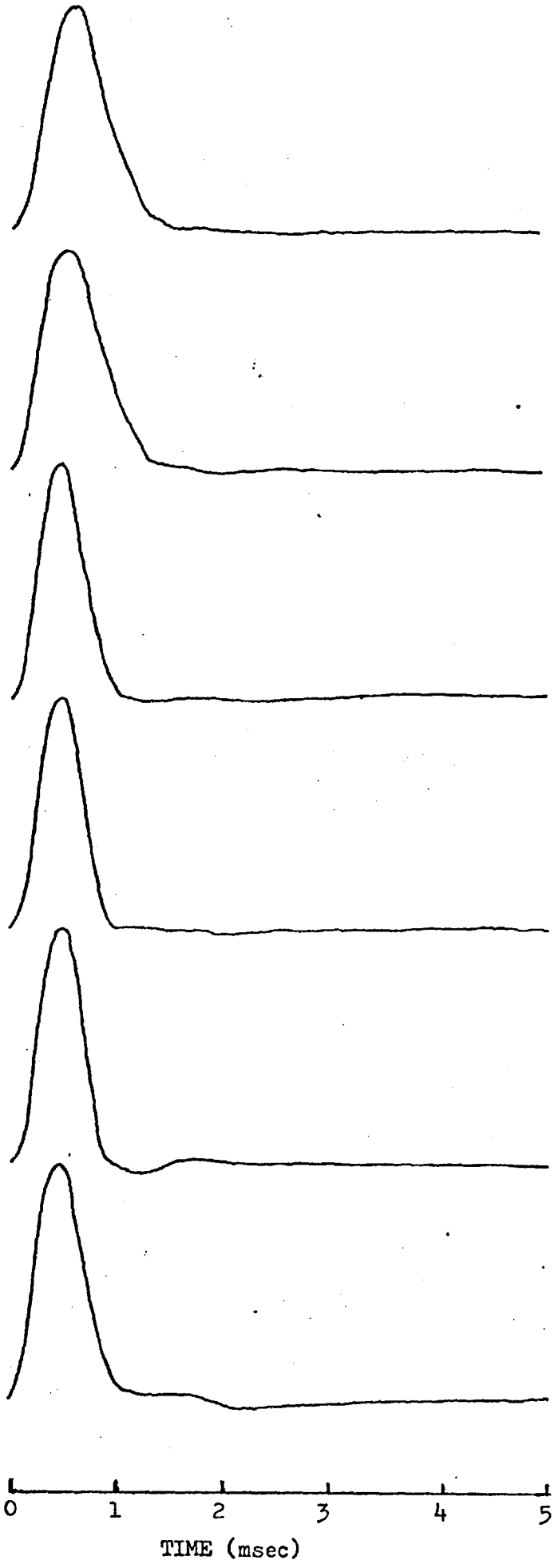


FIGURE 5.7 Perpendicular-Wind Pulse Response at 150 metres (every 50th pulse)

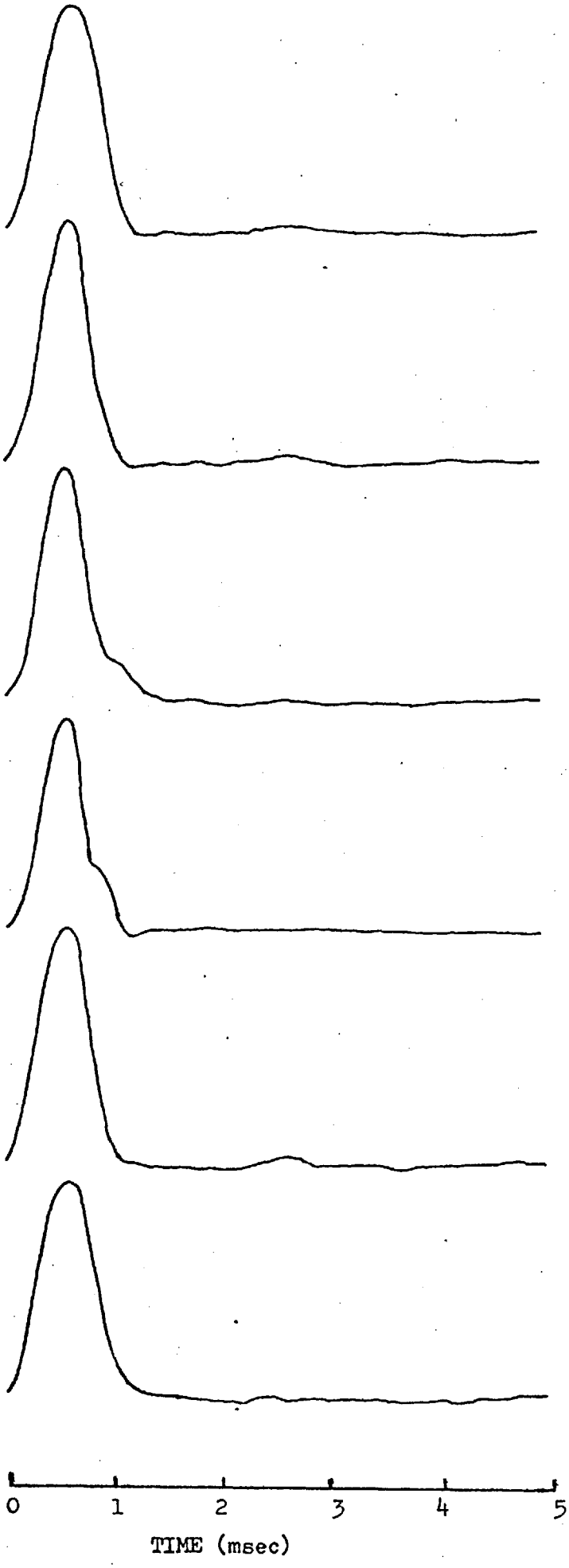


FIGURE 5.8 Perpendicular-Wind Pulse Response at 200 metres (every 50th pulse)

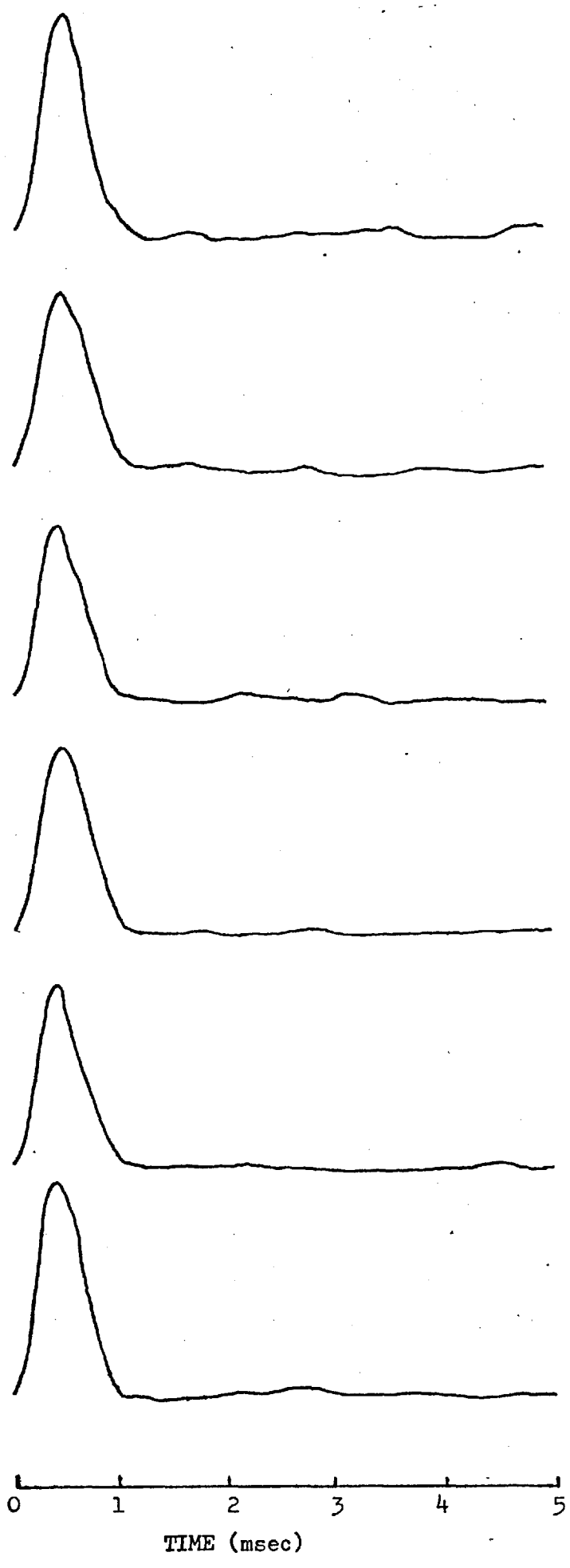


FIGURE 5.9 Perpendicular-Wind Pulse Response at 650 metres (every 50th pulse)

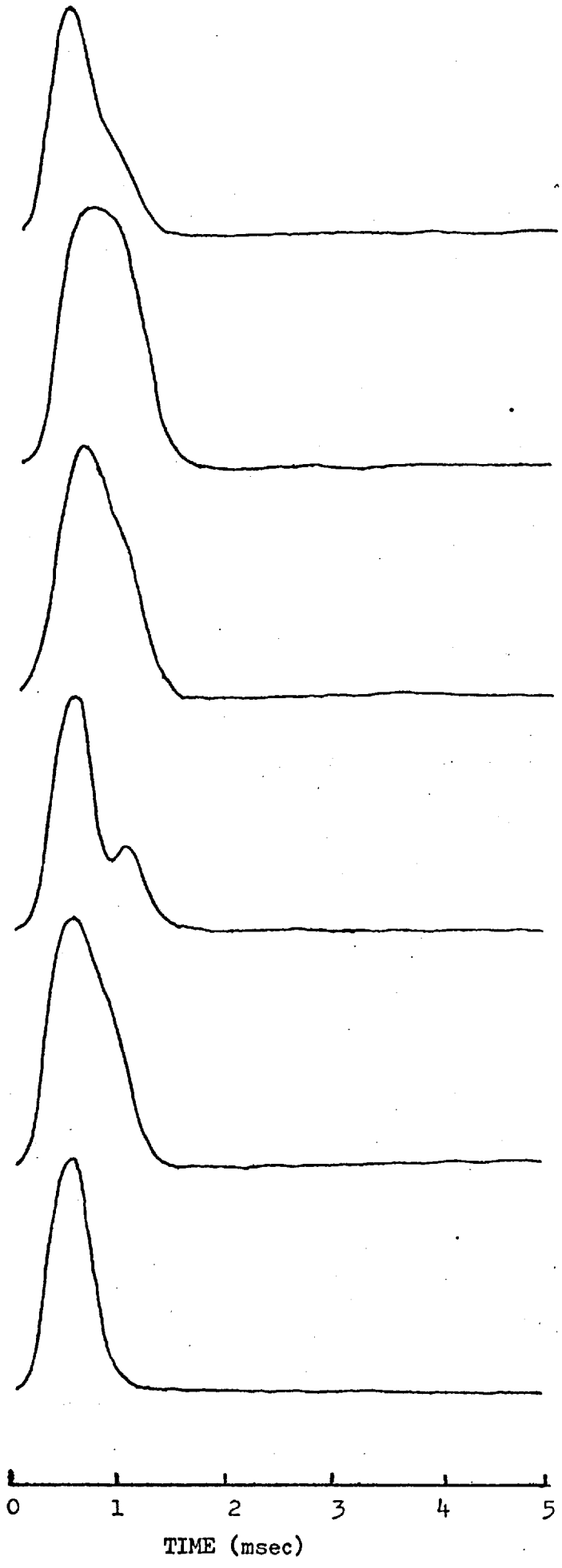


FIGURE 5.10 Parallel-Wind Pulse Response at 150 metres (every 50th pulse)

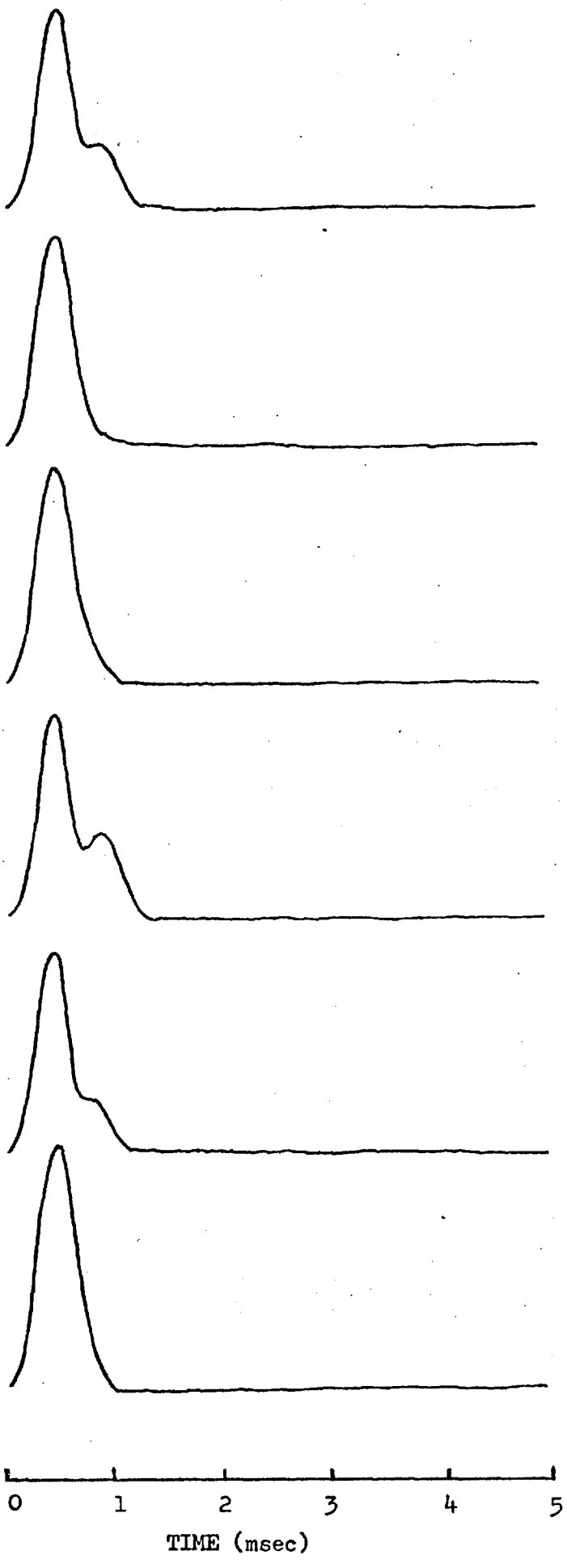


FIGURE 5.11 Parallel-Wind Pulse Response at 200 metres (every 50th pulse)

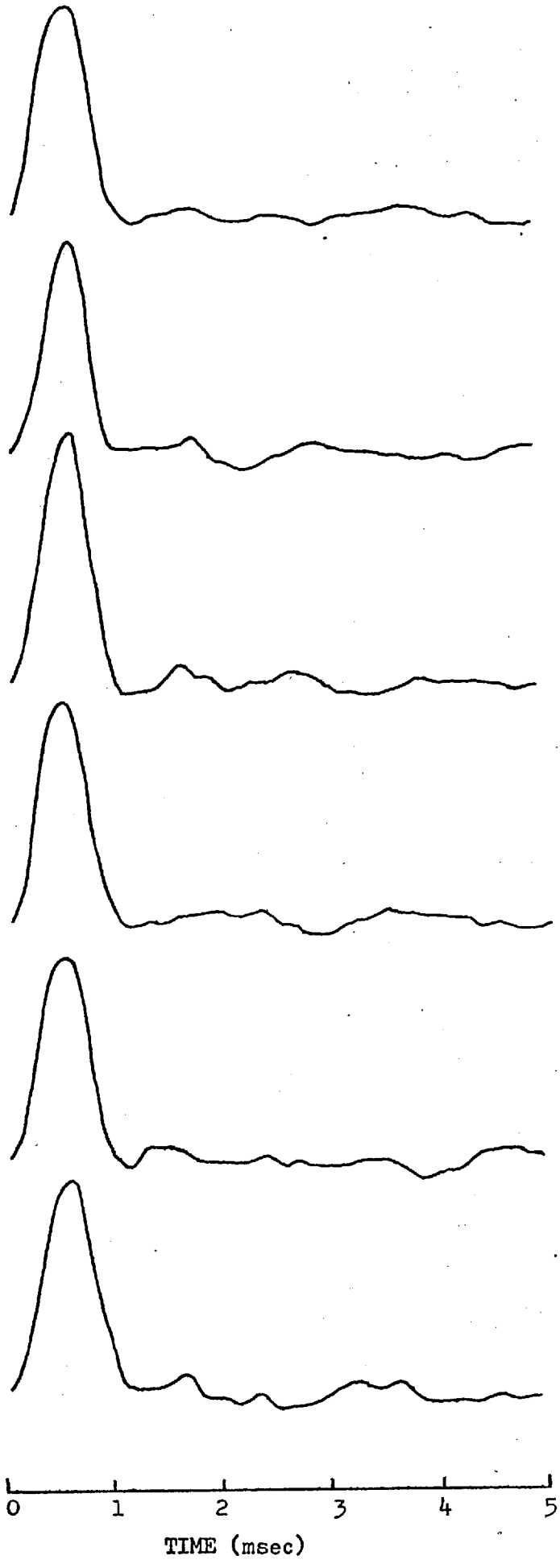


FIGURE 5.12 Parallel-Wind Pulse Response at 650 metres (every 50th pulse)

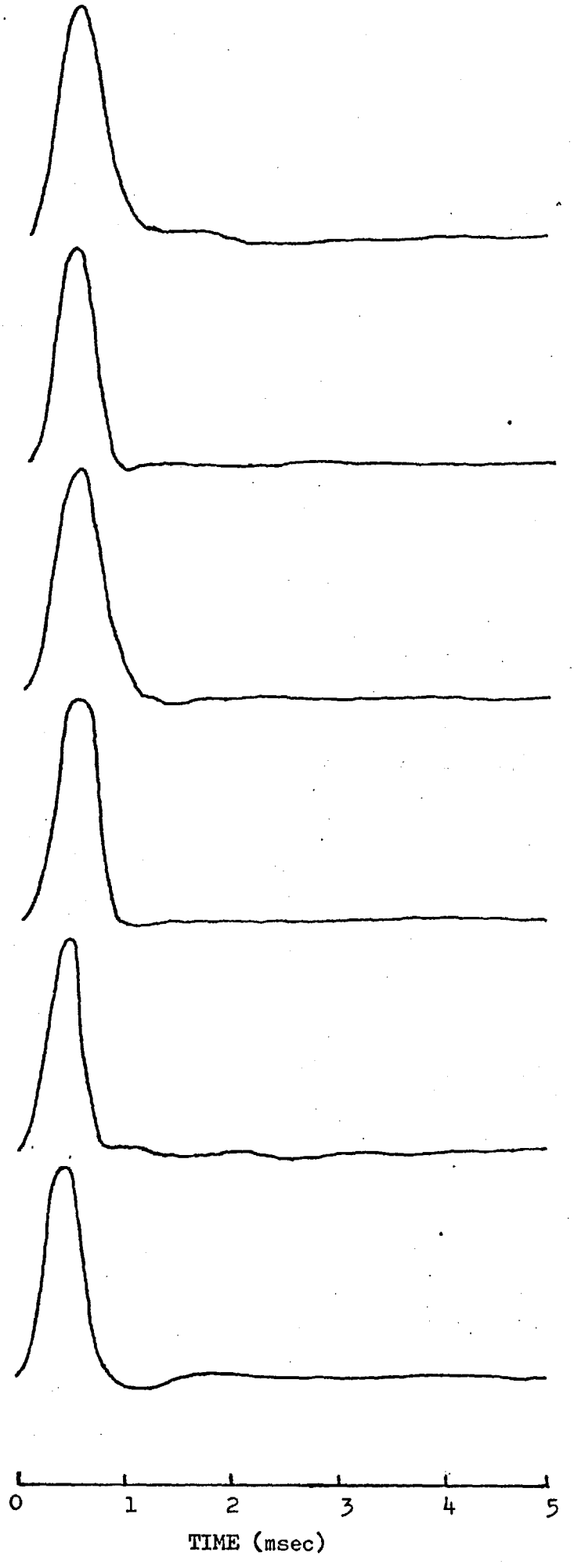


FIGURE 5.13 Perpendicular-Wind Pulse Response at 150 metres (every 150th pulse)

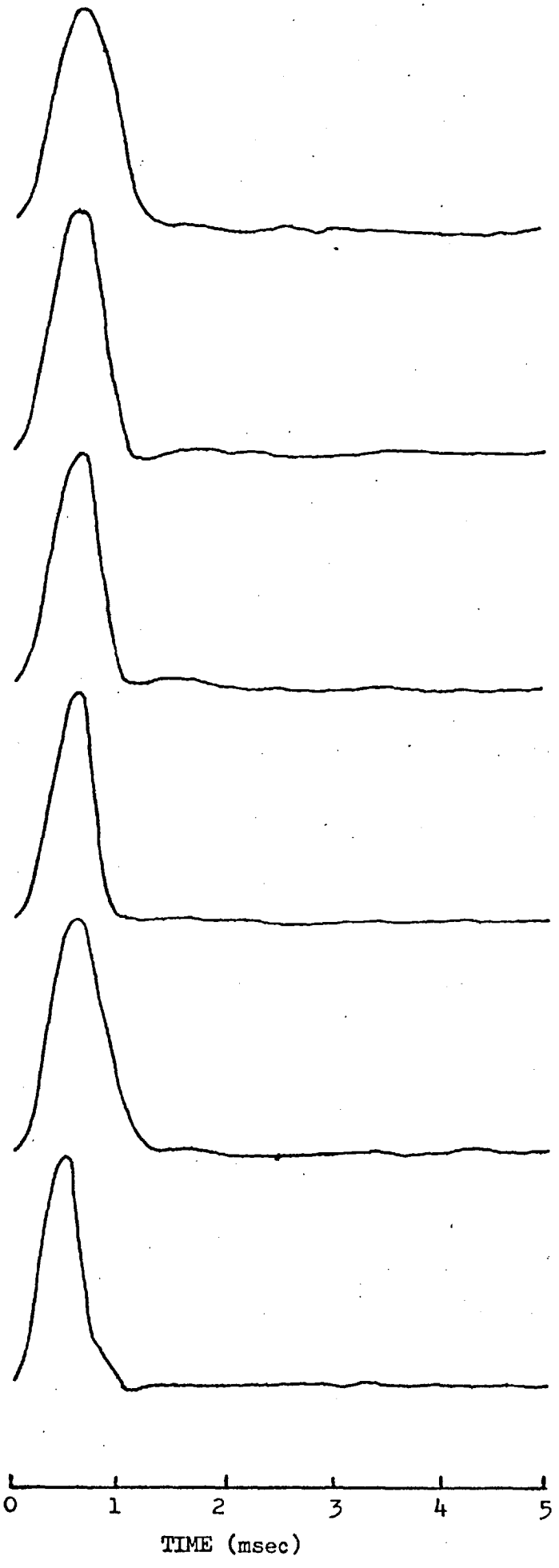


FIGURE 5.14 Perpendicular-Wind Pulse Response at 200 metres (every 150th pulse)

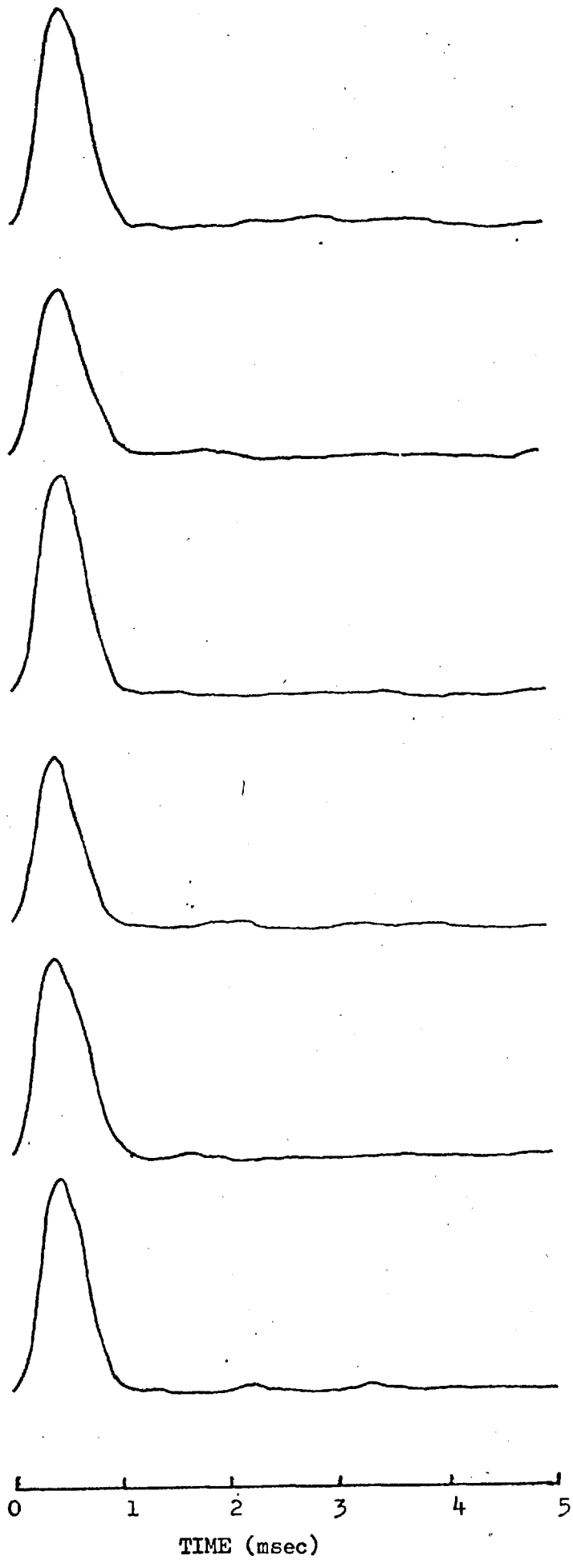


FIGURE 5.15 Perpendicular-Wind Pulse Response at 650 metres (every 150th pulse)

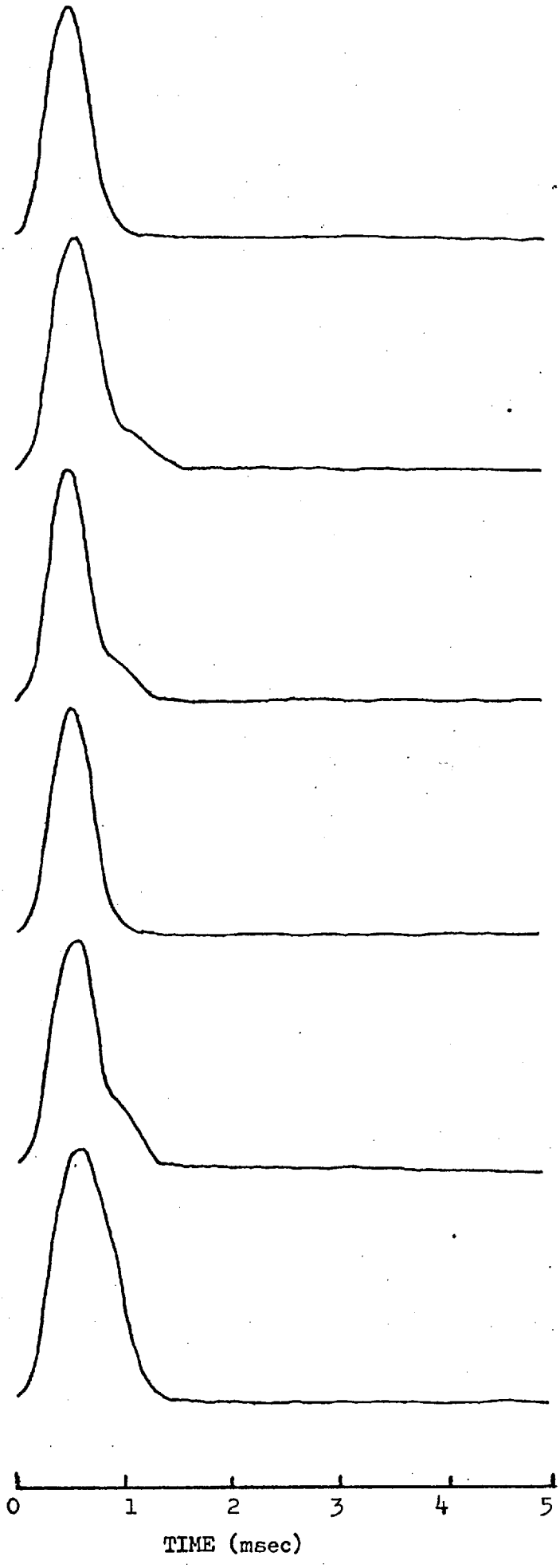


FIGURE 5.16 Parallel-Wind Pulse Response at 150 metres (every 150th pulse)

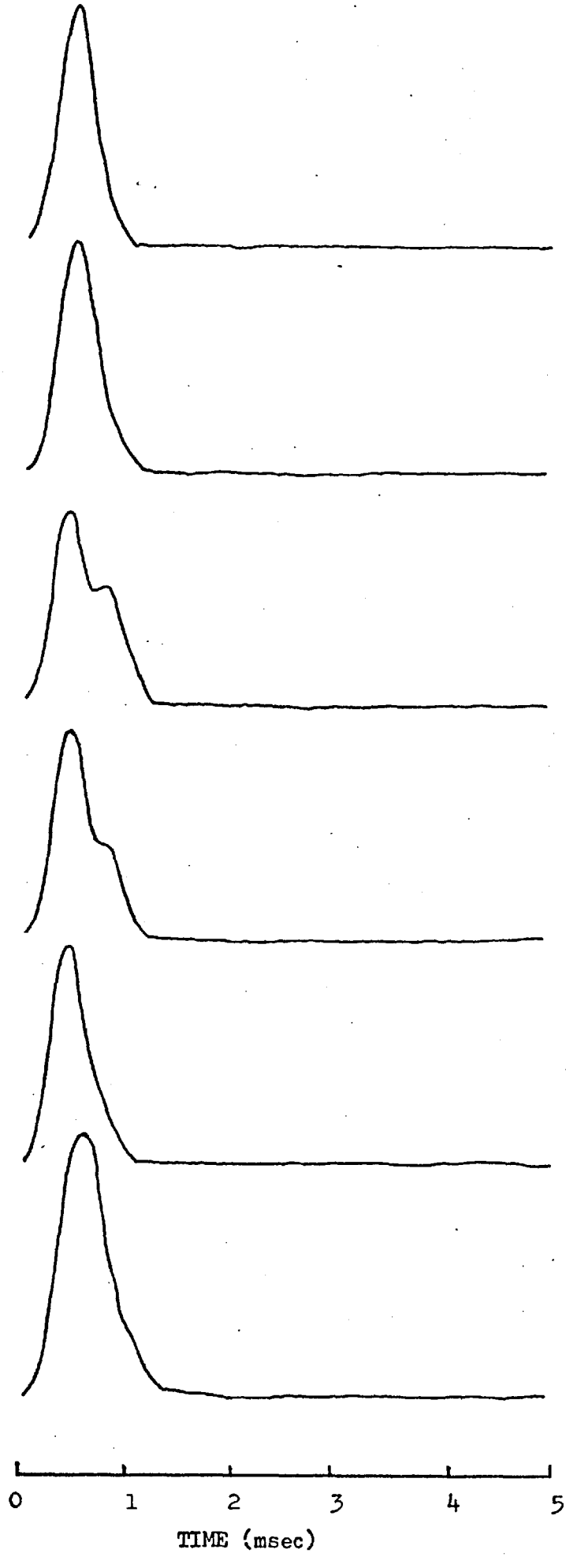


FIGURE 5.17 Parallel-Wind Pulse Response at 200 metres (every 150th pulse)

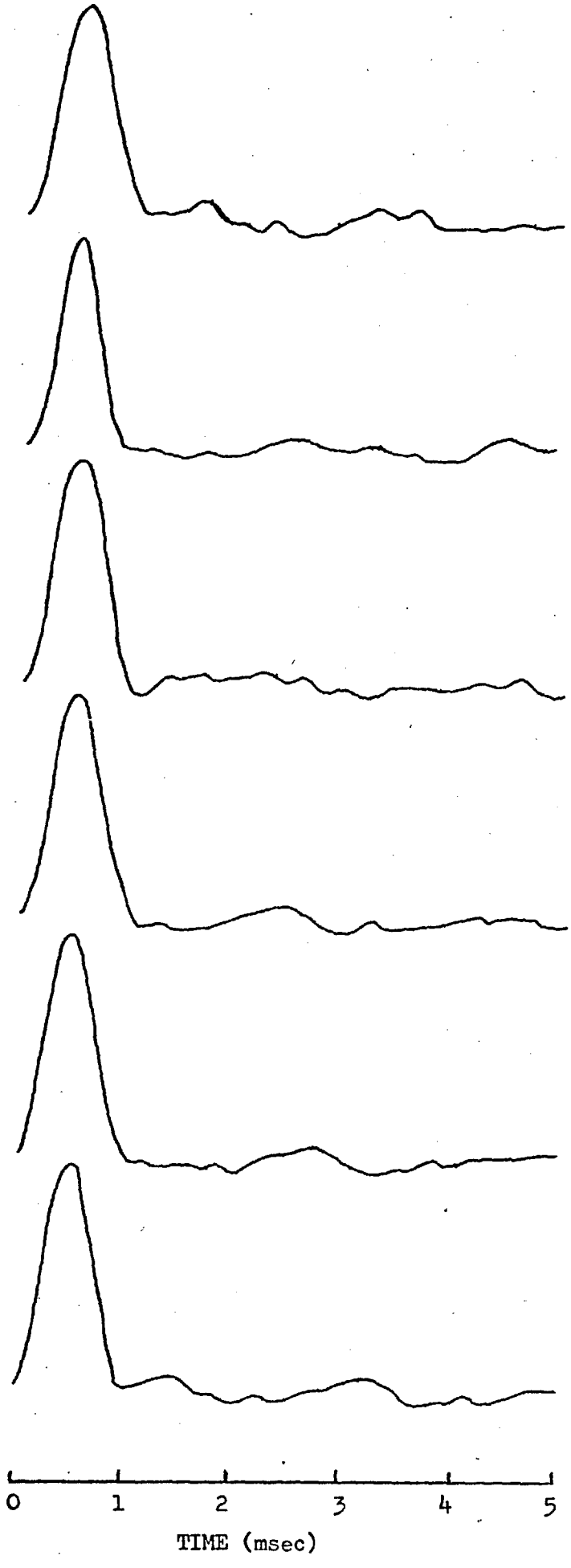


FIGURE 5.18 Parallel-Wind Pulse Response at 650 metres (every 150th pulse)

A general observation which can be made from an analysis of the results shown in FIGURES 5.1 to 5.6 is that, in each figure, the shape and amplitude of the received data-pulses remain quite constant on a pulse-to-pulse basis. Thus, as shown in each of the figures, the pulse response appears to remain relatively constant, over a time interval of 38.4 msec, for a particular range and prevailing wind direction.

An indication of the effect of the wind direction on the pulse response can be seen from a comparison of FIGURES 5.1 and 5.2 with FIGURES 5.4 and 5.5. In the case of a wind parallel to the direction of transmission, as illustrated by the pulse responses in FIGURES 5.4 and 5.5, the multipath interference is such that the data-pulse width is increased considerably. However, in the perpendicular-wind case, as shown in FIGURES 5.1 and 5.2, the effect of the multipath interference is much reduced and the pulse dispersion of the channel does not appear to be as great as in the parallel-wind case. In general, the responses shown in FIGURES 5.1 to 5.6 indicate that multipath and pulse dispersion effects do not exist much beyond about 1.5 msec in the case of either wind direction. It should be noted, however, that there are some slight indications of pulse dispersion and multipath beyond 1.5 sec. This can be seen from a consideration of the responses shown in FIGURES 5.3 and 5.6. These results, which were obtained at a range of 650 metres, illustrate that some 'ripple' exists in the responses beyond 1.5 msec. It is thought that multipath resulting in echo effects could be a cause of this ripple.

Typical pulses responses obtained when considering every 50th data-pulse are shown in FIGURES 5.7 to 5.12. From the figures, it can be seen that, on a trace-to-trace basis, significant changes occur in both the general shape of the received pulse and the pulse amplitude.

In particular, this effect appears to be most pronounced when the wind is parallel to the direction of transmission. This is illustrated in FIGURES 5.10 to 5.12. In each figure, it can be seen that significant changes in both the shape and amplitude of the data-pulses occur within the time interval of 1920 msec shown in the figure.

Further evidence of the nature of the multipath interference can be obtained by considering the responses shown in FIGURE 5.11. It can seen from the figure that the multipath signal appears first to increase and then to decrease in the space of three or four traces. The time of this variation ranges from approximately 700 to 1000 msec. These values approximately correspond to the time of the first zero-crossing of the autocorrelation functions presented in Chapter 3.

In FIGURES 5.13 to 5.18, which are results obtained by considering every 150th data-pulse, it can be seen that, just as in the case when every 50th pulse was considered, there are considerable changes in the shape and amplitude of the data pulses and further that, in each figure, this variation occurs on a trace-to-trace basis. The extent of the pulse amplitude fluctuations is illustrated particularly in FIGURES 5.16 to 5.18. The responses shown in these figures were obtained under the parallel-wind propagation condition. A comparison of FIGURES 5.16 to 5.18 with FIGURES 5.13 to 5.15 shows that the amplitude fluctuations are larger in the parallel-wind case than in the corresponding case of a perpendicular-wind .

5.3 Summary of Results

It is important to note that the pulse responses presented in this chapter are the result of only a preliminary investigation of aspects relating to the pulse response of the channel. Although the results are only provisional, they appear to be sufficiently uniform for some

general indicative conclusions to be drawn.

One of the most significant observations which can be made is that beyond approximately 1.5 msec, there is little multipath interference or pulse dispersion. This would indicate that if data was transmitted at a rate less than about 600 bits/second, then there would few false alarm errors due to multipath effects. However, if the data-rate was in excess of 600 bits/second, then errors due to false alarms arisng from multipath interference would be introduced. This, in fact, has been observed and is shown in FIGURES 4.6 and 4.10.

The material presented in FIGURES 5.7 to 5.12 provides an indication of the 'fading-rate' of the multipath interference. From a consideration of the figures, it can be calculated that fading-rates of the order of 1 Hz to 2 Hz occur and that these values are in agreement with results relating to signal amplitude fluctuations presented in Chapter 3. This type of information about the fading-rate of the channel is a highly important parameter in the design and implementation of adaptive or automatic equalisers. However, more work is required in the investigation of the pulse response of the system in order to effectively implement such methods of improving system performance Also, the effects of increased range, and the associated increased multipath, need to be investigated further.

CHAPTER SIX

SUMMARY AND CONCLUSIONS

Introduction

In this chapter, the work presented in the thesis is summarised and the conclusions which can be drawn from the results are described in detail. Also, some suggestions are made relating to further research.

6.1 General Summary

Although the interest in underwater data communication has increased considerably in recent years, there are many aspects relating in particular to underwater data transmission that have not yet been fully investigated. The aim of the work reported on in this thesis was to investigate some of these aspects and to provide information about them. It was intended mainly that certain important quantitative results relating to the performance of a particular data transmission system be obtained, and that the results be interpreted in terms of physical and climatic conditions.

An ASK data transmission system was designed and tests using the system were carried out in a large inland reservoir. The system is described in Chapter 2, and an outline of the experimental procedures adopted is also presented in the chapter. A presentation and analysis of results relating to signal amplitude fluctuations is given in Chapter 3 and, in Chapter 4, the performance of the ASK system is studied in terms of the measured bit-error probabilities. In Chapter 5, a preliminary practical investigation into the pulse response of the ASK system is presented and the results are discussed.

6.2 Summary of Results

In Chapter 3, the results of tests relating to the amplitude

fluctuations of data pulses, transmitted over ranges of 150, 200 and 650 metres, are presented. Four parameters of the signal fluctuations were computed. These were: the frequency spectrum of the envelope of the signal, the autocorrelation function of the signal envelope, the probability density function of the sampled signal, and the coefficient of variation (or RMS amplitude fluctuation) of the received pulses.

An analysis of the computed amplitude frequency spectra and the autocorrelation functions of the signal envelope has indicated that the amplitude fluctuations of the received signal are dependent mainly on the signal arriving from the surface-reflected transmission path. A further study of these experimental results has revealed that the signal fluctuations caused by the moving surface of the water are affected by the direction of the prevailing wind, and it has been found that when the prevailing wind direction is approximately parallel to the transmission path, the effect of the surface-reflected signal on the received signal is strongest. This fact was deduced from an analysis of the amplitude frequency spectra. The results obtained also indicate the effect of the surface-reflected path signal for a wind perpendicular to the transmission path. However, under both experimental wind conditions, the spectrum of the envelope of the received data-pulses has been found to be similar to the amplitude spectrum computed from a consideration of the wave-spectra theory of Neumann and Pierson (1966), and the analysis of the signal autocorrelation functions provides further evidence of this effect.

The probability density functions (PDFs) of the received data pulses were computed from recorded data taken under a variety of propagation and climatic conditions. It has been shown that if the experimental data is divided according to the prevailing wind direction

(as in the case of the autocorrelation functions and the amplitude frequency spectra), then it is possible to compare the observed PDFs with well-known distributions. In the case of a wind parallel to the direction of transmission, the measured PDF has been shown to resemble a Gaussian distribution, while in the perpendicular-wind case, the experimentally determined PDF appears to tend towards a Rician distribution.

A statistical analysis was carried out on the measured PDFs and one of the statistics, the coefficient of variation, was studied in detail in Chapter 3. Two main causes of signal amplitude fluctuations were identified and separated from an analysis of experimental data recorded under parallel-wind and perpendicular-wind propagation conditions. It has been found that for a parallel-wind, the signal amplitude fluctuations are caused by both the effects of the surface-reflected path signal and the thermal inhomogeneities in the medium. However, with a perpendicular-wind, the main cause of signal fluctuation has been shown to be due to the thermal inhomogeneities within the medium. It has also been shown that for a wind which was approximately perpendicular to the transmission path, the fluctuations due to thermal inhomogeneities agree closely with those predicted using the theory of fluctuations developed by Chernov (1967). The fluctuations of the signal caused by the effect of moving waves on the water surface have been shown to decrease with increasing range, while the fluctuations due to thermal inhomogeneities have been shown to increase with increasing range.

An investigation relating to the PDFs of the direct-path and surface-reflected path signals was also presented in Chapter 3. It is seen that, under the conditions of a prevailing parallel-wind, the PDF

of the surface-reflected path signal resembles a Rician distribution, and that with a prevailing perpendicular-wind, the PDF of the signal reflected from the surface resembles a Rayleigh distribution. An explanation of these observations is given in terms of conventional scattering theory. The PDF of the direct-path signal under both the parallel and perpendicular-wind conditions has been found to approximate to a Gaussian distribution. This is expected (see Whitmarsh et al, 1957) in view of the ranges and the transmission frequency used in the tests.

Using the experimentally measured PDFs of the surface-reflected and direct-path signal envelopes as a guide, two mathematical models of the received signal envelope PDF have been developed. It is shown that in the case of a wind parallel to the direction of transmission, the PDF of the received signal envelope can be approximated by a Rician distribution, while in the case of a perpendicular-wind, the resulting envelope PDF of the signal approximates to a Gaussian probability distribution. Experimentally measured PDFs have been found to be in close agreement with the mathematical models.

The performance of the ASK data transmission system, in terms of measured bit-error probabilities, was described and analysed in Chapter 4. The results were obtained over a period of several months and it has been found that they could be interpreted more easily if they were divided into two groups, namely those obtained during the period from June to September (summer) and those obtained during the period from October to November (autumn). The reason for dividing the groups in this way was associated with the manner in which the temperature-depth profile of the reservoir changed during the test period. It was found that during the summer period, the temperature-depth profile could change considerably over an interval of a few days, while during the

autumn period, very small changes in the temperature-depth profile were observed during a similar interval.

The results of the bit-error probability tests indicate that, in general, it is possible, when using only 50 milli-Watts peak transmitter power, to transmit digital data over ranges up to 650 metres using a carrier frequency of 150 kHz, and to do so with an average error probability of 1 in 10^3, and that this can be done when transmitting data at rates up to 625 bits/second. The results also indicate that if data is sent at a rate of 1250 bits/second over the same ranges, then this can be done, but that the average error probability is increased to 1 in 10^2. An analysis of the results presented in Chapter 4 has shown that errors in detection arise from two main sources - intersymbol interference and signal amplitude fluctuations. When the digital data is transmitted at rates below about 625 bits/second the detection errors are due mainly to the effect of signal amplitude fluctuations. These fluctuations can arise from both pulse dispersion due to multipath interference, and thermal inhomogeneities in the medium. However, if the data-rate is increased above 625 bits/second, then additional detection errors occur and it is almost certain that they are due to intersymbol interference resulting from the presence of multipath.

The performance of the ASK data transmission system has been found to be very dependent on the time of year during which the tests were carried out. During the summer period (June to September), the performance of the system, in terms of the measured bit-error probabilities, was found to be extremely variable, and that the variation could be significant from day-to-day. During the autumn period (October to November), the system performance was found to be

much less variable. It seems very likely that the variable nature of the system performance during the summer was related directly to the significant variations in the temperature-depth profile that occurred from day-to-day.

The two PDF models developed in Chapter 3 were used in the computation of the average error probability of the data transmission system. Two computations, based on the PDF models derived for the parallel and perpendicular-wind conditions, have been made for each test range. It has been shown, in Chapter 4, that the computed error probabilities based on the parallel-wind and perpendicular-wind PDF models appear to form approximate upper and lower bounds to the experimentally measured error probabilities. In particular, it is shown that for S/N ratios greater than 17 dB, the measured results actually lie within the computed bounds.

From an analysis and consideration of the results of tests relating to the performance of the system in terms of the measured bit-error probabilities, it is possible to draw some conclusions. It has been shown that if the data-rate is less than approximately 625 bits/second, then communication can be carried out over ranges up to 650 metres, and that this can be done with an average bit-error probability of 1 in 10^3. However, if data is transmitted at rates in excess of 625 bits/second and a similar error-rate of 1 in 10^3 is to be maintained, then it will be necessary to take steps to reduce the effects of intersymbol interference and signal amplitude fluctuations. It is suggested that techniques such as adaptive equalisation could be used to achieve this objective.

The pulse response of the ASK system was considered in Chapter 5. Although the investigation reported on in the chapter is only

preliminary, several trends can be observed, and it is possible to draw some indicative conclusions from the results of the investigation. It is seen that the direction of the prevailing wind affects the amplitude and shape of the pulse response. It appears that under the conditions of a parallel-wind, multipath interference causes a considerable time-spreading of the data pulses, but that under the conditions of a perpendicular-wind, this effect is much reduced.

When considering the pulse response of the system in terms of a pulse-to-pulse basis, it is seen that the response varies little during the 38.4 msec analysis interval. However, if the response is considered on the basis of sampling every 50th data pulse, it is observed that both the shape and the amplitude of the pulse response change significantly over a 320 msec period. This is further illustrated in the case when every 150th data pulse is sampled.

The analysis of the pulse response indicates that the multipath interference changes from a maximum effect to a minimum effect in approximately 700 to 1000 msecs. These particular time values compare favourably with the values of the second zero-crossing of the signal envelope autocorrelation functions which are presented in Chapter 3. A conclusion which can be drawn from the experimental investigation presented in Chapter 5 is that if techniques such as adaptive equalisation are to be implemented in order to improve system performance, then the parameters of the equalisers will need to be readjusted at rates of approximately two to ten times per second. The equaliser will also be required to have a sufficient number of delay taps in order to reduce the effects of pulse dispersion over intervals of up to 1.5 msecs.

6.3 Suggestions for Further Research

Although the work reported on in this thesis has provided some valuable new information relating to several aspects of underwater acoustic data transmission, much remains to be done. In this concluding section of the thesis, several additional areas of investigation are suggested and discussed briefly.

The tests relating to the average bit-error probability performance of the ASK system have shown that, under the short-range shallow-water conditions of the inland reservoir, it is possible to carry out communication at a rate of approximately 625 bits/second over ranges up to 650 metres, and to do so with an average bit-error probability that is consistently of the order of 1 in 10^3. However, the investigation has also indicated that if higher data-rates are to be achieved with a similar bit-error probability, then it will be necessary to implement techniques which are capable of reducing the effects of pulse dispersion and intersymbol interference. One possible method of achieving this is to implement adaptive equalisers into the system. A study of adaptive equalisation techniques when applied specifically to the underwater environment would therefore be very useful. The experimental investigation of the pulse response of the channel has provided some valuable information, which is useful in the design of equalisers, relating to the characteristics of the multipath and pulse dispersion. However, this information is only provisional and therefore, a more detailed study of the pulse response of the channel is required.

The experimental investigation presented in the thesis has been based on measurements made on an ASK data transmission system. It has been shown that, when using ASK techniques, it is possible to obtain information about the medium and its effect on system performance in

a simple manner. It would be useful to assess the performance of underwater data transmission systems, under similar propagation conditions, but with other types of modulation methods. An interesting area of research is the comparison of system performance when using ASK, PSK, DPSK and FSK techniques. Other further areas of investigation are carrier extraction methods in PSK systems when operating in a dispersive medium, such as the underwater environment, and also the comparison of various demodulation schemes in terms of the performance of the underwater data transmission system.

The quantitative results relating to the study of signal amplitude fluctuations, presented in Chapter 3, have been shown to be in agreement with several relevent threories. Since the experimental investigation has been carried out using one carrier frequency of 150 kHz, it would be interesting to investigate the validity of the theories when using different carrier frequencies in the ASK system. Further aspects of this type of investigation are the study of the signal fluctuations when using other modulation methods, and the study of phase fluctuations with particular emphasis in PSK, DPSK and FSK systems. Similar types of studies could be carried out, using several modulation methods, on the signal probability density functions.

Perhaps a most interesting and challenging extension of the work presented in this thesis is to apply the measurements and tests in longer-range and deeper-water environments. The tests described in the thesis can be carried out over a variety of transmission ranges and propagation conditions and aspects such as signal amplitude fluctuations and bit-error probabilities can be studied in detail in order that a wider knowledge of underwater data transmission can be obtained.

REFERENCES

ABOTTEEN,R.A., SHEHADEH,N.M., and VANELLI,J.C. : ' Error Probability of a Binary NRZ Signal Over a Parallel Channel ', IEEE Trans. Sonics and Ultrasonics, Vol. SU-21, p300, 1974

ANDREWS,R.S., CONSTANTINIDES,A.G., and TURNER,L.F. : ' Use of Sample-and-Hold Delay Circuits for Synthesising Raised-Cosine Filters ', Proc. IEE, Vol. 121, p169, 1974

ANDREWS,R.S. and TURNER,L.F. : ' An Investigation of the Amplitude Fluctuations of High-Frequency Short-Duration Sound Pulses Propagated Under Short-Range Shallow-Water Conditions ', J. Acoust. Soc. Am., Vol. 58, No. 2, p331, 1975

ANDREWS,R.S. and TURNER,L.F. : ' On the Performance of Underwater Data Transmission Systems Using Amplitude-Shift-Keying Techniques ', IEEE Trans. Sonics and Ultrasonics, Vol. SU-23, p64, 1976

BECHMANN,P. and SPIZZICHINO,A. : "The Scattering of Electromagnetic Waves from Rough Surfaces", Pergamon Press, London, 1963

BENDAT,J.S. : " Principles and Applications of Random Noise Theory ", J.Wiley and Sons, New York, 1958

BENNETT,W.R. and DAVEY,J.R. : "Data Transmission", McGraw-Hill Book Company, New York, 1965

BERGMANN,P.G. : ' Propagation of Radiation in a Medium with Random Inhomogeneities ', Physical Review, Vol. 70, p486, 1946

BERKTAY,H.O., GAZEY,B.K., and TEER,C.A. : ' Underwater Communication-Past, Present and Future ', J. Sound and Vib., Vol. 7, p62, 1968

CAMPANELLA,S.J. and FAVRET,A.G. : ' Time Autocorrelation of Sonic Pulses Propagated in a Random Medium ', J. Acoust. Soc. Am., Vol. 46, p1234, 1969

CHERNOV,L.A. : "Wave Propagation in a Random Medium", Dover Publications, New York, 1967

GODDARD,G.C. : 'An Underwater Acoustic Telemeter for Use in a Multipath Channel', Ph.D. Thesis, University of Birmingham, 1970

GOLD,B. and RADER,C.M. : "Digital Processing of Signals", McGraw-Hill Book Company, New York, 1969

HEARN,P.J. : 'Underwater Acoustic Telemetry', IEEE Trans. Comm. Tech., Vol. COM-14, p839, 1966

KINSLER,L.F. and FREY,H.R. : "Fundamentals of Acoustics", J. Wiley & Sons, London, 1962

LIEBERMAN,L. : 'The Effects of Temperature Inhomogeneities in the Ocean on the Propagation of Sound', J. Acoust. Soc. Am., Vol. 23, p563, 1951

MACKENZIE,K.V. : 'Long-Range Shallow-Water Signal Level Fluctuations and Frequency Spreading', J. Acoust. Soc. Am., Vol. 34, p.61, 1962

MARCUM,J.I. : 'Table of Q-Functions', Rand Research Memo, RM339, 1950

MARSH,D.E. and ROWLANDS,R.O. : 'Upper Bounds on the Information Rate for Underwater Acoustic Communication', Int. Conf. Comm., 1968

MARSH,H.W., SHULKIN,M. and KNEALE,S.G. : 'Scattering of Underwater Sound by the Sea Surface', J. Acoust. Soc. Am., Vol. 33, 1961

MASON,W.P. : "Electromechanical Transducers and Wave Filters", Van Nostrand Company, London, 1948

McCARTNEY,B. : 'Acoustics in Oceanography', IEE Colloquim on Civil Applications of Underwater Acoustics, May 1975

MEDWIN,H. : 'Specular Scattering of Underwater Sound from the Wind-Driven Surface', J. Acoust. Soc. Am., Vol. 41, p1485, 1967

MILLER,C.S. and BOHMAN,C.E. : 'An Experiment in High-Rate Underwater Telemetry', IEEE Conf. Eng. in Ocean Environment, 1972

MINTZER,D. : 'Wave Propagation in a Randomly Inhomogeneous Medium', J. Acoust. Soc. Am., Vol. 25, p422, 1953

MITSON,R. : 'Sonar Observations in Fishery Research', IEE Colloquim on Civil Applications of Underwater Acoustics, May 1975

NESBITT,R. and BERKTAY,H.O. : "An Electronic Tracking System for Acoustic Telemetry", Br. Acoust. Soc., Spring Mtg., April 1971

NEUMANN,G. and PIERSON,W.J. : "Principles of Physical Oceanography", Prentice-Hall, Englewood Cliffs, New Jersey, 1966

NICHOLS,R.H. and YOUNG,H.J. : 'Fluctuations in Low Frequency Acoustic Propagation in the Ocean' , J. Acoust. Soc. Am., Vol.43, p716, 1968

OKERLUND,J.H. : 'A Phase-Shift-Keyed Acoustic Data Link', Int. Conf. Comm., Seattle, 1973

OPPENHEIM,A.V. and SCHAFER,R.W. : "Digital Signal Processing", Prentice-Hall, Englewood Cliffs, N.J., 1975

PARVULESCU,A. and CLAY,C.S. : 'Reproductibility of Signal Transmissions in the Ocean', Radio Elec. Eng., Vol. 29, p223, 1965

RICE,S.O. : ' Mathematical Analysis of Random Noise ', in " Selected Papers on Noise and Stochastic Processes ", N.Wax, ed., Dover Publications, New York, 1954

ROWLANDS,R.O. and QUINN,F.G. : 'Transmission Rate Limits in Underwater Acoustic Telemetry', in "Underwater Acoustics - Vol. 2", ed. V.M.Albers, 1967

SAGAR,F.H. : 'Acoustic Intensity Fluctuations and Temperature Microstructure in the Sea', J. Acoust. Soc. Am., Vol. 32, No. 1, 1960

SAGAR,F.H. : 'Near Ocean Turbulence and Acoustic Intensity Fluctuations Measured at Ultrasonic Frequencies', Ultrasonics International Proc., London, 1973

SCHWARTZ,M. : "Information, Transmission, Modulation and Noise", McGraw-Hill Book Company, New York, 1970

SCHWARTZ,M., BENNETT,W.R. and STEIN,S. : "Communication Systems and Techniques", Mc-Graw-Hill Book Company, New York, 1966

SKUDRZYK,E : ' Scattering in an Inhomogeneous Medium ', J. Acoust. Soc. Am., Vol. 29, p50, 1957

STANFORD,G.E. : 'Low-Frequency Fluctuations of a CW Signal in the Ocean', J. Acoust. Soc. Am., Vol. 55, p968, 1974

STEINBERG,J.C. and BIRDSALL,T.G. : 'Underwater Sound Propagation in the Straits of Florida', J. Acoust. Soc. Am., Vol. 39, 1966

STONE,R.G. and MINTZER,D. : 'Range Dependence of Acoustic Fluctuations in a Randomly Inhomogeneous Medium', J. Acoust. Soc. Am., Vol. 34, p647, 1962

TATARSKI,V.I. : "Wave Propagation in a Turbulent Medium", Dover Publications, New York, 1967

TUCKER,D.G. and GAZEY,B.K. : "Applied Underwater Acoustics", Pergamon Press, London, 1966

TURNER,L.F. and ANDREWS,R.S. : 'Data Transmission Through the Underwater Dispersive Channel', Proc. NATO Advanced Study Institute on New Directions in Signal Processing, Darlington, 1974

URICK,R.J. : 'Fluctuation Spectra of Signals Transmitted in the Sea and Their Meaning for Signal Detectability ', 8th International Congress on Acoustics, Symposium on Underwater Acoustics, Birmingham, 1974

URICK,R.J. : "Principles of Underwater Sound for Engineers", McGraw-Hill Book Company, New York, 1967

WEATHERBURN,C.E. : " Mathematical Statistics ", Cambridge University Press, 1961

WELSBY,V.G. and DUNN,J.R. : 'A High-Resolution Electronic Sector-Scanning Sonar', J. Brit. Inst. Radio Engrs, Vol. 26, p205, 1963

WHITMARSH, D.C. : 'Underwater Acoustic Transmission Measurements', J. Acoust. Soc. Am., Vol. 35, p2014, 1963

WHITMARSH,D.C., SKUDRZYK,E. and URICK,R.J. : 'Forward Scattering of Sound in the Sea and Its Correlation with the Temperature Microstructure', J. Acoust. Soc. Am., Vol. 29, p1124, 1957

APPENDIX A

MEAN VALUE OF RICIAN DISTRIBUTION

The median value of the Rician distribution can be computed when,

$$\int_{\bar{r}}^{\infty} f_r(r)dr = 0.5 \qquad \ldots\ldots \text{(A.1)}$$

where,

$$f_r(r) = \frac{r}{\sigma^2} \exp\left[-\frac{(r^2+A^2)}{2\sigma^2}\right] I_o\left(\frac{rA}{\sigma^2}\right) \qquad \ldots\ldots \text{(A.2)}$$

By substitution of Equation (A.2) into (A.1), then it can be shown that Equation (A.1) can oe expressed in terms of the Q-function as given by Marcum (1950) or,

$$Q\left\{\frac{A}{\sigma}, \frac{\bar{r}}{\sigma}\right\} = 0.5 \qquad \ldots\ldots \text{(A.3)}$$

The parameter, A, which is the 'specular' component of the Rician distribution, will approximate the median value, $\bar{r}$, under certain conditions, and for small values of skew, the median value will be approximately equal to the mean value.* $\bar{r}$, expressed as a fraction of A, is shown as a function of A/σ in FIGURE A1. The values shown were computed from Equation (A.3) using the Q-function tables. From the figure it can be seen that A can be considered as the median (and hence mean) value of the distribution to within 5% for $A/\sigma \geq 4.5$. In terms of the coefficient of variation, then the above will be true if V is less than 0.22. For these particular value of V, the skew of the Rician distribution will be small. In the experimental tests, the condition that V be less than 0.22 was met for all the PDFs considered.

* see Weatherburn, (1961)

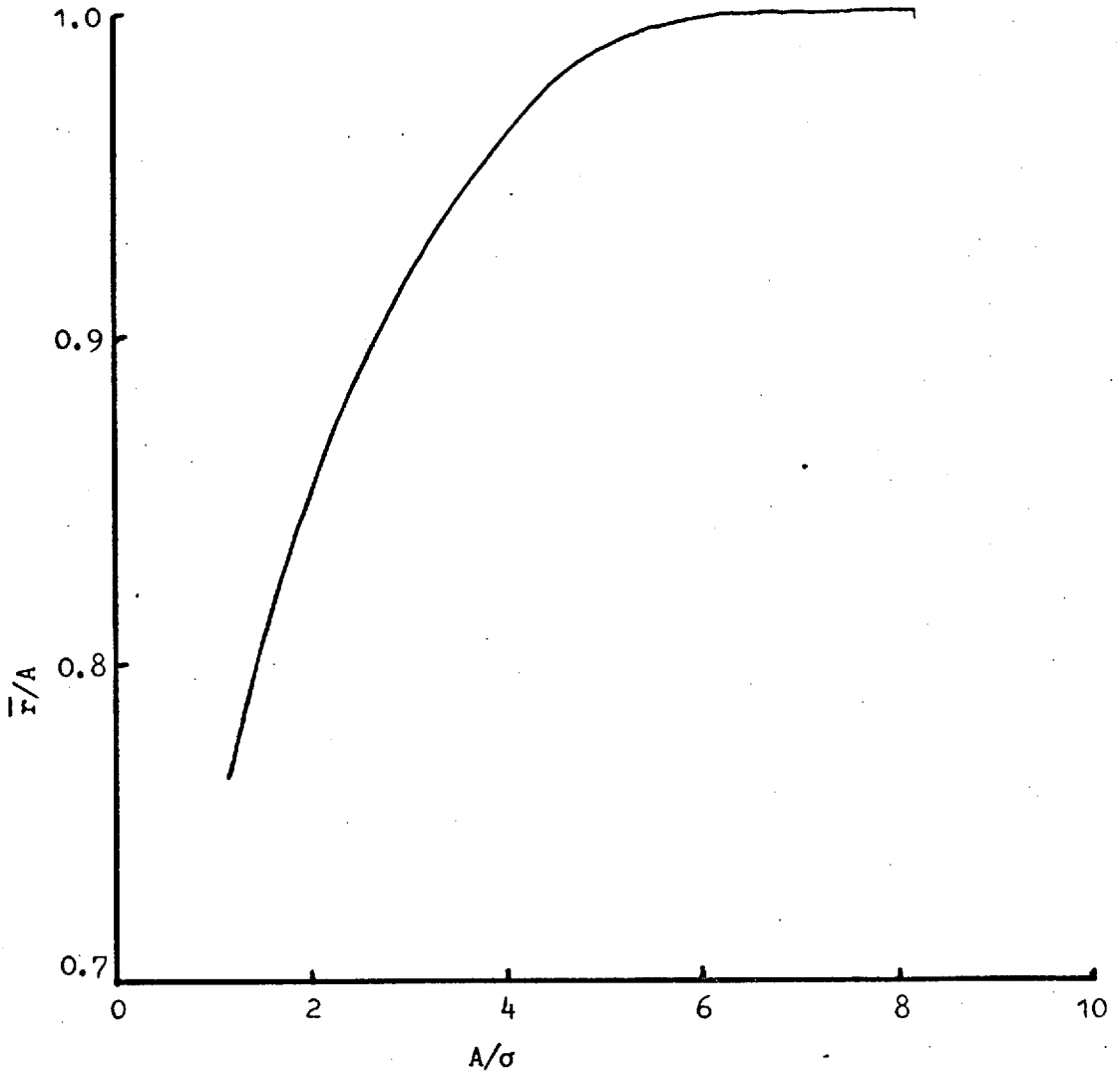


FIGURE A1. $\bar{r}$ as a Fraction of A

APPENDIX B

COMPUTATION OF SPECTRA USING THE FAST FOURIER TRANSFORM (FFT)

Because of the finite number of summations which are used in computations and by its implementation, the fast Fourier transform (FFT) provides a biased estimate of the power spectrum (and consequently the amplitude frequency spectrum) of a signal. It has been shown by Oppenheim and Shafer (1975), (pp 541-548), that the estimation of power spectra using the FFT method is always biased and that the variance of the estimation does not approach zero as the number of samples or points is increased. However, a better estimate of the power spectrum can be obtained by using smoothing or averaging techniques such as Bartlett's procedure.

One interesting point concerning the estimation of power spectra using FFT routines is that as the number of samples used in the computation increases, the rapidity of the fluctuations in the spectrum estimate increases because the uncorrelated frequency samples with zero covariance move closer together and the variance of the estimated spectrum approaches a finite, non-zero value (Oppenheim and Shafer, p545). This fluctuation can be observed in the amplitude frequency spectra shown in FIGURES 3.1 to 3.6 in Chapter 3. A further example, taken from Oppenheim and Shafer (p547) is shown in FIGURE B.1. The information shown in the figure clearly illustrates that the rapidity of fluctuations in the computed power spectrum increases with increasing numbers of data samples.

Bartlett's procedure can be used to smooth power spectra and thereby provide a good estimate of the true spectra. The procedure consists of taking N samples of data and dividing the N samples into K groups, each with M samples, such that KM=N. The FFT of each of the

ω = frequency (rad/sec.)

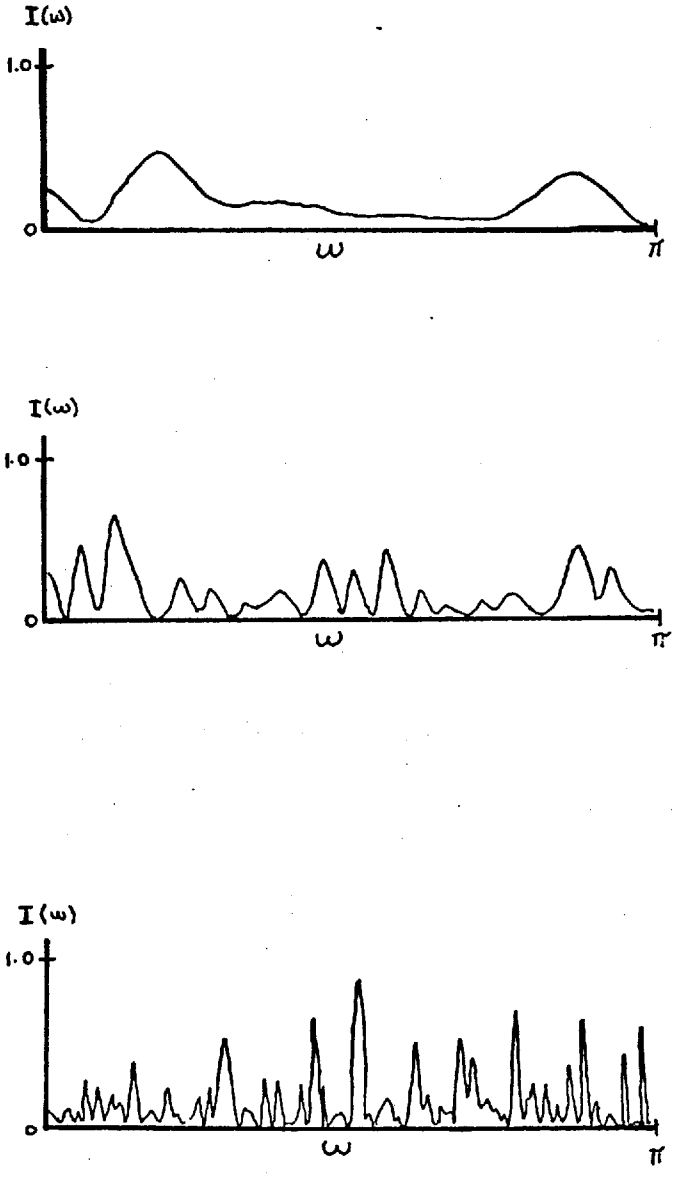


FIGURE B.1 Power Spectra for Sample Lengths of N = (a) 14, (b) 51, and (c) 135

K groups of data is then computed and the K FFTs are added together. The effect of this operation is, however, to decrease the frequency resolution in the spectrum when compared to an N-bit FFT. A simple illustration of this technique is shown in FIGURE B.2 (Oppenheim and Shafer, p569) in which 14000 samples of data are first divided into 27 groups, each containing 512 samples, and then into 280 groups, each containing 50 samples of data. The effect of this operation is clearly shown in the figure.

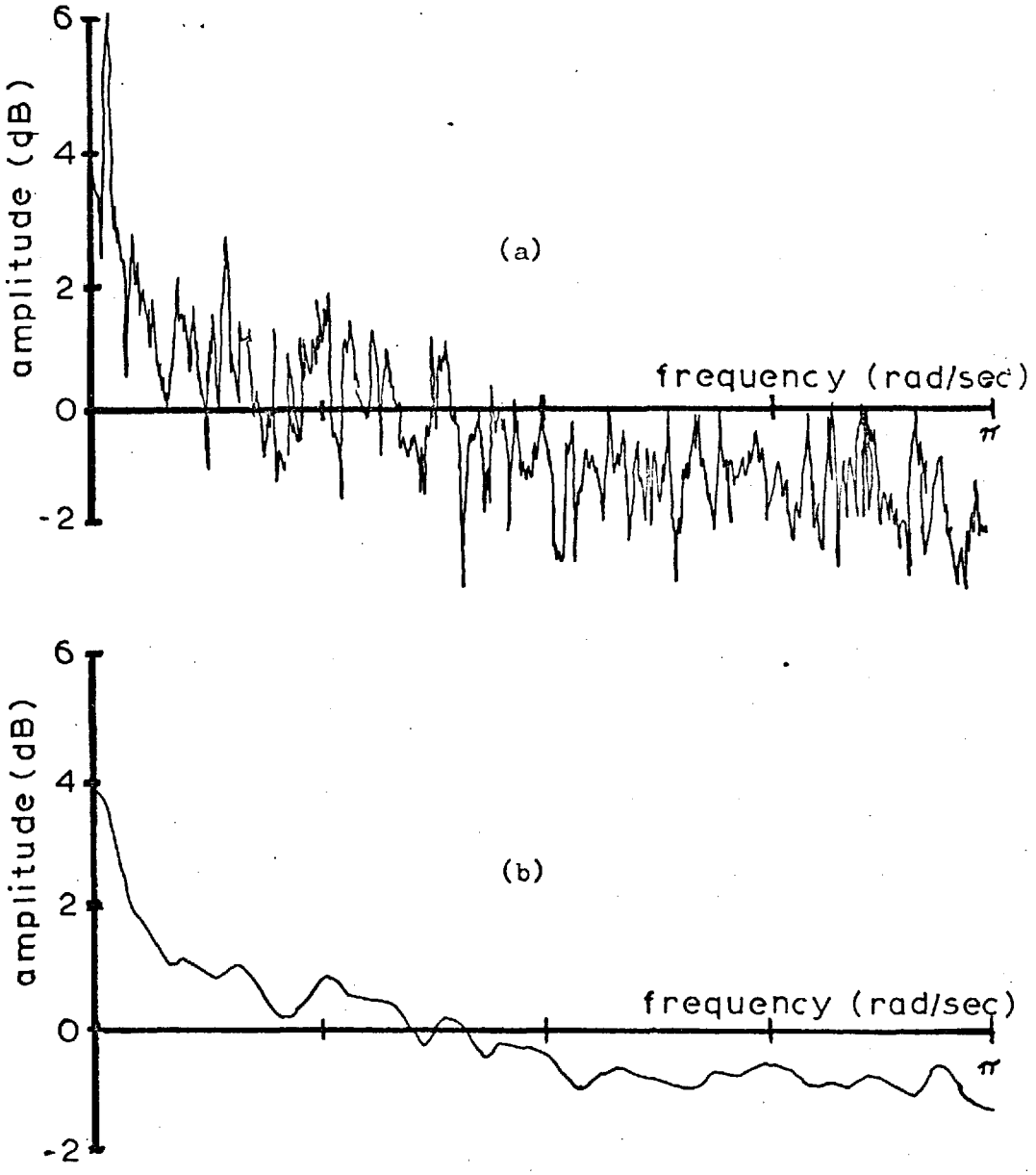


FIGURE B.2 Power Spectrum Estimates Using Bartlett's Procedure for N = 14000, and M = (a) 512, and (b) 50

APPENDIX C

EXPONENTIAL-COSINE AUTOCORRELATION FUNCTION

The exponential-cosine autocorrelation function has been widely reported in many situations such as valve noise, radar-fading and atmospheric turbulence (Bendat, 1958, p.189). In its simplest form, the function can be given as (Bendat, p.202),

$$R(\tau) = A \exp\left[-k|\tau|\right]\cos(c\tau) \qquad \ldots\ldots \text{(C.1)}$$

and the power spectrum of (C.1) can be shown to be,

$$G(\omega) = \frac{2}{\pi}\int_0^{\infty} R(\tau)\cos(\omega\tau)\, d\tau$$

$$= \left(\frac{2Ak}{\pi}\right)\left[\frac{\omega^2 + (k^2 + c^2)}{\omega^4 + 2(k^2-c^2)\omega^2 + (k^2+c^2)}\right] \qquad \ldots\ldots \text{(C.2)}$$

If $3c^2 > k^2$, then $G(\omega)$ has a single maximum which occurs at ω_1, where

$$\omega_1 = (k^2+c^2)^{\frac{1}{4}}\left[2c - (k^2+c^2)^{\frac{1}{2}}\right]^{\frac{1}{2}} \qquad \ldots\ldots \text{(C.3)}$$

In the case in which $3c^2 > k^2$, the power spectrum, $G(\omega)$ appears in the form shown in FIGURE C.1(a), and the corresponding autocorrelation function, R( ), can be represented in the form shown in FIGURE C.1(b).

In addition, if $c^2 \gg k^2$, or, if the frequency, c, of the cosine term in Equation (C.1) is much larger than the exponential decay term, k, then the maximum (peak) in the power spectrum occurs at ω_1', where,

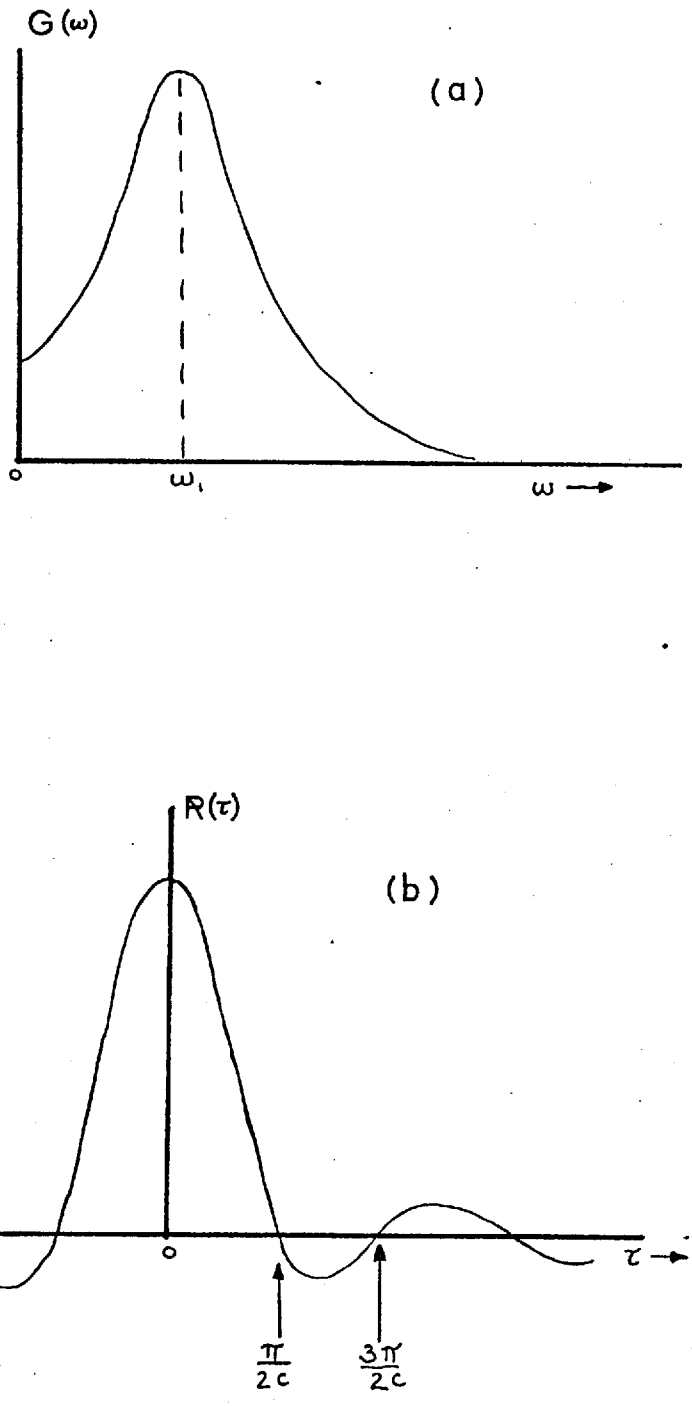


FIGURE C.1 (a) Power Spectrum and (b) Autocorrelation Function of the Simple Exponential-Cosine Form

$$\omega_1' \simeq (c^2)^{\frac{1}{4}} (2c - c)^{\frac{1}{2}}$$

$$= c \qquad \ldots\ldots (C.4)$$

and thus, the peak in the power spectrum occurs at the frequency of the cosine term in the autocorrelation function.

Although the spectra shown in FIGURES 3.1 to 3.6 are amplitude frequency spectra, they appear to resemble, in shape, the power spectrum shown in FIGURE C.1(a). There is also similarity between the measured autocorrelation functions shown in FIGURES 3.7 to 3.10 and the autocorrelation function shown in FIGURE C.1(b). However, it is noted that the Fourier transform of the square of Equation (3.1) is much more complicated than the simple expression given by Equation (C.1), but the experimental evidence suggests that the spectra and autocorrelation functions shown in FIGURES 3.1 to 3.10 can be simply represented by the forms shown in FIGURE C.1.

In FIGURE C.1(b), the times of the first two zero-crossings of the autocorrelation function are indicated. These times are used in Chapter 3 to compare the similarity of the autocorrelation functions and power spectra, which are shown in FIGURES 3.1 to 3.10, to the simple exponential-cosine form.

APPENDIX D

COMPUTATION OF NOISE SPECTRUM

If white noise is band-pass filtered about a centre frequency, f_o, with an overall bandwidth B, such that $B/f_o \ll 1$, then after envelope detection the baseband noise power spectrum is of the form (see Rice, 1954),

$$W(f) = \frac{K}{B}\left(1 - \frac{f}{B}\right) + \frac{K}{2}\delta(f) \qquad \ldots\ldots (D.1)$$

where K = constant
$\delta(f)$ = unit impulse at the origin
B = overall bandwidth = 2 x baseband bandwidth

The power spectrum given by (D.1) is illustrated in FIGURE D.1.

The total noise power in the band 0 to B Hz is therefore,

$$\alpha_t^2 = \frac{K}{B}\int_0^B \left(1 - \frac{f}{B}\right) df + \frac{K}{2} = K \quad \text{Watts} \qquad \ldots\ldots (D.2)$$

However, in the bandwidth 0 to B/2 Hz, corresponding to the baseband, the noise power is given by the shaded area in FIGURE D.1, or as,

$$\alpha_p^2 = \alpha_t^2 - \left(\tfrac{1}{2}\,\frac{K \cdot B}{2B \cdot 2}\right) = \frac{7K}{8} \text{ Watts} \qquad \ldots\ldots (D.3)$$

Thus, the total r.m.s. noise voltage which would be measured in the band 0 to B/2 Hz is,

$$\alpha_p = \sqrt{\frac{7K}{8}} \quad \text{Volts} \qquad \ldots\ldots (D.4)$$

In the computation of the amplitude frequency spectra presented in Chapter 3, the r.m.s. noise voltage, α_p, was measured over a

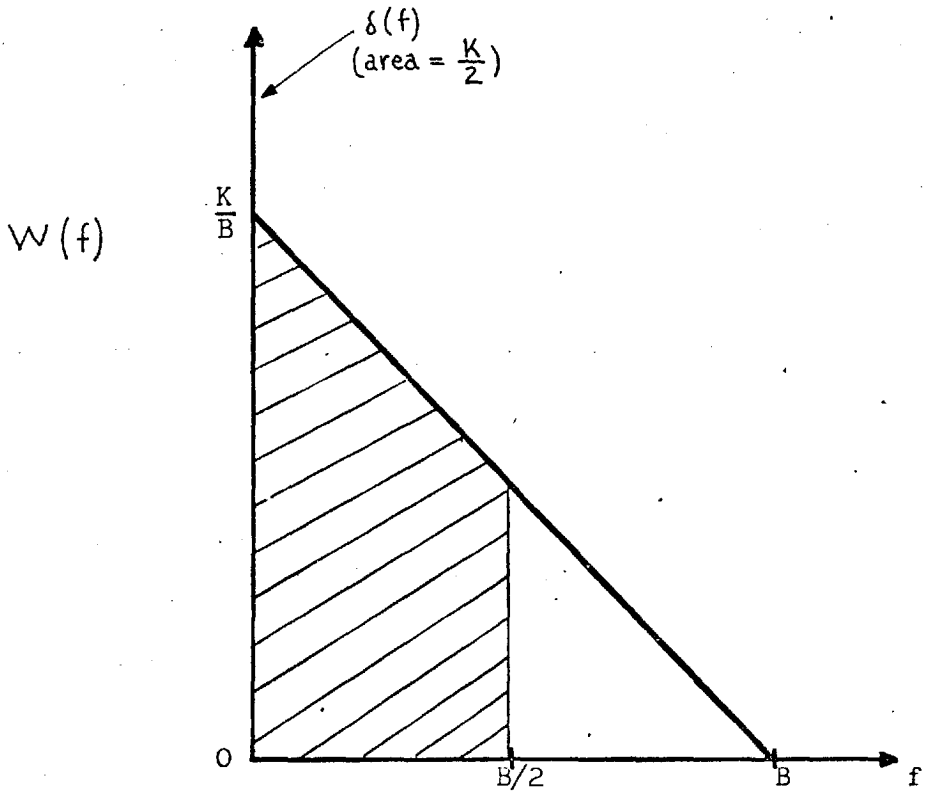


FIGURE D.1. Noise Power Spectrum After Detection

bandwidth of 4.5 kHz. However, the received signals were then low-pass filtered at 20 Hz in order to compute the amplitude frequency spectra. In this narrow band, the noise power spectrum can be considered to be essentially constant and the noise spectral density is approximately,

$$W'(f) = \frac{K}{B} \quad \text{Watts/Hz} \qquad \ldots\ldots (D.5)$$

Expressed in terms of α_p, the measured r.m.s. noise voltage, the noise power spectrum can be written as,

$$W'(f) = \frac{8\alpha_p^2}{7B} \qquad \ldots\ldots (D.6)$$

and hence, the amplitude frequency spectrum is given by,

$$A(f) = \sqrt{W'(f)} = 2\alpha_p \sqrt{\frac{2}{7B}} \qquad \ldots\ldots (D.7)$$

In the tests relating to the measurement of the amplitude frequency spectra, 0.8 msec duration raised-cosine pulses, repeating every 6.4 msec, were used to modulate a 150 kHz carrier signal. The d.c. component of such a sequence can be computed as,

$$S_{dc} = \frac{1}{8T} \int_0^T \frac{h}{2}(1 + \cos(\pi f T)) \, dt$$

$$= h/16 \qquad \ldots\ldots (D.8)$$

where h = amplitude of pulse (peak amplitude)

T = duration of pulse in seconds

f = frequency in Hz

The d.c. component of the measured amplitude frequency spectra can be located in FIGURES 3.1 to 3.6, and thus the noise spectrum can be drawn in each of the figures, as illustrated. For a peak signal-to-r.m.s. noise level of 30 dB (typical value), i.e., $h/\alpha_p \cong 30$, then

$$\frac{S_{dc}}{A(f)} = \frac{h}{16} \cdot \frac{1}{2\alpha_p}\sqrt{\frac{7B}{2}}$$

$$= \frac{30}{32}\sqrt{\frac{7 \times 9000}{2}} = 166 \qquad \ldots\ldots \text{(D.9)}$$

or, $S_{dc}/A(f) = 44$ dB.

Thus, the noise spectrum level is approximately 44 dB below the d.c. component of the signal spectrum.

From an analysis of FIGURES 3.1 to 3.6, it can be seen that the computed, approximate, noise spectrum level is well below the levels of the fluctuation spectra and hence, the effects of background noise on the fluctuation spectra can be considered to be negligible.